

---

Electronic Thesis and Dissertation Repository

---

8-20-2024 11:30 AM

## Modular Open-Source Photovoltaic-Powered DC Nanogrid for Application-Specific Designs

Md Motakabbir Rahman, *Western University*

Supervisor: Pearce, Dr Joshua M., *The University of Western Ontario*

A thesis submitted in partial fulfillment of the requirements for the Master of Engineering Science degree in Electrical and Computer Engineering

© Md Motakabbir Rahman 2024

Follow this and additional works at: <https://ir.lib.uwo.ca/etd>



Part of the [Power and Energy Commons](#)



This work is licensed under a [Creative Commons Attribution 4.0 License](#).

---

### Recommended Citation

Rahman, Md Motakabbir, "Modular Open-Source Photovoltaic-Powered DC Nanogrid for Application-Specific Designs" (2024). *Electronic Thesis and Dissertation Repository*. 10346.  
<https://ir.lib.uwo.ca/etd/10346>

This Dissertation/Thesis is brought to you for free and open access by Scholarship@Western. It has been accepted for inclusion in Electronic Thesis and Dissertation Repository by an authorized administrator of Scholarship@Western. For more information, please contact [wlsadmin@uwo.ca](mailto:wlsadmin@uwo.ca).

## Abstract

Decreasing cost of green energy producing solar panels has significantly boosted their popularity. Despite this, the power electronics associated with PV systems remain closed-source, expensive, and not easily compatible or expandable. This limits accessibility, especially for low-power applications. This research addresses these issues by adopting and analyzing DC nanogrid technology, converting it into a modular, open-source hardware system that users can easily assemble and expand. Detailed small signal analysis of the DC nanogrid was conducted, followed by the design of controllers and an effective energy management system. The system's stability was also thoroughly analyzed. Subsequently, hardware was developed and tested to ensure adaptability and modularity. The resulting system offers higher efficiency by serving most loads in DC, eliminating the need for AC conversion and concomitant conversion losses. This technology is particularly suitable for applications in ambulances, mini clinics, tents, expedition vehicles, houses, and camps where grid power is unreliable or unavailable.

## Keywords

DC nanogrid, Photovoltaic, Off grid, Modular PV system hardware, Open source microgrid

## Summary for Lay Audience

The cost of solar photovoltaic (PV) panels has been decreasing steadily, but the associated power electronics, such as converters, maximum power point trackers, and inverters, have not seen similar reductions. This discrepancy limits the accessibility and potential of solar power. The goal of this research was to develop an alternative PV system solution that is more accessible for the general users. The aim was to create a system that people can easily replicate, assemble, and use to power small-scale setups with solar energy. To achieve this, various microgrid technologies and topologies were explored. DC nanogrids were identified as the most promising alternative to conventional PV systems. This research focused on making the nanogrid modular by examining converter topologies and control methodologies. It was determined that three different converters—dedicated for PV, battery, and load—were necessary. The system's operation was first simulated, and then the system was mathematically modeled to check the stability of the bus under various conditions, ensuring it could handle additional PV units, batteries, or loads without issues. The results confirmed the system's stability under different disturbances.

Next hardware was designed. Initially, a prototype was created on a protoboard, later a final hardware of modular nanogrid was developed incorporating a hybrid control technique. In this setup, local converters manage their operations while a master controller oversees the entire nanogrid, making critical decisions such as managing excess loads and controlling power generation. The master controller also handles data logging and monitoring, sending information to a Raspberry Pi display equipped with a graphical user interface to show the system's performance.

The research identified ambulances and mini clinics as ideal candidates for adopting this hardware, given that most of their equipment can operate on battery power or directly from 6V or 12V supplies. By using two buck converters, along with PV and battery converters, these vehicles can be powered throughout the year. The PV and battery sizes were optimized through simulations. While there is room for further development, this system introduces a novel approach to PV systems and DC grids, making it accessible for general users to adopt and implement.

## Co-Authorship Statement

This master's thesis contains three co-authored works that have been published, submitted for review, or are intended for submission in peer reviewed journals. The author's contributions associated with the three articles are as follows.

### **Details of article 1 used for Chapter 2 and 3:**

**M. M. Rahman** and J. Pearce, "Modular Open Source Solar Photovoltaic-Powered DC Nanogrids with Efficient Energy Management System," *Solar Energy and Sustainable Development Journal*, vol. 13, no. 1, Art. no. 1, Feb. 2024, doi: 10.51646/jsesd.v13i1.169.

Author Contributions:

Md Motakabbir Rahman: Developed the simulations and gathered data; analyzed the data and contributed to writing the manuscript; authored all sections related to design, small signal modeling, and plotted results; presented findings.

Joshua M. Pearce: Provided conceptualization and study design; research supervision; secured funding; edited the manuscript; supplied resources; managed submission.

### **Details of article 2 used for Chapter 4:**

**M. M. Rahman**, S Khan and J. Pearce, "Open-source Hardware Design of Modular Solar DC Nanogrid," (to be published).

Author Contributions:

Md Motakabbir Rahman: Designed, assembled, and validated the electrical hardware; developed the enclosures for the converters and stands; completed the final assembly and software integration; authored all sections of the manuscript related to electrical design, assembly, and system integration; performed simulation and stability analysis; plotted results and presented findings.

Sara Khan: Authored sections of the manuscript on converter topology and controller design; compared the system to existing literature.

Joshua M. Pearce: Provided conceptualization and research supervision; secured funding; edited the manuscript; supplied resources; managed submission

**Details of article 3 used for Chapter 5:**

**M. M. Rahman, S Khan, KS Hayibo, and J. Pearce, “An Application of a Modular Open-Source Solar Photovoltaic-Powered DC Nanogrid to Ambulances,”** (to be published)

Author Contributions:

Md Motakabbir Rahman: Designed the system for the ambulance and modified the nano grid for compatibility; estimated the load, designed, and simulated the optimized PV system; authored all sections of the manuscript related to electrical design and system integration; and performed simulations; plotted results and presented findings.

Sara Khan: Authored sections related to the equipment inside the ambulance, assessed their compatibility with the DC nano grid, and compared the system with existing work.

Koami Soulemene Hayibo: Flexible solar panel installation and PV performance analysis on ambulance roof.

Joshua M. Pearce: Provided conceptualization and research supervision; secured funding; edited the manuscript; supplied resources; managed submission.

## Acknowledgments

My deepest gratitude goes to my supervisor, Dr. Joshua Pearce, whose guidance and support have been invaluable throughout this research. Dr. Pearce not only introduced me to the concept of open-source hardware but also enlightened me on its vast benefits. His visionary approach inspired the development of a modular and affordable nanogrid system, aimed at making solar power accessible to all. His encouragement and insights have been pivotal in shaping this thesis, and I am profoundly grateful for his mentorship. His unwavering faith in me, especially during challenging times, has been a source of immense motivation and strength. It is truly a privilege to have such a mentor in one's academic journey.

Special thanks are due to my colleagues at the FAST research group for their remarkable contributions. The development of the open-source SAMA software for the optimization of PV systems has been instrumental in advancing this research. Additionally, the creation of the open-source SCADA system, BREAD, provided significant inspiration for developing the communication protocol between the converters in the nanogrid. I am deeply appreciative of their innovative work and the collaborative spirit they brought to this project. Special thanks to Koami S Hayibo, Uzair Jamil, and Giorgio Antonini for the valuable discussions, both academic and beyond, which have helped me overcome many hurdles during this journey.

I am also grateful to my course teachers and professors. Through their courses, I gained invaluable knowledge about DC-to-DC converters, power systems, and the importance of robust protection in electrical circuits. This foundational understanding was crucial for the development of this project. Thank you for your guidance and the depth of knowledge you imparted.

Finally, my affectionate appreciation goes to my family and Riya Roy for their unwavering faith and continuous encouragement throughout my academic education. My heartfelt thanks to my wife, Sara Khan, for her unwavering support, both mentally and academically, during my journey at Western University. Her contributions to writing the nanogrid hardware paper have been invaluable.

# Table of Contents

Abstract .....	ii
Summary for Lay Audience .....	iii
Co-Authorship Statement.....	iv
Acknowledgments.....	vi
Table of Contents .....	vii
List of Tables .....	xi
List of Figures .....	xiii
List of Appendices .....	xvii
List of Abbreviations .....	xviii
List of Symbols .....	xix
Chapter 1 .....	1
1 Introduction .....	1
1.1 DC Nanogrid.....	2
1.2 Converter topology and controllers .....	3
1.3 DC bus voltage selection .....	6
1.4 Application-specific PV systems .....	7
1.5 Reliable Power Supply for Ambulance and Mini Clinics.....	9
1.6 Motivation and objectives of the thesis .....	10
1.7 Outline of thesis .....	11
Chapter 2.....	13
2 Methodology .....	13
2.1 Introduction.....	13
2.2 Methods.....	16
2.2.1 System Architecture:.....	16

2.2.2	Energy Management System (EMS): .....	17
2.3	Controller design.....	18
2.3.1	PV Array Converter & Controller: .....	18
2.3.2	Customer Load Converter Controller: .....	20
2.3.3	Energy Storage System (ESS) Controller:.....	21
2.4	Simulation results.....	23
2.4.1	Case 1: Variation in PV power generation .....	23
2.4.2	Case 2: Variation of load .....	24
2.4.3	Case 3: Isolation of Battery.....	26
Chapter 3	.....	28
3	Stability analysis .....	28
3.1	Small signal modelling of converters .....	28
3.1.1	Boost converter's transfer function and input/output impedance derivation .....	29
3.1.2	Buck converter's transfer function and input/output impedance derivation .....	32
3.1.3	Bidirectional converter's transfer function and input/output impedance derivation .....	35
3.2	Bus voltage stability analysis.....	37
3.2.1	Impedance scanning.....	37
3.2.2	Fast Fourier Transform (FFT) Analysis.....	41
3.3	LQR controller design and performance.....	41
3.3.1	LQR controller design: .....	42
3.3.2	LQR controller performance:.....	45
3.3.3	FFT analysis:.....	46
3.4	Conclusions.....	47
Chapter 4	.....	48

4	Hardware experimental setup and results .....	48
4.1	Introduction.....	48
4.2	Materials and Methods.....	49
4.2.1	System architecture.....	49
4.2.2	Control strategy.....	50
4.2.3	Controllers design.....	53
4.2.4	Converter design.....	54
4.2.5	Bidirectional Battery converter design .....	56
4.2.6	PV Boost converter design.....	58
4.2.7	Buck converter design.....	60
4.2.8	Master Controller design.....	62
4.2.9	Communication bus .....	64
4.2.10	Inductor design.....	65
4.2.11	Bill of materials.....	66
4.2.12	Arduino codes and GUI .....	67
4.2.13	Interface and GUI .....	68
4.2.14	Step by step integration and commissioning process .....	69
4.3	Final Hardware and Result.....	70
4.3.1	Final nanogrid hardware .....	70
4.3.2	Stability of 24V bus voltage under load disconnection .....	71
4.4	Discussion.....	71
4.5	Conclusions.....	72
	Chapter 5.....	74
5	Application of OS Nanogrid in Ambulance.....	74
5.1	Typical load of ambulance.....	74
5.1.1	Defibrillator.....	75

5.1.2	Suction unit .....	75
5.1.3	Ventilators.....	76
5.1.4	Portable Oxygen Concentrators (POCs).....	76
5.1.5	Nebulizer.....	76
5.1.6	Infusion Pump.....	77
5.1.7	Summary of emergency equipment’s power requirements .....	77
5.2	PV installation capacity and Load estimation.....	79
5.2.1	Maximum PV installation capacity.....	79
5.2.2	Selection of PV panels .....	80
5.2.3	Annual load assumed of an ambulance.....	82
5.2.4	Simulation of PV and battery.....	83
5.2.5	Modification of Nanogrid for ambulance applications .....	84
5.3	Results.....	86
5.3.1	PV optimization for the location of London and Addis Ababa .....	86
5.3.2	Final assembled DC nanogrid for Ambulance.....	92
5.3.3	Load converters performance under load change .....	92
5.4	Discussion.....	93
Chapter 6	.....	96
6	Conclusions and Future scope.....	96
6.1	Conclusions.....	96
6.2	Thesis contributions .....	97
6.2.1	Publications from this thesis .....	97
6.3	Future scope .....	97
References	.....	99
Appendices	.....	118
Curriculum Vitae	.....	130

## List of Tables

Table 1.1 Comparative analysis of various converter topologies proposed in the literature ....	3
Table 2.1 Controller parameters of boost converter .....	18
Table 2.2 Critical parameters of Buck converters .....	21
Table 2.3 Critical parameters of bidirectional buck boost converter .....	22
Table 2.4 Basic Parameters of PV Battery System Under STC .....	23
Table 2.5 Constant DC load for case 1 .....	23
Table 2.6 Variable DC load for case 2.....	25
Table 2.7 Parameters for case 3 .....	26
Table 4.1. System specifications.....	55
Table 4.2. Converter components and controller parameters calculation.....	56
Table 4.3. Function of each traced in the communication bus .....	64
Table 4.4. Design parameters of inductors. ....	66
Table 4.5. Summary of total cost of the system.....	66
Table 4.6. Arduino codes and GUI of the DC nano grid system are all licensed with GNU GPL v3.....	67
Table 5.1 Typical loads of equipment inside an ambulance .....	77
Table 5.2 Area of surface of an Ambulance available for PV installation .....	79
Table 5.3 Comparison between rigid panel vs flexible panel for Ambulance.....	81
Table 5.4. Optimizing PV systems parameters.....	84
Table 5.5 Comparison PV system optimization between different cases.....	86

Table A.1. 3D printed parts required for assembly of the frame of the DC nano grid all licensed with CERN OHL-S 2.0.....	118
Table A.2. 3-D printing parameters.....	118
Table A.3. 3D printed parts required for assembly of converters and master controller all licensed with CERN OHL-S 2.0.....	122

## List of Figures

Figure 1.1 Conventional off-grid PV system diagram.....	8
Figure 2.1 Architecture of DC nanogrid.....	15
Figure 2.2 Block diagram of control system.....	17
Figure 2.3 EMS algorithm .....	18
Figure 2.4 (a) Controller for isolated PV directly connected with DC load. (b) Controller for battery connected PV array. (c) Battery charge controller. (d) Load voltage controller. ....	20
Figure 2.5 Case 1: PV power variation (a) power flows (PV, ESS and DC load) and (b) DC bus voltage. ....	24
Figure 2.6 Case 2: PV power variation (a) power flows (PV, ESS and DC load) and (b) DC bus voltage. ....	25
Figure 2.7 Case 3: Isolation of battery (a) power flows (PV, ESS and DC load), (b) DC bus voltage and (c) SoC of battery. ....	27
Figure 3.1 (a) boost converter circuit (b) Small AC signal equivalent circuit model of boost converter, (c) AC signal equivalent circuit model of boost converter from output side .....	30
Figure 3.2 (a) Equivalent input impedance measurement(b) Equivalent output impedance measurement of boost converter .....	32
Figure 3.3 (a) buck converter circuit (b) Small AC signal equivalent circuit model of buck converter, (c) Small AC signal equivalent circuit transferred to output side.....	33
Figure 3.4 (a) Equivalent input impedance measurement (b) Equivalent output impedance measurement of buck converter .....	35
Figure 3.5 Bidirectional converter circuit.....	36
Figure 3.6 Nyquist plot of total output impedance and input impedance.....	39

Figure 3.7 (a) Bode plot of total output impedance and total input load impedance (b) Bode plot of the total DC bus impedance.....	40
Figure 3.8 FFT analysis of the bus voltage under the disturbance on the boost converter's input side.....	41
Figure 3.9 Block diagram of the LQR controller.....	43
Figure 3.10 Block diagram of LQR controller with integral action .....	44
Figure 3.11 Output voltage response boost converter of the LQR controller and PI controller. ....	46
Figure 3.12 FFT analysis of the bus voltage under with LQR controller.....	47
Figure 4.1. Architecture of DC Nano grid.....	50
Figure 4.2. Control strategy (a) Hybrid control model of modular DC nano grid and (b) Detail connection diagram .....	52
Figure 4.3. PV controller for boost converter.....	53
Figure 4.4. (a) Schematic of bidirectional converter for battery, (b) 3D assembled PCB of bidirectional converter.....	58
Figure 4.5. Assembled bidirectional battery converter.....	58
Figure 4.6. (a) Schematic of boost converter for PV, (b) 3D assembled PCB of Boost converter.....	59
Figure 4.7. Assembled Boost converter for PV.....	60
Figure 4.8. (a) Schematic of buck converter for 24V load, (b) 3D assembled PCB of Buck converter .....	62
Figure 4.9. Buck converter PCB with components (a) front side (b) back side.....	62

Figure 4.10. (a) Schematic of Master controller, (b) 3D assembled PCB of master controller. .....	63
Figure 4.11. Master controller PCB layout and assembly. ....	64
Figure 4.12. Schematic of Communication bus.....	65
Figure 4.13. Assembled and extended communication bus.....	65
Figure 4.14. DC nano grid GUI for data monitoring. ....	68
Figure 4.15. Nanogrid final hardware (a) front view (b) back view.....	70
Figure 4.16. The bus voltage after sudden disconnection of 30W load (0-70sec).....	71
Figure 5.1 External dimensions of Mercedes Benz ABL-XLT-SL Ambulance [186]. ....	79
Figure 5.2 Top view of ambulance with PV panels placement .....	81
Figure 5.3 Monthly load assumed of an ambulance. ....	83
Figure 5.4 DC nanogrid in electrical box for the ambulance.....	85
Figure 5.5 Electrical wiring of an ambulance. ....	85
Figure 5.6. Optimized PV and battery performance for London, Ontario (Case 1). ....	87
Figure 5.7. PV and battery performance with three PV panels and 2kW battery in London, ON (Case 2). ....	88
Figure 5.8. PV and battery performance with 350 W of PV and 1kW battery for Addis Ababa (Case 3). ....	89
Figure 5.9. PV and battery performance with 175W of PV and 2kW battery for Addis Ababa (Case 4). ....	90
Figure 5.10. Hourly PV, load and battery charging/discharging power for case 4 in Addis Ababa. ....	91

Figure 5.11. Battery state of charge hourly for case 4 in Addis Ababa. ....	91
Figure 5.12. Hardware of nanogrid for ambulance. ....	92
Figure 5.13. Bus voltage and 6V converter voltage variation due to load change (0-70sec). .	93
Figure 5.14. Bus voltage and 12V converter voltage variation due to load change (0-70sec)	93
Figure A.1 Parts required for assembly of frame. ....	120
Figure A.2. Assembly process of the frame. ....	120
Figure A.3. Assembled frame. ....	121
Figure A.4. Rendered 3D image of master controller encloser .....	122
Figure A.5. Rendered 3D image of final assembly of Nano grid. ....	123

## List of Appendices

Appendix A: Integration of converters .....	118
Appendix B: Bill of materials of DC nanogrid hardware .....	124

## List of Abbreviations

MPPT	: Maximum Power Point Tracker
PSO	: Particle Swarm Optimization
FA	: Firefly Algorithm
ACO	: Ant Colony Optimization
P&O	: Perturb and Observe
SOC	: State of Charge
PV	: Photovoltaic
PID	: Proportional, Integral and Derivative Controller
AEM	: Anion Exchange Membrane
SOC	: State of Charge
EMS	: Energy Management System
FFT	: Fast Fourier Transform
PM	: Phase Margin
GM	: Gain Margin
ESS	: Energy Storage System
OSAT	: Energy Management System
ECG	: Electrocardiogram
POCs	: Portable Oxygen Concentrators
SPWM	: Sinusoidal Pulse Width Modulation
LCOE	: Levelized cost of energy
NPC	: Net present cost
COE	: Cost of energy
STC	: Standard Test Conditions
SSA	: State-Space Averaging
ASM	: Averaged Switch Model
AED	: Automated external defibrillator
POC	: Portable Oxygen Concentrators
ALS	: Advanced Life Support

## List of Symbols

$K_p$	: Proportional gain
$K_i$	: Integral gain
$D$	: Nominal duty cycle
$D'$	: Complement of the nominal duty cycle $D$ , where $D'$ is defined as $(1 - D)$
$\omega_z$	: Zero frequency
$Q$	: Quality factor
$Z_{in}$	: Input impedance
$Z_o$	: Output impedance
$Z_{ocl}$	: Closed loop output impedance
$Z_{icl}$	: Closed loop input impedance
$Z_{tsource}$	: Total source side impedance
$Z_{tload}$	: Total load side impedance
$Z_{bus}$	: Total bus impedance
$J$	: Cost function
$Q$	: State weighting matrix
$R$	: Control weighting matrix
$K$	: LQR gain matrix
$P$	: Unique positive definite solution of algebraic Riccati equation (ARE).

# Chapter 1

## 1 Introduction

The inherent limitations in the accessibility and scalability of traditional photovoltaic (PV) systems restrict their widespread adoption, particularly in small-scale applications. To overcome these challenges, an alternative approach involving modular DC nanogrids presents a promising solution. DC nanogrids, characterized by their decentralized structure and compatibility with renewable energy sources, offer enhanced flexibility and ease of deployment compared to conventional PV systems. By leveraging modular converter topologies and advanced control strategies, this approach aims to deliver a more user-friendly and scalable solution for solar energy utilization, enabling efficient assembly, replication, and customization of small-scale solar installations, thus making solar power more accessible and adaptable across diverse applications including emergency healthcare system and ambulance.

The nanogrid is defined as a distribution network combining renewable and conventional power resources, capable of supplying a group of clustered loads with a maximum capacity in the range of 2-20 kW [1]. Typically, it is referred to as a building block of microgrids, which usually consist of a mesh of small nanogrids serving power demands over a larger area. The distinction between microgrids and nanogrids is often ambiguous, primarily differing in their maximum power supply capacity and range. The capacity of the nanogrid is typically confined to supplying electrical power within a single household to cluster of households [2]. The integration of renewable energy resources makes it more economically friendly and helps reduce the carbon footprint. Thus it is also defined as a grid that generates power using renewable energy sources and that supplies power up to few watts to 5 kW for residential loads [3]. Since the nanogrid is capable of supplying power to a limited range over a specific distance, it is well-suited for applications where grid electricity is unavailable or costly. Because of the restrictions on maximum power capacity and area coverage, it is suitable to supply power to application-specific types of loads, typically single household loads, small residential loads, hospitals, libraries, ambulances, etc.

## 1.1 DC Nanogrid

Nanogrid functions as a network connection to integrate renewable energy resources as a potential source of energy generation. Renewable resources, especially photovoltaics naturally generate DC power, and supplying this DC power directly to loads eliminates conversion losses and increases system efficiency. Given that nanogrid supplies local loads over a limited range, it is more feasible to deliver power directly without converting it to AC. Therefore, DC nanogrid is more economical than AC nanogrid. Studies comparing the structure, components, feasibility, pros, and cons of AC and DC nanogrid conclude that DC grids outperform AC grids [4]. Converter-based distribution network shows incredible potential especially when integrated with renewable energy sources [5]. That's why all the distributed energy resources are typically connected to power converters to smooth out the voltage fluctuations and supply power reliably to loads. DC power is directly compatible with these power converters. And combination of distributed energy resources that generate DC power, for instance, solar photovoltaic systems with power DC-DC converters makes an ideal match for generating and distributing power in a new fashion. Solar DC nanogrid is a potential future, especially to tropical places across the globe where solar energy is abundant in nature. The development idea of very small sized solar DC nanogrid grid is proposed for places where grid electricity is still unavailable [6].

Implementing a DC nanogrid is cost-effective compared to an AC grid because it eliminates the need for an inverter. This reduction in equipment can result in around 25% cost savings when supplying power via a DC nanogrid compared to an AC in a specific area [7]. Several examples are found where DC nanogrid is implemented to serve places where grid electricity is either costly or unavailable across the globe. In [8], the feasibility of solar DC nanogrid is discussed where grid electricity is inadequate in a state of India. In [9], the design, hardware implementation, and economics of the nanogrid system were discussed. The economics of a solar DC nanogrid, particularly situated in a region in Africa is analyzed [10]. The net present cost (NPC) and cost of energy (COE) was significantly lower than the diesel generating unit. A case study comprising of 5 household was selected at a location in Nigeria [11] and demonstrated that various configurations of renewable energy sources yielded promising results in terms of levelized cost of energy (LCOE) and

net present cost (NPC) compared to the local diesel fuel-operated grid system. Considering all the aspects of nanogrid, solar PV DC nanogrid emerges as the ultimate solution for providing a clean, affordable, and reliable power supply tailored to specific requirements.

## 1.2 Converter topology and controllers

A nanogrid has the potential to operate as a stand-alone system without integrating with the AC grid, but the intermittent nature of renewable energy resources may necessitate connecting the AC grid to the DC distribution network to ensure a continuous power supply. This connection necessitates an AC/DC converter to link the AC supply to the bus network. The smooth operation of the DC nanogrid largely depends on the stability of the bus voltage. Given the possibility of multiple distributed energy resources being connected to the DC nanogrid, along with battery storage or an external utility grid (or both) for continuous power supply, controlling the bus voltage becomes crucial. This is where electronic power converters come into play. Power converters act as interfaces for each element connected to the DC bus, each with different roles but ultimately ensuring the stability of the entire nanogrid system. As such, extensive studies are conducted to identify the best architecture for these converters. Various topologies are examined in terms of design, modes of operation, and control mechanisms and included in Table 1.1 to optimize the performance and stability of the nanogrid.

**Table 1.1** Comparative analysis of various converter topologies proposed in the literature

Converter	Interface	Performance	Hardware Validation	Ref.
Two-stage PWM bidirectional converter	Grid to bus	<ul style="list-style-type: none"> <li>It featured a full bridge rectifier to interact with the grid side and a bidirectional SR dc-dc converter to stabilize dc bus voltage with minimum ripple voltage and faster dynamic responses.</li> <li>Significant reduction in dc-link capacitor without compromising</li> </ul>	Yes	[12]

		dynamics decoupling and bidirectional current protection.		
Switched Boost Inverter (SBI)	Grid to bus	<ul style="list-style-type: none"> <li>• Inverter is capable of supplying both ac and dc power simultaneously.</li> <li>• Modified conventional PWM control technique and implemented in digital domain to control SBI</li> </ul>	Yes	[13]
Cascaded two-stage bidirectional converter	Grid to bus	<ul style="list-style-type: none"> <li>• Featured a Dual Active Bridge (DAB) converter followed by a bidirectional dc-ac converter.</li> <li>• Operates in three different modes (power surplus mode, power deficit mode and idle mode).</li> </ul>	Yes	[14]
Two-stage bidirectional grid interface converter (BGIC)	Grid to bus	<ul style="list-style-type: none"> <li>• Two bridge topologies: Neutral Point Clamped (NPC) and Full bridge (FB) are examined in terms of their efficiency.</li> <li>• Efficiency was found greater when first stage converter was controlled by NPC topology and second stage by a full bridge NPC structure.</li> </ul>	No	[15]
High-gain bidirectional dc-dc converter	Bus to battery storage	<ul style="list-style-type: none"> <li>• Converter topology was developed based on high voltage gain with a three-state switching cell while operating in both buck mode and boost mode.</li> <li>• Converter ensured stability in both grid-connected and islanded mode of the nanogrid, reducing voltage ripple, eliminating the chance of improper switching between modes of operation and</li> </ul>	No	[16]

		establishing smooth bidirectional power flow.		
Boost derived hybrid converter (BDHC)	Bus to loads	<ul style="list-style-type: none"> <li>• A single stage BDHC design was proposed for simultaneously supplying ac and dc loads in a solar PV integrated DC nanogrid system.</li> <li>• Featured a voltage source inverter H-bridge structure for the substitution of boost converter switch.</li> <li>• Efficiency is higher than conventional DC nanogrid converter where dedicated converters are required for each component.</li> </ul>	Yes	[17]
Fourth-order bidirectional dc-dc converter (FoBiDC)	Bus to battery storage	<ul style="list-style-type: none"> <li>• Exhibited continuous bus side and battery side operation with minimum ripple while minimizing the effect of non-linearity for multiple converter-based system.</li> </ul>	Yes	[18]
Bidirectional modular PV battery system (BMPBS)	PV to bus	<ul style="list-style-type: none"> <li>• A small battery was connected to each individual PV module which was further integrated with a single stage dc-dc converter.</li> <li>• Problems associated with PV modules like module mismatch, module open circuit due to partial shading or any other reasons were eliminated by using this converter topology.</li> </ul>	Yes	[19]

For connecting the battery to the DC bus, various bidirectional converters are employed, including high-gain bidirectional converters and fourth-order bidirectional converters (FoBiDC), which minimize ripples and enhance grid stability. To mitigate the intermittent nature of PV, two-stage PWM bidirectional converters, two-stage bidirectional grid

interface converters (BGIC), and cascaded bidirectional converters are utilized. These configurations typically incorporate a DC-DC converter followed by a rectifier circuit, facilitating grid integration with the nanogrid and improving system stability. While researchers are exploring more efficient converter topologies, the absence of a modular multiconverter-based nanogrid system that supports easy integration and expansion remains a gap. This research is motivated to prioritize the hardware development of nanogrid systems, setting aside advanced converter topologies and AC grid integration for future exploration, despite their potential benefits.

### 1.3 DC bus voltage selection

The concept of null net energy (NNE) building can be practically implemented by DC nanogrid [20]. Due to the feasibility of DC nanogrid, it is possible to go completely off-grid and use dc distribution network to supply household loads. In the case of household loads, plenty of tabletop appliances are found that operate efficiently in DC power supplies, such as LED lights, laptops, mobile chargers, television, computer, etc. Taking advantage of appliances operating directly on DC, the implementation of DC house was completed in three different locations (US, Indonesia, and Philippines) to supply basic household loads at a voltage level of 48V DC [21]. Even, apart from the household loads, agricultural loads were also proposed to be supplied from a 48V dc bus [22]. So, the compatibility of DC voltages encourages more research and projects to make a shift toward DC. In a small DC network with a bus voltage of 48V and integration of smart sockets along with a communication network was done to control and measure all the devices that are connected to the system. And from this setup, a substantial power savings (around 30%) is obtained compared to as AC [23]. Therefore, 48V DC is considered a standard voltage level for supplying DC loads compatible with low-voltage DC levels. If a lower voltage is required, buck converters can be used to step down the voltage before interfacing with the load.

Common household appliances, such as washing machines, dryers, coolers, heating systems, stoves, refrigerators, and other kitchen devices, are typically powered by AC. However, some of these appliances can potentially operate on DC power at this voltage level with minor modifications [24]. The advancement of electronic converter technology

made these appliances compatible to work in both AC and DC power supply. A washing machine can be considered an example of a modern appliance where a conventional pole-changing induction motor is replaced by a variable-speed drive. Continuous research and development have been done to make modern appliances compatible with DC distribution networks. In [25], the design idea of a particular home appliance, induction heating was proposed to make it compatible with the DC distribution network. With the advancement of modern appliances, since it is possible to completely go DC, standardization of the voltage level is necessary to connect the loads directly like in conventional AC-powered houses. Two voltage levels were proposed in [26] -one is a high DC voltage of 380 V that is compatible with loads that require high voltage that is mentioned above, and the other is a low voltage level of 48 V. The 380 V DC is selected as a commercial DC distribution standard to connect loads that usually require high voltage to operate. For example, in [27], a high voltage DC distribution network of 380V DC is implemented for a demo house. Even eight different loads are selected randomly and tested to see their response in DC voltage [28]. The response showed a promising future for the shift toward DC. Some standby losses are reported in a study of home appliances particularly by induction stove and laptop when connected to AC, while the significant standby losses become zero if connected to DC [29]. So, to grab the advantages of a DC distribution network, standardization of the voltage level was necessary to make it as standardized as the conventional AC network. In [30], it reviews different DC voltage levels for residential DC nanogrid. In choosing the appropriate DC bus voltage for DC nanogrid, some consideration has been made to ensure user safety, efficiency, and cost savings. Among different low voltage levels ranging from 12V to 100V, 48V voltage level is found to be the best choice for the nanogrid in terms of cost and performance.

## 1.4 Application-specific PV systems

Application-specific PV systems refer to the design of off-grid PV systems tailored to applications, without considering other types of loads into the system. As a foundation for this research, various application-specific PV designs were initially explored, such as an off-grid ball mill for laboratory use, where the goal was to power an open source ball mill

with a 100W panel, a 12V, 8Ah battery, and a PWM battery charge controller, supplying 24V power to the system.[31].

Next, to power an AEM electrolyzer, an off-grid solution was developed [32]. Instead of powering the AEM using a combination of an inverter and an AC-DC converter, an open-source adjustable DC-DC converter was developed to work with a 12V off-grid PV system, directly connected to the DC bus bar. The PV system includes a 12V, 100Ah battery, and a 400W PV panel.

Finally, an off-grid inverter was developed to supply 230V at 60Hz, operating with 24V DC for plasma generation in the hydrogen production process [33]. The inverter was customizable, and with minor modifications, the same circuit could be used with a 48V DC input to supply 120V at the output. These systems utilized conventional solutions, as illustrated in Figure 1.1, where DC-DC converters supply DC loads and inverters supply AC loads, all connected to a common bus bar.

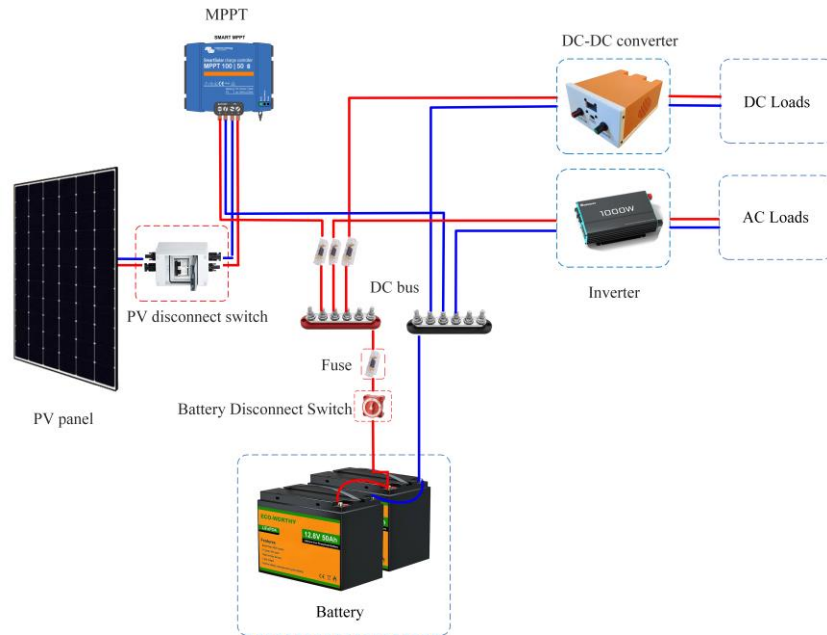


**Figure 1.1** Conventional off-grid PV system diagram

However, such designs have several limitations. They occupy more space, require specialized knowledge for system design, and lack modularity and adaptability. For

example, a 24V inverter cannot be used in a 12V system, and the same applies to MPPTs and converters. Since these components are often sourced from different vendors, they lack direct communication, making system monitoring challenging. Effective monitoring typically necessitates the use of proprietary solutions, which are more expensive and compatible only with products from the same vendor. Thus, a modular PV system is essential to cover multiple applications simultaneously, making the need for a modular DC nanogrid evident.

## 1.5 Reliable Power Supply for Ambulance and Mini Clinics

Ambulances serve as the primary vehicles in pre-hospital emergency medical services (EMS), providing crucial support during medical emergencies [34]. They are equipped with medical equipment, used to transport sick or injured individuals to a hospital. Ensuring an uninterrupted power supply for all medical equipment in ambulances is crucial due to their immeasurable importance in saving human lives [35]. For example, the Free 108 Emergency Ambulance service in Tamil Nadu, India has contributed to reducing the infant mortality rate from 35 to 22 per 1,000 live births, lowering maternal mortality, and saving 120,271 road traffic accident victims through timely interventions [36]. Survival rates for sudden cardiac arrests (SCAs) are significantly higher in public places, exceeding 50%, when defibrillation and CPR are administered promptly, compared to a much lower 3-5% survival rate for SCAs at home, where response times are longer [37]. Observations of over 7,000 adult cardiac patients in King County, Washington, from 1983 to 2000 suggest that early CPR, particularly with dispatcher assistance, can boost survival rates by about 50%, highlighting the life-saving potential of widespread CPR training and use of automated external defibrillators (AEDs) in ambulance and emergency healthcare services could collectively save thousands of lives annually [38].

Most medical equipment on an ambulance has individual batteries that are charged at the hospital; however, many ambulances also provide power [39]. Additionally, solar-photovoltaic (PV) powered ambulances address humanitarian needs in remote, rural, and off-grid areas [40]. Especially in rural areas of Africa and South Asia where grid connectivity is often unavailable or unreliable. In Ethiopia, for example, where the general

energy access rate is 44% and only about 10% in healthcare facilities, and the intensive care treatment is challenging due to the lack of electricity [41]. Altogether around 55,000 healthcare facilities in sub-Saharan Africa lack electricity and are yet to be equipped with solar photovoltaic and battery storage systems [42]. In response, the WHO is advocating for the allocation of essential human and financial resources to develop and implement clean energy plans and sustainable delivery models specifically designed for the needs of the health sectors [43]. Apart from rural areas, a stable backup power supply to these services is crucial [44], particularly during catastrophic disasters or wars when the reliable grid may be disrupted or damaged [45]. It is estimated that 54 percent of the 45 million annual deaths in low- and middle-income countries, or 24.3 million, are due to conditions potentially addressable by prehospital and emergency care, resulting in 932 million years of life lost (YLL) to premature mortality [46]. Solar-powered ambulances and mini clinics can significantly improve healthcare in rural and off-grid areas, potentially saving thousands of lives.

## 1.6 Motivation and objectives of the thesis

To make off-grid solutions more accessible, customizable, and easily adaptable, the concept of a DC nanogrid in a box is both visionary and essential. Open-source designs are increasingly being appreciated and adopted rapidly. Intending to replace conventional off-grid systems with more efficient solutions, the motivation behind this project is to design a DC nanogrid with the following features:

- **Modular Design:** The DC nanogrid features a modular architecture for scalable and easy expansion by connecting additional PV modules and batteries.
- **Open Source:** Licensed under GNU GPLv3 and CERN OHL-S v2, the nanogrid system is open source, promoting collaborative development and innovation.
- **Parametric Energy Management System (EMS):** The EMS uses parametric controls to optimize grid operation based on DC bus voltage and battery state of charge (SoC), ensuring efficient power delivery.

- Flexible Voltage Compatibility: With bidirectional buck-boost converters, the nanogrid accommodates various bus voltage levels, enhancing device and application compatibility.
- Stable Bus Voltage: Incorporates stability analysis with impedance scanning and Fast Fourier Transform (FFT) analysis.
- Application in ambulance: Capable of supplying uninterrupted power for emergency medical equipment inside an ambulance.

## 1.7 Outline of thesis

A chapter-wise summary of this thesis is outlined below:

Chapter 2: This chapter details the system architecture of the proposed DC nanogrid, including system and operational specifications. It discusses the design process for PV converters optimized for solar power integration, buck converters tailored for specific loads, and bidirectional converters designed for seamless battery integration. It also introduces the proposed energy management system and using MATLAB Simulink, this chapter simulates the designed system and presents simulation results under varying irradiance conditions and fluctuating loads.

Chapter 3: This chapter explores the stability analysis of DC nanogrids using impedance scanning method and FFT analysis.

Chapter 4: This chapter focuses on the hardware design of nanogrid and provides experimental results validating their performance. Additionally, it discusses the development of user interfaces and GUIs for system monitoring, presents integration and commissioning procedures, and reports experimental results demonstrating system functionality.

Chapter 5: This chapter identifies typical emergency lifesaving instruments found in an ambulance or a mini clinic and plans load integration and wiring strategies. It estimates and schedules loads for optimized operation, sizes PV arrays and batteries based on

ambulance-specific requirements, documents PV system and battery installation processes in ambulances, and simulates PV and battery operations under varying load conditions relevant to ambulance usage.

Chapter 6: Summarizing key findings and conclusions drawn from the research, this chapter highlights contributions made and proposes future research directions and enhancements for DC nanogrid applications. It concludes with insights into the broader impact and potential applications of the research.

## Chapter 2

### 2 Methodology

Techno-economic advances in photovoltaic (PV) technology have enabled solar PV stand-alone nanogrid to power individual devices using device-specific architectures. To reduce costs and increase accessibility for a wider range of people, a modular open-source system is needed to cover all applications at once. This chapter introduces a modular PV-powered nanogrid system, consisting of a do-it-yourself (DIY) PV system with batteries to allow for off-grid power. The resultant open-source modular DC nanogrid can deliver DC power to loads of different voltage levels, which is possible because of the efficient and parametric energy management system (EMS) that selects modes of operation for the grid based on DC bus voltage and state of charge of batteries. Simulation results are found using MATLAB/Simulink, verify the coordination between the EMS and the PV-battery system under varying PV power generation and load conditions. This EMS has the potential to enable easy personalization of a vast area of applications and expand appropriate technology for isolated communities.

#### 2.1 Introduction

The United Nations has stressed the critical importance of modern energy services access through its Sustainable Development Goal (SDG) 7, which seeks to provide access to affordable, reliable, and sustainable modern energy for all people on earth [47]. The world has made some progress on this front, as the number of people without access to electricity declined from 1.2 billion in 2010 to 759 million in 2019 [48]. These numbers, however, can be misleading as Ayaburi et al., estimate that 3.5 billion people lack “reasonably reliable” access to electricity services [49]. Extending the electric grid is costly [50], [51] and even providing full power with PV and backup to a building can be cost prohibitive despite the clear benefits that it brings [52]. Recent decreases in PV costs [53], [54] offer economically viable power for a range of contexts [55], [56], but high initial investment requirements (particularly for electrical storage that still must decrease for widespread adoption [57]) and technical complexity created barriers to adoption for most consumers.

The potential for providing device specific power is a way that can expand reasonably reliable electricity services to billions of people.

Although the initial idea of the nanogrid was for supplying power to individual homes [23], advancements in solar photovoltaic (PV) technology have expanded its applications. Stand-alone nanogrids are now also used to power individual devices, such as in on-site solar-powered LED street light projects, where PV modules are mounted on poles , with batteries and controllers equipped in a box [58], [59]. Solar-powered electric vehicle (EV) chargers with distinguished architectures have been developed [60], [61]. Solar PV and solar thermal collector-based complete water desalination systems [62], and solar-powered air conditioning, refrigeration, and water cooling [63], [64] have been proposed. Similarly, solar irrigation systems have been designed to supply PV-generated power to single-phase motor/pump [65], [66]. Some similar developments are solar-powered cellular base stations [67], and solar-powered extruders [68] and 3-D printers [69], [70]. These single-device solutions introduced new architectures for each device, rather than a single modular parametric solution that could work for all devices. Consequently, they were unable to leverage the scale of PV production, resulting in higher costs. Furthermore, these examples suggest that most of these loads or devices operate on DC, but their PV solutions involve unnecessary conversion from DC to AC and then back from AC to DC. To reduce costs and increase accessibility for a wider range of people, a modular open-source system is needed to cover all applications at once.

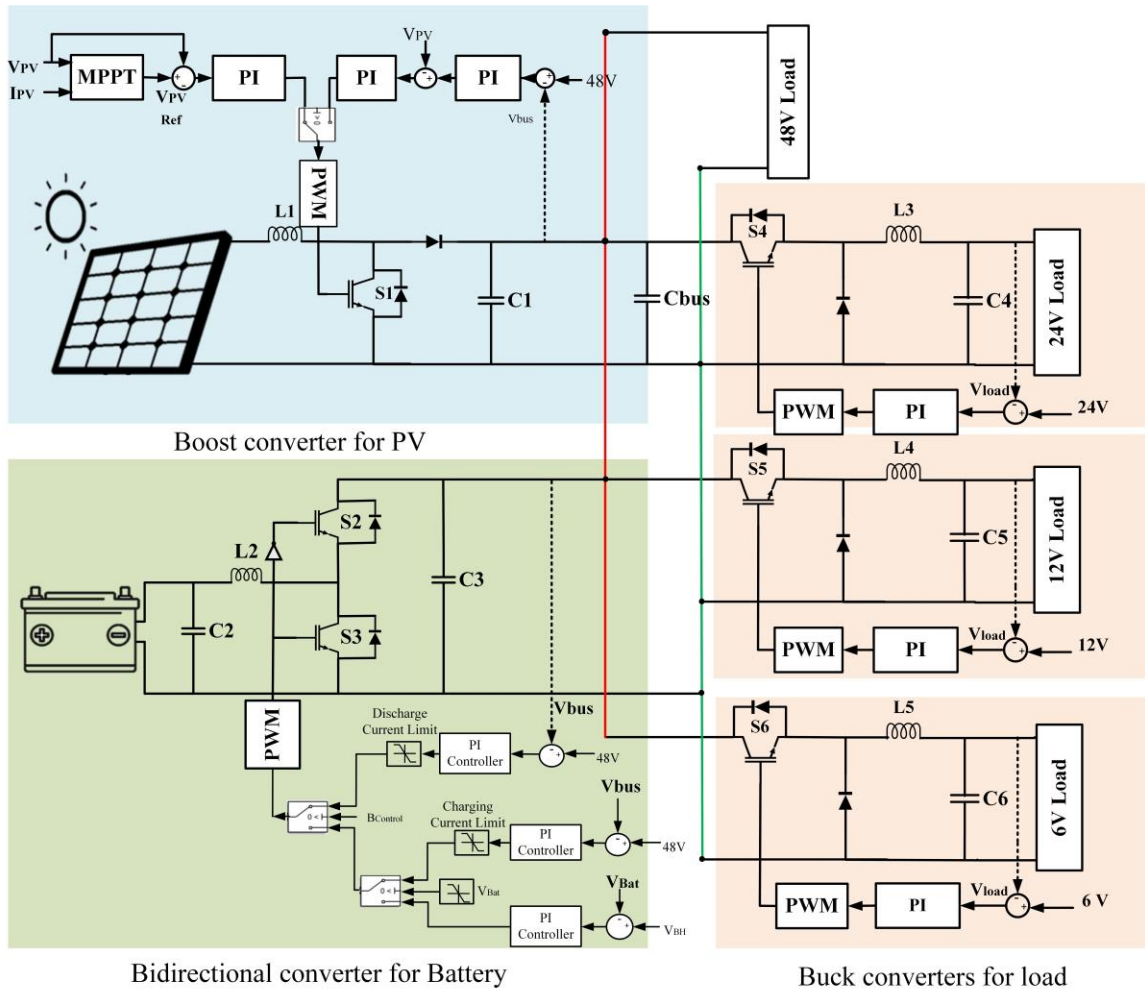


**Figure 2.1** Architecture of DC nanogrid

To do this, this research introduces a modular PV-powered nanogrid system [71] with batteries to efficiently deliver DC power to loads operating at various voltage levels. It is licensed open source under GNU GPLv3 and CERN OHL-S v2. The novelty of this work is the energy management system (EMS), which employs parametric controls and selects optimal operating modes for the grid based on the DC bus voltage and battery state of charge (SOC). This setup enables the PV converter, bidirectional battery charging converter, and load converter to operate independently, following commands issued by the central EMS. These units will be interconnected in a modular fashion to a common DC bus, enhancing the overall robustness and flexibility of the solution. Additionally, this arrangement can facilitate the implementation of various charging and MPPT (maximum

power point tracking) algorithms easily. This open-source EMS design can serve as a versatile and customizable solution for both current and future solar-powered individual devices. The chapter is structured as follows: Section 2.2 presents a concise elucidation of the configuration and EMS of the DC nanogrid. Section 2.3 outlines the design procedure of the controllers and their specifications. Section 2.4 encompasses the time domain simulation for three distinct scenarios.

## 2.2 Methods

### 2.2.1 System Architecture:

In the nanogrid architecture (Figure 2.1), a 2kW boost converter is used to interface the PV system with the DC bus. On the other side, a bidirectional buck-boost converter of 5kW and three buck converters (total 1.6kW) connect respectively a lithium-ion (li-ion) battery and loads of different voltage levels to the grid [72], [73].

In choosing the appropriate DC bus voltage for DC nanogrid, some consideration has been made to ensure user safety, efficiency, and cost savings. Among different bus voltage levels, 48V voltage level is found to be the best choice for the nanogrid in terms of cost and performance [74]. The nanogrid is also modelled in such a way that the generation can easily be scaled up by connecting additional PV modules and their interface converters with the bus. Similarly, additional batteries can be introduced with a bidirectional converter to support any expansion of loads or storage requirements. The centralized control by the energy management system (EMS) can accommodate any variation in DC load and weather conditions. Thus, this research introduces the modular and adaptive architecture of a PV system with free and open source control system [75]. However, it is crucial to ensure that the cumulative ratings of the solar panels, batteries, and loads do not surpass the originally specified power limits of the nano-grid. The source code for this project is released under GNU GPL v3[76]. Where all cases slated for investigation in this literature are included in Simulink file format. Open source development allows for rapid innovation [77], [78] and has been called for in the PV sector [79]. Additionally, the nanogrid variants can be used to power specific devices and solar powering of open source appropriate technology (OSAT) [80].

### 2.2.2 Energy Management System (EMS):

Previously, the power management systems used in nanogrid operate based on the battery voltage [81], while the DC bus voltage is used as an information carrier for mode selection [82], [83]. Other PV and battery parameters such as PV output power, SOC and power limit of the battery, DC loads, and the load demands are also used by the power management systems to decide the operation modes of the system [84]. In this EMS, decisions are made based on DC bus voltage and SOC of battery.

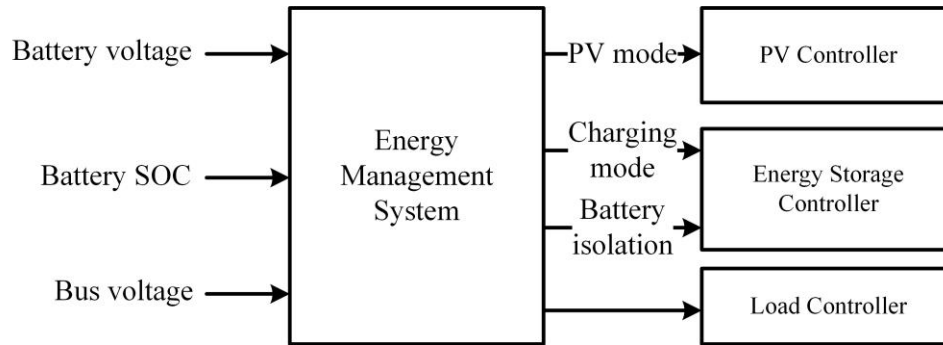


**Figure 2.2** Block diagram of control system

Usually, a DC nanogrid has three different operation modes: 1) power surplus, 2) deficit and 3) battery isolation, based on the instructions given by the EMS [85]. In addition, the EMS coordinately controls [86] all the interface controllers in a centralized manner by providing three different output signals: 1) battery charging/discharging signal, 2) battery isolation signal, and 3) PV converter control signal as shown in Figure 2.2. The upper limit of bus voltage for the surplus mode is selected to be  $48+10\%$  (52.8V) and the lower limit for deficit mode is  $48-10\%$  (43.2V). Finally, the decision on idle mode (isolation of battery) is made on the upper and lower limit of SOC of battery [87]. The depth of discharge for battery has been chosen to be 60% [88], [89] and based on that the lower limit of SoC is 35% and upper limit of 95% is selected. The EMS generates all control signals based on the algorithm depicted in Figure 2.3. The entire system is simulated using SIMULINK, and the EMS algorithm is implemented as a MATLAB function.

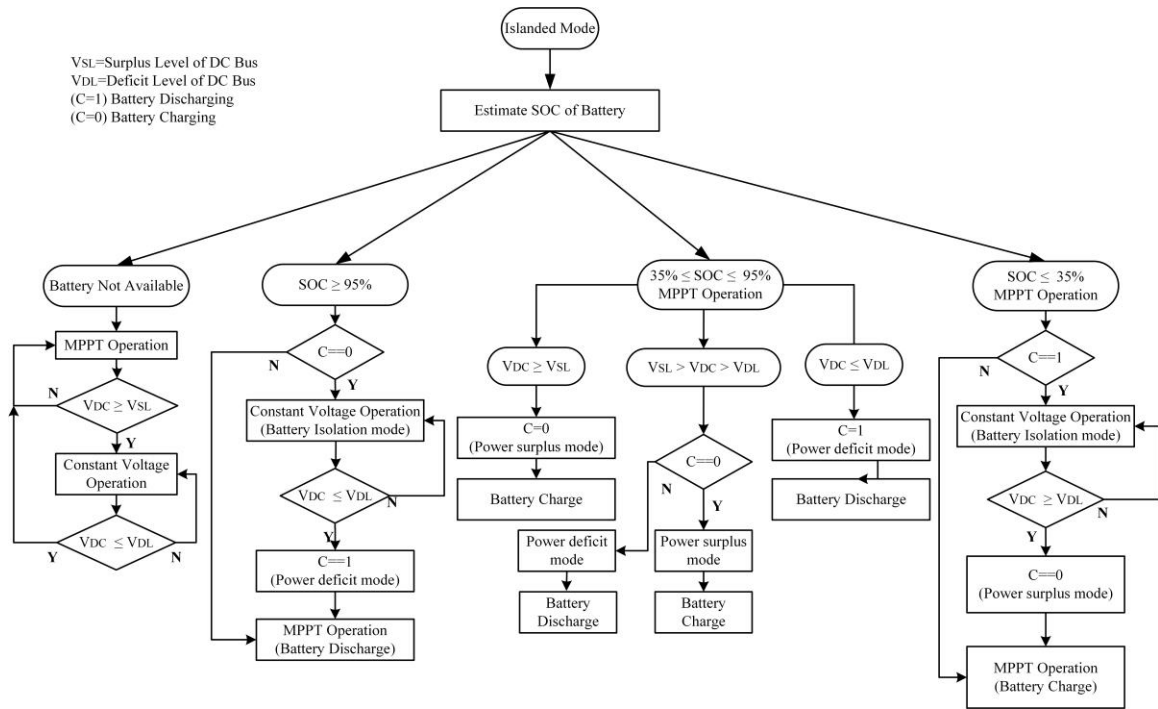


**Figure 2.3** EMS algorithm

## 2.3 Controller design

### 2.3.1 PV Array Converter & Controller:

PV arrays are connected to a boost converter which operates on two modes: MPPT mode and bus control mode. In bus control mode where PV is radially connected to the DC load without battery (isolated), the bus voltage is regulated by the boost converter. The controller in Figure 2.4 (a) is designed for this mode and has a closed PI loop. The PI loop regulates the DC bus voltage and minimizes the transients during load change.

**Table 2.1** Controller parameters of boost converter

Parameter	Boost Converter
Max load power	2,000 W
Input voltage ( $V_S$ )	30 V
Output voltage ( $V_{bus}$ )	48 V
Inductance (L)	$L_1=30 \mu\text{H}$
Output capacitor ( $C_{out}$ )	$C_1= 680 \mu\text{F}$
Proportional gain ( $K_p$ )	0.05
Integral gain ( $K_i$ )	7.5

In MPPT mode, the controller in Figure 2.4 (b) uses MPPT alongside PI controller to maintain the PV arrays at  $V_{MPP}$  to extract the maximum power from the PV array. Various MPPT methods have been introduced in the literature, including particle swarm optimization (PSO) technique [90] and incremental conductance algorithm [91]. These MPPT methods can be categorized into four groups: conventional, intelligent, optimization, and hybrid techniques [92]. Among the conventional MPPT methods, the variable step size incremental conductance MPPT algorithm automatically adjusts the step size to improve MPPT speed and accuracy. The step size is determined based on the derivative of power to voltage of the PV array [93]. Conventional methods are less effective under partial shading and have slower response, whereas intelligent, optimization, and hybrid techniques can handle partial shading more effectively [94], [95]. The optimization methods like PSO [96], Firefly Algorithm (FA), and Ant Colony Optimization (ACO) are best for extracting power from PV under partial shading conditions as they are more accurate, but require expensive hardware [97], [98]. Among all these methods, the perturb and observe (P&O) method is the most popular, and widely used, while artificial intelligence-based methods are fast and stable but require digital applications and multiple sensors [99]. A perturb and observe MPPT algorithm [100] has been used to allow the PV to supply maximum power under varying load condition and varying environmental conditions. The algorithm adjusts the reference PV voltage with a smaller step size of 0.01V to track maximum power, while the PI controller ensures that the PV voltage remains at the reference set by the P&O algorithm. For the PV boost converter, the proportional gain ( $K_p$ ) and integral gain ( $K_i$ ) are selected respectively ( $K_p= 0.05$  and  $K_i=7.5$ ) based on the step response closed-loop transfer function of boost converter with phase margin  $90^\circ$  and the gain margin 16.5dB.

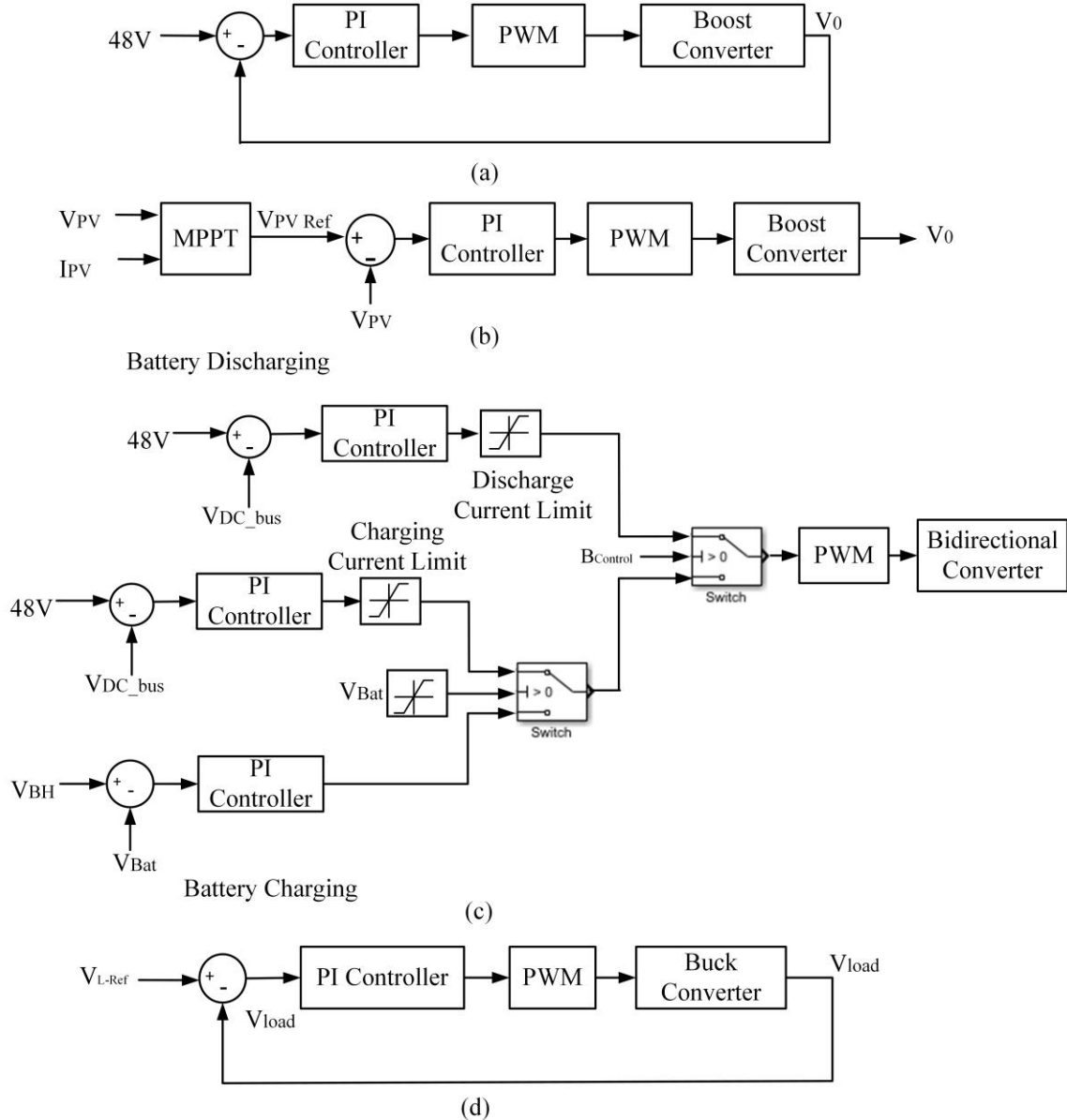


**Figure 2.4** (a) Controller for isolated PV directly connected with DC load. (b) Controller for battery connected PV array. (c) Battery charge controller. (d) Load voltage controller.

### 2.3.2 Customer Load Converter Controller:

Various loads with different voltage levels, such as 48V, 24V, 12V, and 6V, can be connected to the bus bar. Since the bus voltage remains relatively stable at 48V, loads operating at this voltage can be directly connected. However, for loads with other voltage levels, three buck converters equipped with PI controllers (as shown in Figure 2.4 (d)) are

employed. The EMS is responsible for managing load variations and ensuring the stability of both the bus voltage and the load voltages.

To determine the appropriate settings for the load-side buck converters, the proportional gain ( $K_p$ ) and integral gain ( $K_i$ ) are carefully selected based on step response of closed loop transfer function of the converters. And the phase margin and the gain margin for the buck converters 1,2 and 3 are respectively ( $PM=89^\circ$ ,  $GM=26.7$  dB;  $PM=85^\circ$ ,  $GM=20.5$ dB and  $PM=84^\circ$ ,  $GM=21$ dB). Detailed parameters for the buck converters can be found in Table 2.2.

**Table 2.2** Critical parameters of Buck converters

Parameter	Buck Converter 1 (24 V)	Buck Converter 2 (12 V)	Buck Converter 3 (6 V)
Max load power	800 W	600 W	200 W
Input voltage ( $V_s$ )	48	48	48
Output voltage ( $V_0$ )	24	12	6
Nominal duty cycle (d)	50 %	25 %	12.5 %
Inductance (L)	$L_3=60 \mu\text{H}$	$L_4=30 \mu\text{H}$	$L_5=30 \mu\text{H}$
Output capacitor ( $C_{out}$ )	$C_4=220 \mu\text{F}$	$C_5=560 \mu\text{F}$	$C_6=820 \mu\text{F}$
Proportional gain ( $K_p$ )	0.0003	0.001	0.0003
Integral gain ( $K_i$ )	7.962	23.47	15.2

### 2.3.3 Energy Storage System (ESS) Controller:

The battery is tied to the DC nanogrid by a bi-directional buck-boost converter, which can regulate the power flow in either direction. In the power surplus mode, it acts as a buck converter and the battery gets charged and as a boost converter in power deficit mode [101], [102], [103]. In synchronous buck-boost converters, both switches  $S_1$  and  $S_2$  operate alternatively, necessitating complementary gate pulses. The battery charging controller has two independent PI loops for charging and discharging. When the battery control signal is set to logic 1, it facilitates battery charging and current flows from the DC link to the battery direction. In the event of logic 0, it enables battery discharging and current flow from battery to the DC link. The battery discharged only during power deficit mode which is defined by the bus voltage being below 48V, and the discharge current is limited by the maximum discharge current rating of battery which in this case considered 87A. So, during

this power deficit mode, as depicted in Figure 2.4 (c), the controller conducts a comparison between the bus voltage and the reference voltage, initiating battery discharge and the bus voltage raised to 48V. In power surplus mode, the controller initiates battery charging by comparing the battery voltage with the maximum charged voltage ( $V_{BH}$ ), while ensuring that the maximum charging current is limited to 40A through a limiter in the control loop. Considering the battery SOC is below the 95%, the battery voltage will be lower than the maximum charged voltage and the PI controller will compare them would try to charge the battery up to the maximum battery voltage and as soon as the battery SOC becomes beyond 95%, the battery will be isolated from the system. For the bidirectional converter, the proportional gain ( $K_p$ ) and integral gain ( $K_i$ ) along with other parameters are given in Table 2.3 according to the phase margin (PM) and the gain margin (GM) for the charging mode found respectively (PM=  $84^0$ , GM=21dB) and for discharging mode found (PM= $90^0$  and GM=25dB) respectively.

**Table 2.3** Critical parameters of bidirectional buck boost converter

Max load power	5,000 W	5,000 W
Input voltage	$V_{bus} = 48$	$V_{bat} = 24$
Reference voltage	$V_{BH} = 27.93$	$V_{bus} = 48$
Inductance ( $L_2$ )	$L_2 = 120 \mu\text{H}$	$L_2 = 120 \mu\text{H}$
Capacitor	$C_2 = 1000 \mu\text{F}$	$C_3 = 1400 \mu\text{F}$
Proportional gain ( $K_p$ )	0.0005	0.005
Integral gain ( $K_i$ )	2.5	3

## 2.4 Simulation results

To validate the effectiveness of the EMS and nanogrid, three distinct scenarios have been examined: (1) fluctuation in PV generation, (2) variation in load, and (3) battery isolation triggered by overcharge protection or low state of charge (SOC). This section presents time domain simulations of dc bus voltage and power flow for each case. The specifications of PV array and the battery bank under standard test conditions (STC) are given in Table 2.4.

**Table 2.4** Basic Parameters of PV Battery System Under STC

Parameter	Value
PV maximum power ( $P_{PV}^{MPPT}$ )	1532 W
PV maximum power voltage ( $V_{MPPT}$ )	29.3 V
Battery capacity	200 Ah
Battery fully charged voltage ( $V_{BH}$ )	27.94 V
Battery nominal voltage	24 V
Battery maximum charging current	40 A
Nominal discharge current	86.96 A
PV maximum power ( $P_{PV}^{MPPT}$ )	1532 W

### 2.4.1 Case 1: Variation in PV power generation

In this case, the nanogrid operates under varying irradiance conditions, leading to fluctuations in PV generation. Based on the simulation results depicted in Figure 2.5, initially the solar irradiation is set at  $1,000\text{W/m}^2$ , with an ambient temperature of 300K and a maximum PV output of 1,532W. Consequently, all DC loads listed in Table 2.5 are supplied by the PV source, while any excess power is directed towards charging the battery.

**Table 2.5** Constant DC load for case 1

Voltage level	Load
24 V load	576 W
12 V load	344 W
6 V load	80 W
Total	1000 W

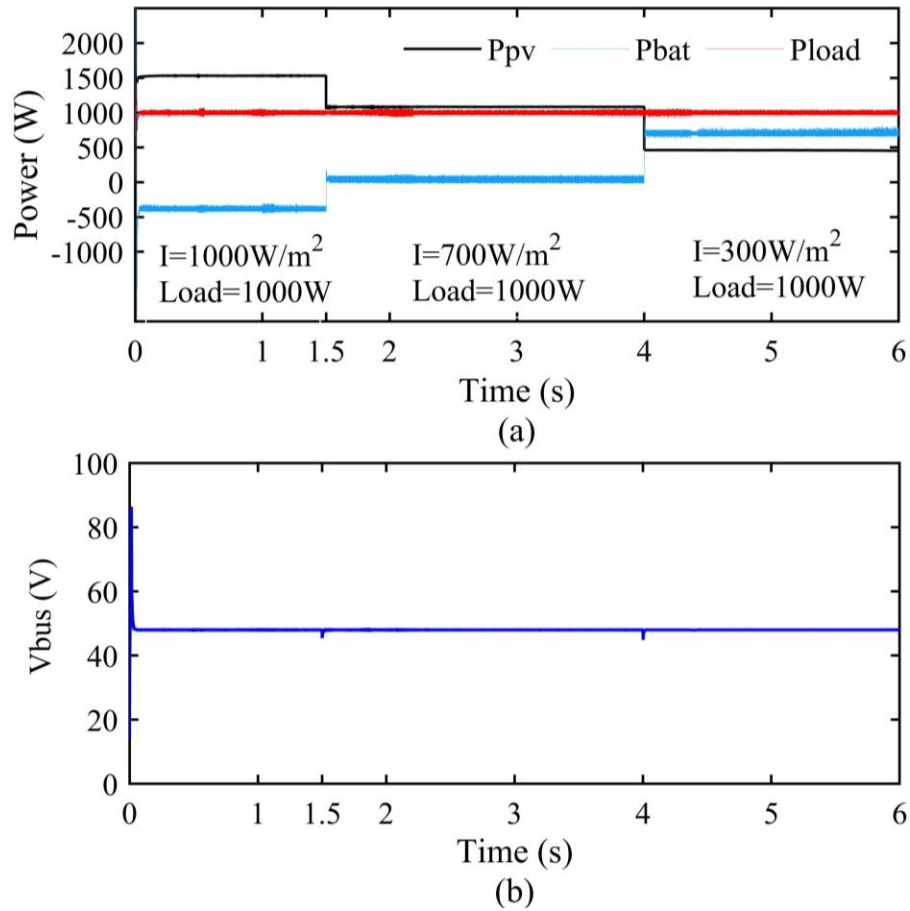


**Figure 2.5** Case 1: PV power variation (a) power flows (PV, ESS and DC load) and (b) DC bus voltage.

At the 1.5 sec, there was a transition in irradiance to  $700\text{ W/m}^2$ , the PV output decreased to 1083 W, yet the system continued to operate with a surplus of power. During this period, the battery was charged with an excess power of 83W. Subsequently, at the 3.5s, the irradiance was further reduced to  $300\text{ W/m}^2$ . The PV power output decreased to 462 W, causing the system to enter a power deficit mode. But the dc bus voltage remained steady at 48V throughout the simulation period.

#### 2.4.2 Case 2: Variation of load

Based on the simulation results at Figure 2.6, the DC bus voltage exhibits stability even as the DC loads fluctuate in accordance with Table 2.6. Throughout the entire simulation, the power generated by the PV source remains constant at 775W, corresponding to an irradiance level of  $500\text{ W/m}^2$ . Initially, the system operates in a power deficit mode since

the load exceeds the PV power. Subsequently, a slight reduction in the loads to 800W at 1.5sec leads to a decrease in the power supplied by the battery. The system, however, continues to remain in a power deficit mode. Finally, at the 4 sec, a significant decrease in the load to 400W shifts the system into power surplus mode, allowing the system to charge the battery with 375W.

**Table 2.6** Variable DC load for case 2

Voltage level	(0-1.5) sec	(1.5-4) sec	(4-6) sec
24 V load	576 W	288 W	192 W
12 V load	144 W	232 W	72 W
6 V load	280 W	280 W	136 W
Total	1000 W	800 W	400 W

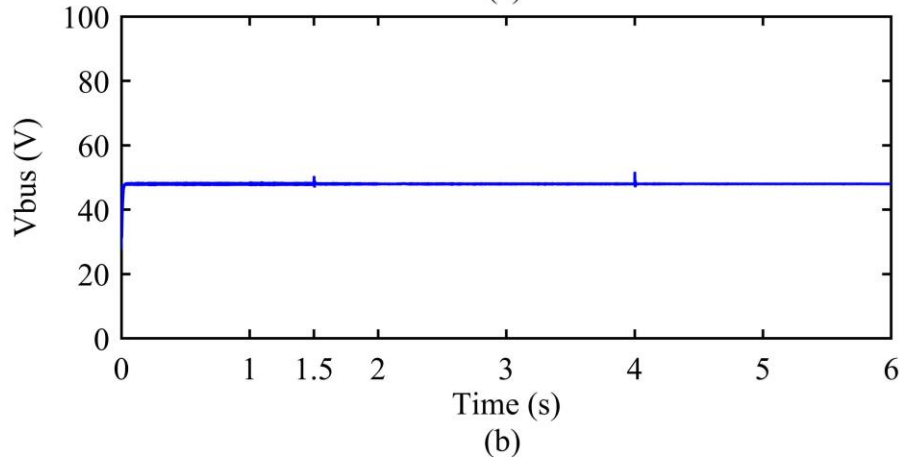
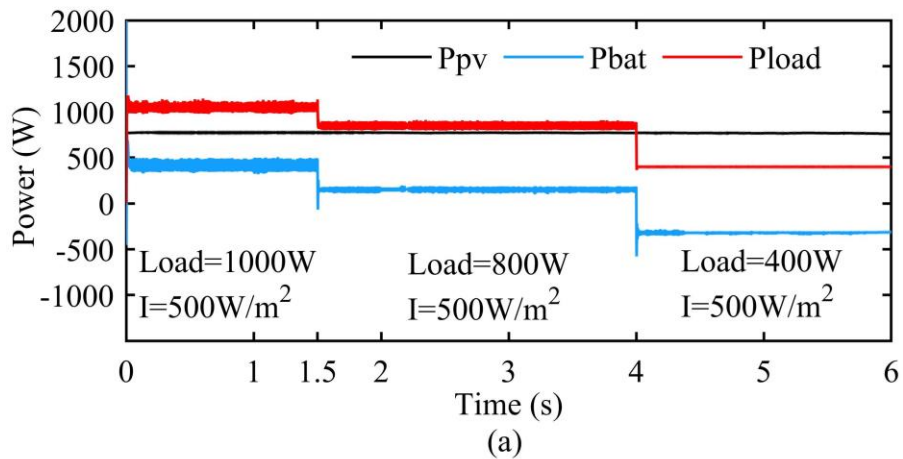


**Figure 2.6** Case 2: PV power variation (a) power flows (PV, ESS and DC load) and (b) DC bus voltage.

### 2.4.3 Case 3: Isolation of Battery

During typical operational conditions, when the battery's state of charge (SOC) remains within the prescribed lower (35%) and upper (95%) limits, the PV array diligently tracks the maximum power point voltage ( $V_{MPP}$ ) as provided by the MPPT algorithm. In power deficit mode, when the SOC drops below 35%, or in power surplus mode, when the SOC exceeds 95%, the EMS isolates the battery from the system until normal power conditions are restored, power surplus (charging mode) for critically discharged batteries and power deficit (discharge mode) for fully charged batteries. In these instances, the PV module operates as an independent power source, ensuring continuous power supply to the loads while maintaining the bus voltage at 48V, provided sufficient solar irradiance is available. If the solar power is insufficient, the bus voltage may drop below 48V, leading to a gradual shutdown of the loads as the voltage reaches critically low levels.

To confirm the isolation condition, the SOC of the battery is set at 94.995% and the system is operating in a power surplus mode ( $P_{pv} > P_{load}$ ). The study considers the parameters outlined in Table 2.7. Figure 2.7 illustrates that the battery becomes isolated from the system as soon as its SOC reaches 95% (at 2.4 seconds). The battery remains in isolation until the system transitions back into power deficit mode ( $P_{pv} < P_{load}$ ) at 4 seconds, triggered by a change in irradiance to  $300\text{W/m}^2$ . Subsequently, the battery initiates discharge.

**Table 2.7** Parameters for case 3

Power mode	Surplus	Isolated	Deficit
Irradiance	$700\text{ W/m}^2$	$700\text{ W/m}^2$	$300\text{ W/m}^2$
$P_{PV}$	1083 W	600 W	462 W
DC load	600 W	600 W	600 W
$P_{BAT}$	-483 W	-	138 W

The time domain simulation effectively demonstrates that the system and EMS consistently maintain the optimal power flow among the PV source, battery, and load across various scenarios. Furthermore, the bus voltage is maintained at 48V. During load and irradiance variations, however, notable fluctuations are observed in the bus voltage, primarily due to the interactions between converters and their resonant frequencies. Hence, in the next

chapter, a comprehensive stability analysis will be conducted to discern the underlying causes and develop alternative controllers to mitigate these transients effectively.

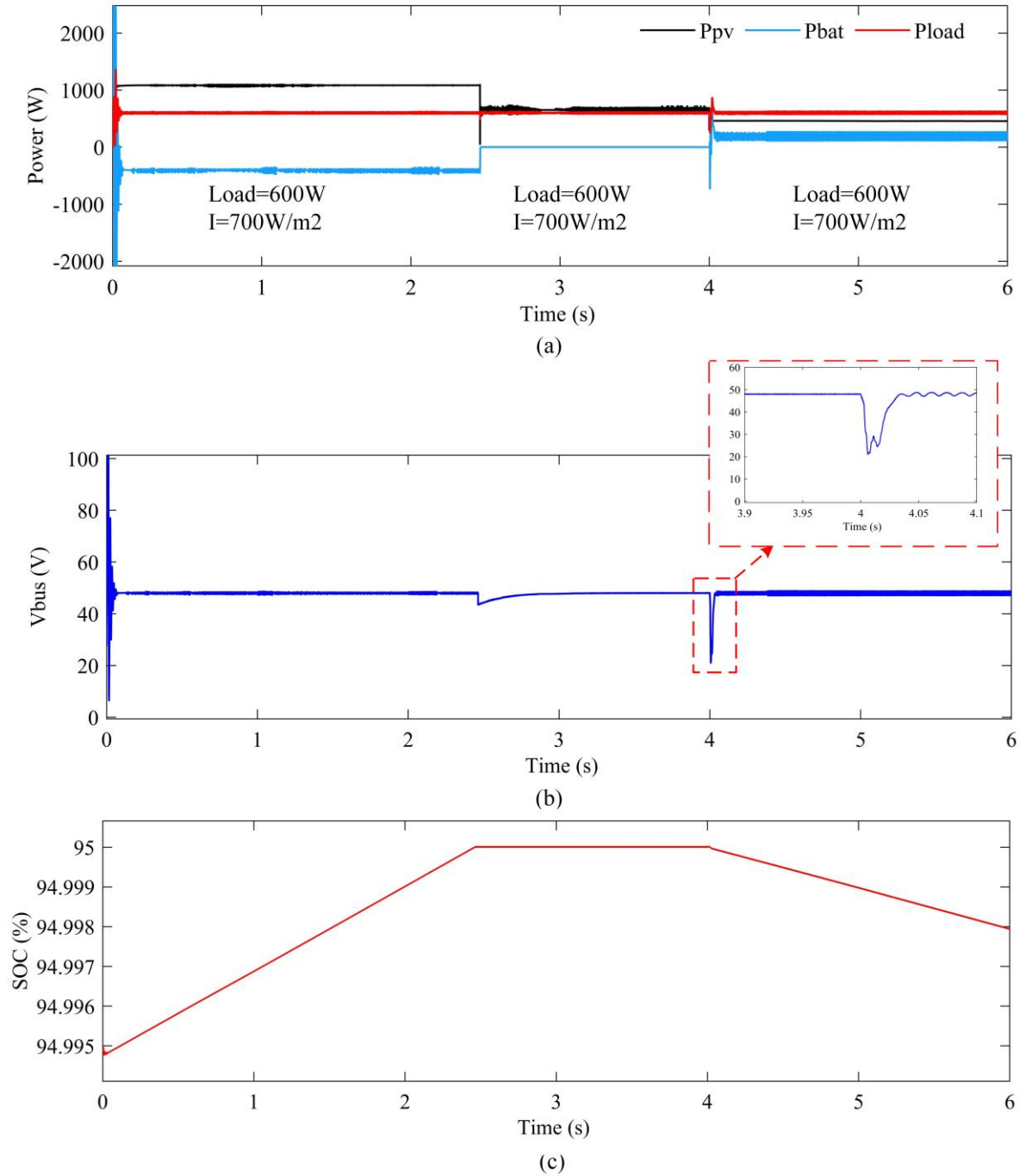


**Figure 2.7** Case 3: Isolation of battery (a) power flows (PV, ESS and DC load), (b) DC bus voltage and (c) SoC of battery.

## Chapter 3

### 3 Stability analysis

To analyze system stability, small signal modeling is necessary. This chapter details the small signal modeling of the DC nanogrid system, enabling comprehensive stability analysis of the bus voltage under disturbances using impedance scanning and Fast Fourier Transform (FFT), leading to the development of an LQR (Linear Quadratic Regulator) controller as a replacement for the conventional PI (Proportional Integral) controllers for better transient stability of the system.

#### 3.1 Small signal modelling of converters

For designing the controllers for the converters and understanding the transients and stability of the overall system, it is essential to grasp the dynamic behavior of the converters. This requires small signal modeling or mathematical modeling of each converter. Different modeling techniques exist for converters, as traditional modeling methods are unsuitable due to the presence of switches.

Small signal modeling of power converters involves various methods to analyze and design control systems, ensuring stability and dynamic performance. Common techniques include State-Space Averaging (SSA) for linearizing state-space equations, Averaged Switch Model (ASM) for focusing on average behavior, PWM Switch Model for duty cycle-output relationships, and Discrete-Time Modeling for digital control systems. Circuit Averaging simplifies analysis by averaging inductor currents and capacitor voltages, while Phasor Transformations analyze sinusoidal perturbations in the frequency domain.[104]

Appropriate method is chosen based on specific analysis needs and converter types. For understanding the different converter topologies used in this research and figuring out the relationships between them, circuit averaging techniques have been utilized for small signal modeling of the converters. This approach will be discussed in detail for each converter separately.

### 3.1.1 Boost converter's transfer function and input/output impedance derivation

The small signal ac equivalent circuit model of the boost converter as shown in Figure 3.1 (b), which is equivalent model of boost converter shown in Figure 3.1(a). The duty cycle ( $d(s)$ ) to output voltage ( $V_o(s)$ ) transfer function is derive by setting the source voltage to zero and pushing all the elements to the output side creates an equivalent circuit shown in Figure 3.1(c). And  $D$  is the nominal duty cycle of the boost converter and  $D' = 1 - D$ .

Now the average equivalent circuit has two dependent voltage and current sources, and to determine the transfer function, first the transfer function for circuit with voltage only is determined,

$$\begin{aligned}\frac{V_o(s)}{d(s)} &= \left(\frac{V_0}{D'}\right) \frac{\left(R \parallel \frac{1}{sC}\right)}{\left(R \parallel \frac{1}{sC}\right) + \frac{sL}{D'^2}} \\ &= \left(\frac{V_0}{D'}\right) \left(\frac{\frac{R}{1+sRC}}{\frac{R}{1+sRC} + \frac{sL}{D'^2}}\right) \\ &= \left(\frac{V_0}{D'}\right) \left(\frac{RD'^2}{RD'^2 + s^2RLC + sL}\right)\end{aligned}\tag{3.1}$$

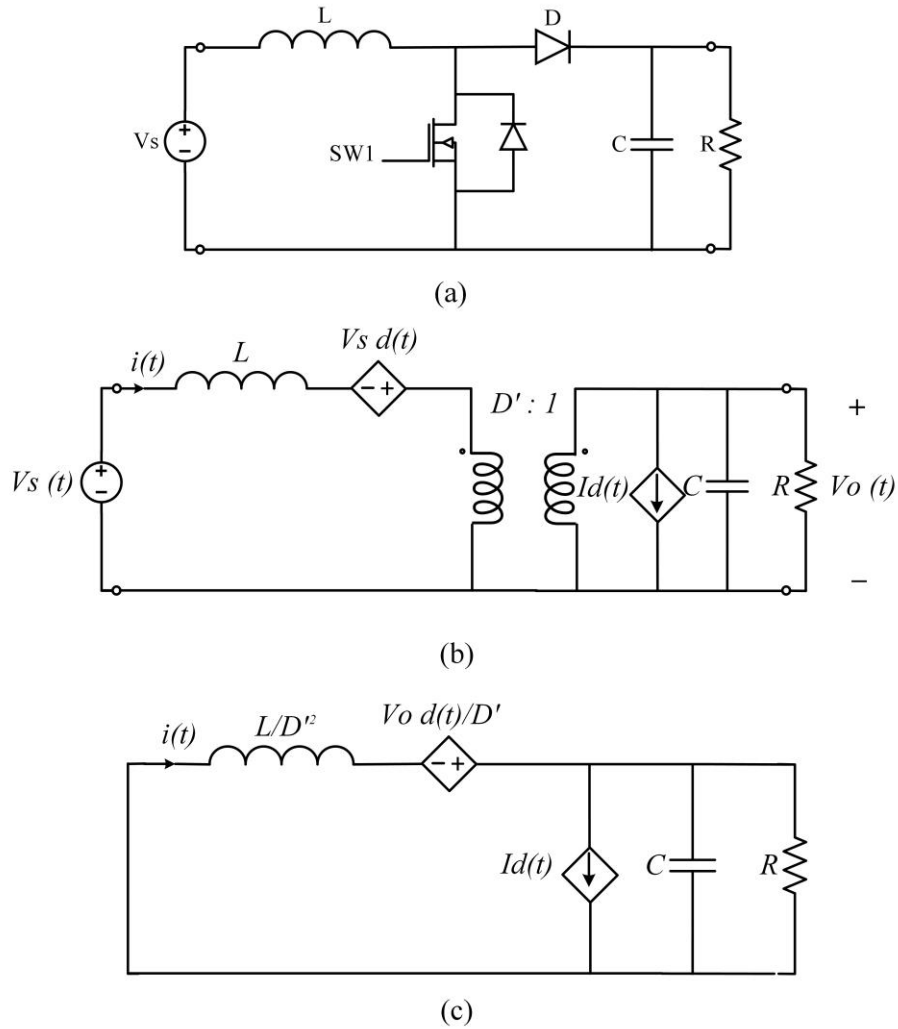


**Figure 3.1** (a) boost converter circuit (b) Small AC signal equivalent circuit model of boost converter, (c) AC signal equivalent circuit model of boost converter from output side

Next the transfer function with current source only is determined,

$$\frac{V_o(s)}{d(s)} = -I \left( \frac{sL}{D'^2} \parallel \frac{1}{sC} \parallel R \right) \quad \text{where, } I = \frac{V_o}{D'R}$$

$$\frac{V_o(s)}{d(s)} = -\frac{V_o}{D'R} \left( \frac{sL}{D'^2} \parallel \frac{1}{sC} \parallel R \right)$$

$$= -\frac{V_o}{D'R} \left( \frac{1}{\frac{D'^2}{sL} + sC + \frac{1}{R}} \right)$$

$$\begin{aligned}
&= -\frac{V_0}{D'R} \left( \frac{1}{\frac{RD'^2 + s^2RLC + sL}{sRL}} \right) \\
&= -\frac{V_0}{D'R} \left( \frac{sRL}{RD'^2 + s^2RLC + sL} \right) \tag{3.2}
\end{aligned}$$

Finally, the overall transfer function of the boost converter is the summation of the two transfer functions found in Equation (3.1) and (3.2) and the final transfer function becomes,

$$\begin{aligned}
\frac{V_0(s)}{d(s)} &= \frac{V_0}{D'} \left( \frac{RD'^2}{RD'^2 + s^2RLC + sL} \right) - \frac{V_0}{D'} \left( \frac{SL}{RD'^2 + s^2RLC + sL} \right) \\
&= \frac{V_0}{D'} \left( \frac{RD'^2 - sL}{RD'^2 + s^2RLC + sL} \right) \\
&= \frac{V_S}{D'^2} \left( \frac{RD'^2 - sL}{RD'^2 + s^2RLC + sL} \right) \tag{3.3}
\end{aligned}$$

After normalizing the transfer function ( $G_c$ ),

$$G_c(s) = \frac{V_S}{D'^2} \left( \frac{1 - \frac{sL}{RD'^2}}{1 + s^2 \frac{LC}{D'^2} + s \frac{L}{RD'^2}} \right) \tag{3.4}$$

From where the zero frequency ( $\omega_z$ ), natural frequency ( $\omega_0$ ) and quality factor ( $Q$ ) can be obtained for boost converter,

$$\omega_z = \frac{RD'^2}{L}, \omega_0 = \frac{D'}{\sqrt{LC}}, \text{ and } Q = RD' \sqrt{\frac{C}{L}} \tag{3.5}$$

Now the equivalent input and output impedance circuit is shown in Figure 3.2 (a)(b):

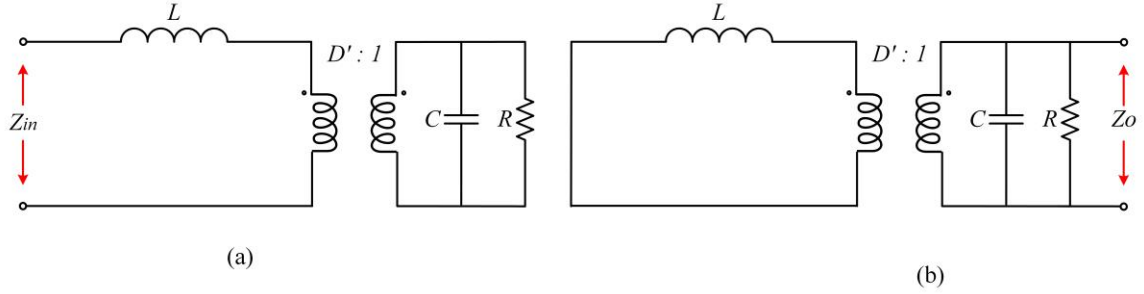


**Figure 3.2** (a) Equivalent input impedance measurement (b) Equivalent output impedance measurement of boost converter

From the equivalent circuit for input impedance ( $Z_{in}$ ) measurement,

$$\begin{aligned}
 Z_{in} &= sL + D'^2 \left( R \parallel \frac{1}{sC} \right) \\
 &= sL + D'^2 \left( \frac{R}{1 + sRC} \right) \\
 &= \frac{s^2LRC + sL + RD'^2}{1 + sRC} \tag{3.6}
 \end{aligned}$$

Output impedance ( $Z_o$ ),

$$\begin{aligned}
 Z_o &= \left( \frac{sL}{D'^2} \parallel R \parallel \frac{1}{sC} \right) \\
 &= \frac{sLR}{s^2LRC + sL + RD'^2} \tag{3.7}
 \end{aligned}$$

### 3.1.2 Buck converter's transfer function and input/output impedance derivation

The small signal ac equivalent circuit model of the buck converter is shown in Figure 3.3 (b) according to the buck converter circuit. And the transfer function of the converter is determined from the output side of the converter, so all the components are pushed toward the output side and then the transfer function is determined.

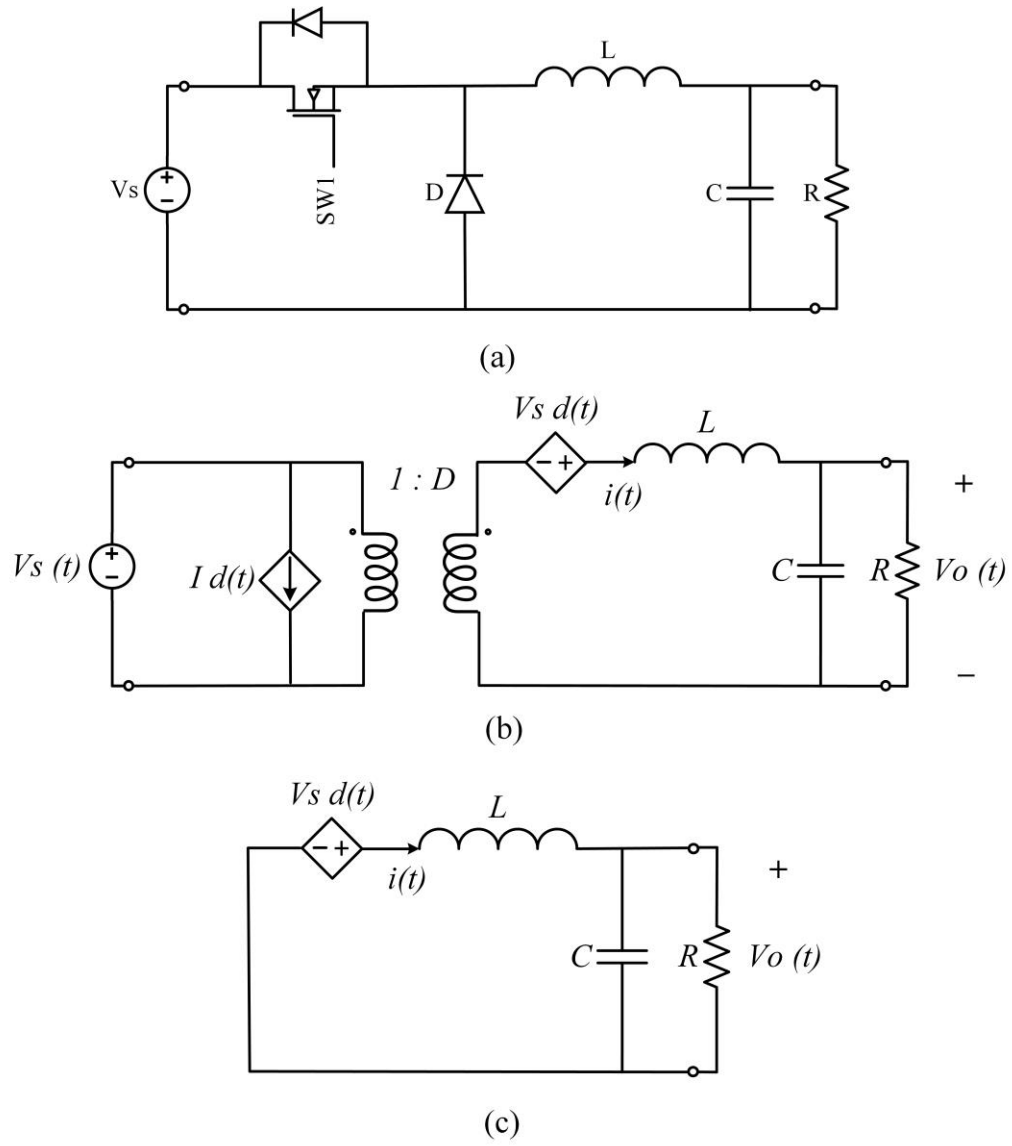


**Figure 3.3** (a) buck converter circuit (b) Small AC signal equivalent circuit model of buck converter, (c) Small AC signal equivalent circuit transferred to output side

Setting the source voltage to zero and pushing all the elements to the output side of the transformer provides the equivalent circuit at Figure 3.3(c). As the equivalent circuit has only one dependent source, so the transfer function is given by,

$$\begin{aligned}
 \frac{V_0(s)}{d(s)} &= \frac{V_s \left( R \parallel \frac{1}{sC} \right)}{\left( R \parallel \frac{1}{sC} \right) + sL} \\
 &= V_s \left( \frac{\frac{R}{1 + sRC}}{\frac{R}{1 + sRC} + sL} \right) \\
 &= V_s \left( \frac{R}{R + s^2RLC + sL} \right) \tag{3.8}
 \end{aligned}$$

This can be expressed in the normalized form

$$G_c(s) = V_s \left( \frac{1}{1 + s^2LC + s\frac{L}{R}} \right) \tag{3.9}$$

From where the natural frequency ( $\omega_0$ ) and quality factor ( $Q$ ) can be obtained for buck converter,

$$\omega_0 = \frac{1}{\sqrt{LC}}, \quad Q = R\sqrt{\frac{C}{L}} \tag{3.10}$$

Now to calculate the input and output impedance of the converter, the equivalent input and output impedance circuit is shown in Figure 3.4 (a)(b).

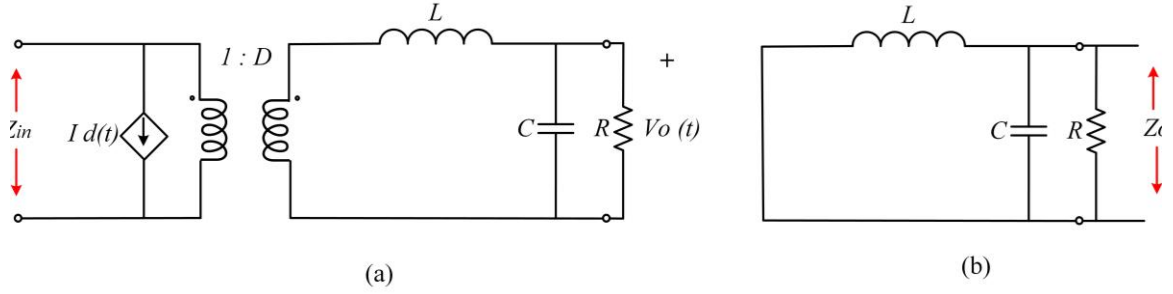


**Figure 3.4** (a) Equivalent input impedance measurement (b) Equivalent output impedance measurement of buck converter

The input impedance is calculated of the buck converter is,

$$\begin{aligned}
 Z_{in} &= \frac{1}{D^2} \left( sL + \left( R \parallel \frac{1}{sC} \right) \right) \\
 &= \frac{1}{D^2} \left( sL + \left( \frac{R}{1 + sRC} \right) \right) \\
 &= \frac{1}{D^2} \left( \frac{s^2LRC + sL + R}{1 + sRC} \right) \tag{3.11}
 \end{aligned}$$

And the output impedance is,

$$\begin{aligned}
 Z_o &= \left( sL \parallel R \parallel \frac{1}{sC} \right) \\
 &= \frac{sLR}{s^2LRC + sL + R} \tag{3.12}
 \end{aligned}$$

### 3.1.3 Bidirectional converter's transfer function and input/output impedance derivation

A bidirectional converter combines the operation of both buck and boost converters. When the battery is charging, the converter operates in buck mode; when the battery discharges, it acts in boost mode. The transfer function and the input-output impedance for the bidirectional converter will be like those of the buck converter and boost converter,

depending on the mode of operation. These parameters, already determined in the previous sections, can thus be calculated as follows.

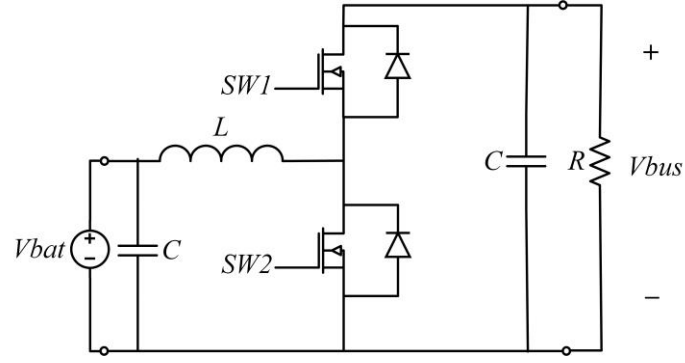


**Figure 3.5** Bidirectional converter circuit

i) In buck mode:

$$G_c(s) = V_S \left( \frac{1}{1 + s^2 L_2 C_2 + s \frac{L_2}{R_{bat}}} \right) \quad (3.13)$$

$$G_c(s) = V_S \left( \frac{1}{1 + s^2 L_2 C_2 + s \frac{L_2}{R_{bat}}} \right) \quad (3.14)$$

$$Z_o = \frac{s L_2 R_{bat}}{s^2 L_2 R_{bat} C_2 + s L_2 + R_{bat}} \quad (3.15)$$

ii) In boost mode:

$$G_c(s) = \frac{V_S}{D'^2} \left( \frac{1 - \frac{s L_2}{R D'^2}}{1 + s^2 \frac{L_2 C_3}{D'^2} + s \frac{L_2}{R D'^2}} \right) \quad (3.16)$$

$$Z_{in} = \frac{s^2 L_2 R C_3 + s L_2 + R D'^2}{1 + s R C_3} \quad (3.17)$$

$$Z_o = \frac{sL_2R}{s^2L_2RC_3 + sL_2 + RD'^2} \quad (3.18)$$

## 3.2 Bus voltage stability analysis

In the time domain simulation, fluctuations in the bus voltage were noted when alterations occurred in the load and irradiance. In this section both impedance scanning and FFT analysis will be utilized to evaluate the stability of the DC nanogrid system and ascertain the reasons behind these voltage fluctuations.

### 3.2.1 Impedance scanning

The impedance scanning has been used extensively with the Nyquist Plot to analyze the small signal stability of interconnected systems [105]. This method serves as a valuable tool for assessing the stability of converter-based interconnected systems, enabling the identification of harmonics originating from both sources and load converters. Moreover, it conducts a comprehensive analysis of the entire system by considering the input-output characteristics (impedance) of each subsystem [106]. One drawback of impedance scanning is that it requires investigating stability at different subsystem interfaces. To address this, the overall nanogrid system is first split into two portions: source side impedance  $Z_S$  and load side impedance  $Z_L$ . In accordance with Nyquist theory, Small Signal Stability (SSS) can be determined by the ratio of  $\frac{Z_S}{Z_L}$ . The system is stable if the Nyquist plot of  $\frac{Z_S}{Z_L}$  curve doesn't encircle (-1,0) point in the negative plane [107], [108]. To obstruct the circle and insure the small signal stability, it is suggested that the source impedance should be much smaller than the load impedance of the converter within all frequency ranges, i.e.,  $|Z_S| \ll |Z_L|$  [109].

In the nanogrid, when the PV and battery are connected to the system and contribute to serving the load, the input side impedance should be the sum of the PV boost converter and the boost mode of the battery converter. The closed-loop output impedance of the boost converter can be expressed as follows:

$$Z_{ocl}(s) = \frac{Z_o(s)}{1 + T(s)} \quad (3.19)$$

Where the open loop output impedance of PV boost converter and boost mode of bidirectional converter (battery discharging mode) is,

$$Z_o = \frac{sLR}{s^2LRC + sL + RD'^2} \quad (3.20)$$

And the loop gains T(s) of the boost converter with PI controller is,

$$T(s) = \left( K_p + \frac{K_i}{s} \right) \times \frac{V_S}{D'^2} \left( \frac{1 - \frac{sL_2}{RD'^2}}{1 + s^2 \frac{L_2 C_3}{D'^2} + s \frac{L_2}{RD'^2}} \right) \quad (3.21)$$

And since the source converters are connected in parallel so the total impedance ( $Z_{tsource}$ ) can be written as the following:

$$Z_{tsource} = \frac{Z_{ocl1} \times Z_{ocl2}}{Z_{ocl1} + Z_{ocl2}} \quad (3.22)$$

On the other hand, the load side consists of three different buck converters serving different voltage level loads. Thus, the output side impedance is the sum of the impedances of all the buck converters. The closed-loop input impedance ( $Z_{icl}(s)$ ) of the buck converter can be expressed as follows [110],

$$Z_{icl}(s) = \frac{Z_i(s) \times R_2 \times (1 + T(s))}{R_2 - D^2 \times T(s) \times Z_i(s)} \quad (3.23)$$

Where the open loop input impedance of buck converter and buck mode of the bidirectional converter (battery charging mode) is,

$$Z_i = \frac{1}{D^2} \left( \frac{s^2LRC + sL + R}{1 + sRC} \right) \quad (3.24)$$

The loop gains  $T(s)$  of the buck converter with PI controller is,

$$T(s) = \left( K_p + \frac{K_i}{s} \right) \times V_s \left( \frac{1}{1 + s^2 LC + s \frac{L}{R}} \right) \quad (3.25)$$

And since the source converters are connected in parallel so the total impedance ( $Z_{tload}$ ) can be written as the following,

$$Z_{tload} = \frac{Z_{icl1} \times Z_{icl2} \times Z_{icl3}}{Z_{icl1} \times Z_{icl2} + Z_{icl2} \times Z_{icl3} + Z_{icl3} \times Z_{icl1}} \quad (3.26)$$

Eventually the total DC bus impedance ( $Z_{bus}$ ) can be expressed as follows,

$$Z_{bus} = \frac{Z_{tsource} \times Z_{tload}}{Z_{tsource} + Z_{tload}} \quad (3.27)$$

The frequency response of the source impedance, load impedance, and total DC bus impedance is analyzed by partitioning the total impedance of the system into output and input impedance elements. The Nyquist plot of the source-to-load impedance ratio is then employed to evaluate the system's stability. Figure 3.6 presents the Nyquist plot as a function of frequency, demonstrating a significant separation from the  $(-1,0)$  point. Consequently, it is evident that the system can be deemed stable.

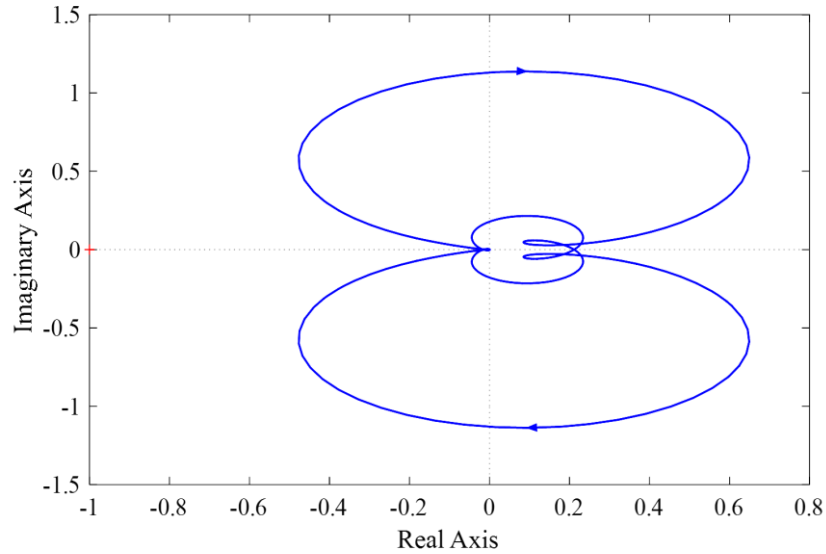
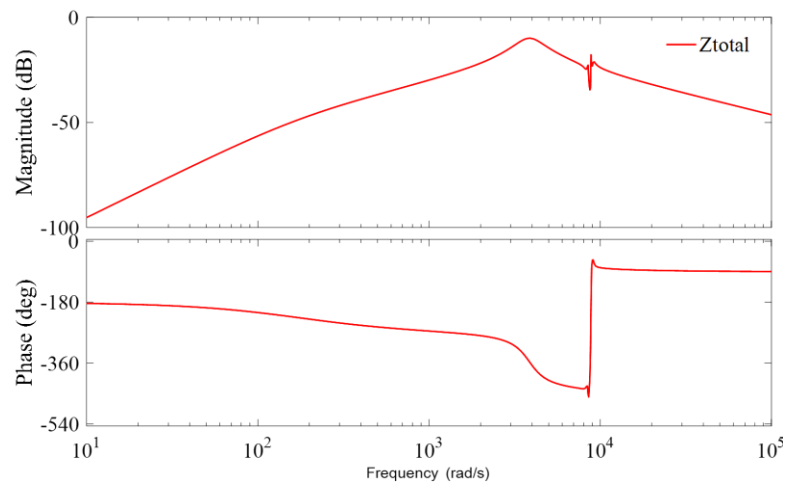
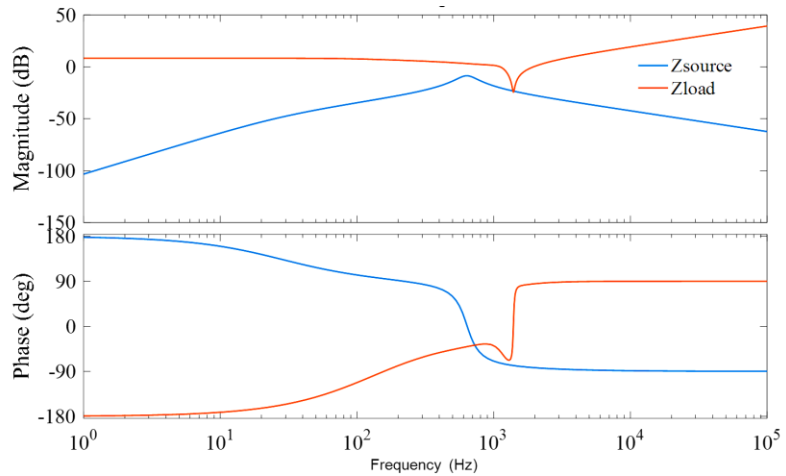


**Figure 3.6** Nyquist plot of total output impedance and input impedance

Moreover, upon examining the Bode plot of both the input and output impedance, it is evident that the magnitude of the source side output impedance consistently remains lower than that of the load side input impedance. This characteristic ensures the stability of the DC nanogrid across a wide frequency range. Analyzing the frequency response of the overall bus voltage in Figure 3.7 (b) reveals that the frequency mode responsible for the observed oscillation is 580Hz and 1300 Hz, closely aligning with the resonance frequency of the boost and bidirectional converter. Excluding these resonance peaks, however, results in the overall magnitude of the impedance response remaining within acceptable limits.



(a)



(b)

**Figure 3.7** (a) Bode plot of total output impedance and total input load impedance (b)

Bode plot of the total DC bus impedance.

### 3.2.2 Fast Fourier Transform (FFT) Analysis

From impedance analysis it is evident that oscillations are likely attributed to the interaction among the DC converters on the source side, as their resonance frequency is closer to the disturbance frequency range. It is, however, not possible to identify the exact source of disturbance from the impedance scanning. Thus, to identify the exact source of the oscillation, a Fast Fourier Transform (FFT) analysis is conducted [111]. Initially, an AC source with a frequency of 580 Hz and amplitude of 500mV is introduced to the source side of the boost converter. Subsequently, the DC bus voltage undergoes FFT analysis. The results of the FFT analysis indicate that the peak of the oscillation aligns closely with the frequency of the applied AC disturbance, confirming that the source converter is responsible for the oscillation in the DC bus voltage, specifically contributing to the 580 Hz oscillation on the bus.

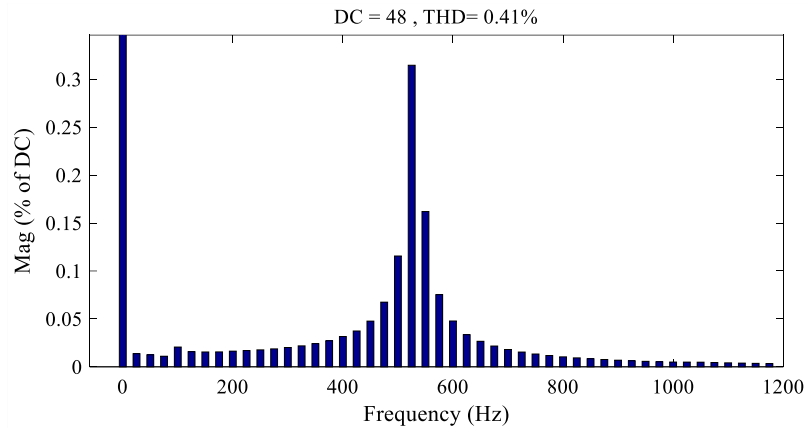


**Figure 3.8** FFT analysis of the bus voltage under the disturbance on the boost converter's input side.

### 3.3 LQR controller design and performance

As mentioned in the preceding section, both the boost converter and bidirectional converter have been identified as the underlying causes of the transients observed in the bus voltage. To address these oscillations and improve the stability of the DC nanogrid, the application of optimal control techniques is recommended [112]. Various optimal control methods are available, including the Linear Quadratic Regulator (LQR), Linear Quadratic Gaussian

(LQG), and Model Predictive Control (MPC). For this particular study, the LQR control scheme will be employed, allowing for the control of the boost converter [113]. This control technique is different from conventional PI controller and requires small signal state space modelling of the converter to design the controller.

### 3.3.1 LQR controller design:

The boost converter can be represented by the following two equations in state space modelling.

$$\dot{x} = Ax + Bu \quad (3.28)$$

$$y = Cx + Du \quad (3.29)$$

where input and output matrix are considered as,

$$x = \begin{bmatrix} i_L \\ v_o \end{bmatrix} \text{ and } u = [d]$$

Using small signal modelling technique and after averaging and linearizing the state equations of the boost converter can be found,

$$\dot{x} = \begin{bmatrix} 0 & -\frac{(1-D_1)}{L} \\ \frac{(1-D_1)}{C} & -\frac{1}{R \times C} \end{bmatrix} x + \begin{bmatrix} \frac{V_{in}}{L \times (1-D_1)} \\ -\frac{V_{in}}{R \times C \times (1-D_1)^2} \end{bmatrix} u \quad (3.30)$$

$$y = [0 \quad 1] x + [0] u \quad (3.31)$$

A controller is designed that produces optimal responses of the closed loop system, in the sense of minimizing a performance index or cost function J which can be defined as,

$$J = \int_0^{\infty} (x^T Q x + u^T R u) dt \quad (3.32)$$

where Q is the state weighting matrix and R is the control weighting matrix. The control signal is defined as

$$u = -Kx \quad (3.33)$$

The LQR controller gain matrix  $K$  must be determined in such a way that it enhances the performance of the system while minimizing a cost function  $J$ . The block diagram of the LQR controller is shown in Figure 3.9.

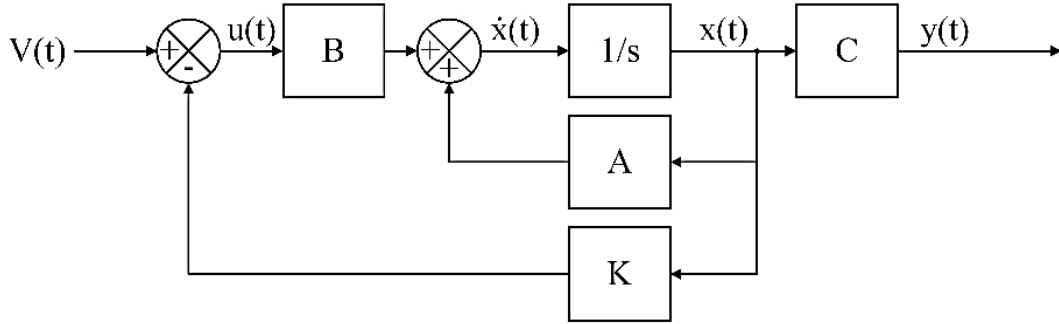


**Figure 3.9** Block diagram of the LQR controller

With  $K$  being the LQR gain matrix, which is given by,

$$K = R^{-1}B^T P \quad (3.34)$$

where  $P$  is the unique positive definite solution of the algebraic Riccati equation (ARE).

$$A^T P + PA - PBR^{-1}B^T P + Q = 0 \quad (3.35)$$

By selecting a proper  $Q$  and  $R$  the LQR gain matrix can be obtained. However, the conventional LQR controller lacks an integral component, and since the boost converter itself does not possess an integrator, it is not possible to achieve a steady-state error of zero solely through state feedback control. To address this limitation, an extended version of the LQR controller is employed, incorporating an integrator. The error between the desired output and the actual output is fed into an integrator, resulting in the creation of a new state variable denoted as  $\dot{z}$ . This new state variable is then multiplied by the integrator gain, represented as  $K_i$ , and subsequently added to the control input as shown in Figure 3.10 [114].

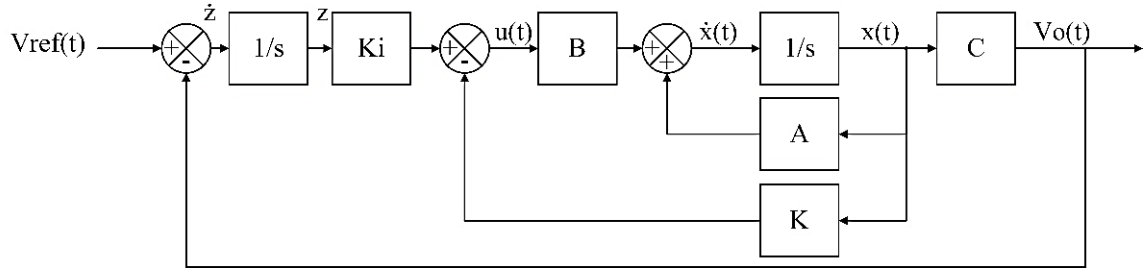


**Figure 3.10** Block diagram of LQR controller with integral action

With the inclusion of integral, the control signal ( $u$ ) becomes,

$$u = K_i z - Kx \text{ and } \dot{z} = V_{ref} - V_o$$

So now the state equation with the integrator becomes,

$$\begin{bmatrix} \dot{x} \\ \dot{z} \end{bmatrix} = A_f \begin{bmatrix} x \\ z \end{bmatrix} + B_f u \quad (3.36)$$

$$y = C_f \begin{bmatrix} x \\ z \end{bmatrix} \quad (3.37)$$

Where,

$$A_f = \begin{bmatrix} A & -BK & BK_i \\ -C & & 0 \end{bmatrix}$$

$$B_f = \begin{bmatrix} 0 \\ 0 \\ 1 \end{bmatrix}$$

$$C_f = [C \quad 0]$$

The gain matrix is determined using MATLAB's (R2023a) LQR function from the Control System Toolbox, which computes the optimal gain matrix ( $K$ ) and the solution ( $S$ ) to the associated algebraic Riccati equation. The resulting gain matrix can be expressed as follows,

$$K_d = [K \quad -K_i] \quad (3.38)$$

Q and R are selected arbitrarily based on the controller response and using the MATLAB command the value of K matrix gain, and integral gain is determined.

$$Q = \begin{bmatrix} 1 & 0 & 0 \\ 0 & 0.1 & 0 \\ 0 & 0 & 100000 \end{bmatrix}$$

$$R = [10]$$

$$K = [0.3190 \quad 0.0301] \text{ and } K_i = 100.0000$$

### 3.3.2 LQR controller performance:

The new state  $\dot{z}$  is found by subtracting the measured output voltage of the boost converter from the reference. And the duty cycle of the boost converter, represented as  $d$ , can be determined based on the control input  $u$  generated by the LQR controller. The duty cycle is fed into a pulse width modulation (PWM) generator to generate the necessary pulses for the switch. Figure 3.11 compares the response of the boost converter under LQR and PI control. To evaluate the transient stability of each controller, a slight change in the input side voltage (from 26V to 30V) was introduced at 0.3 seconds. This comparison highlights their performance and recovery time in maintaining the output voltage at 48V. The results clearly demonstrate that the LQR controller with integral control exhibits superior performance in attaining steady-state conditions at a faster time compared to the PI controller.

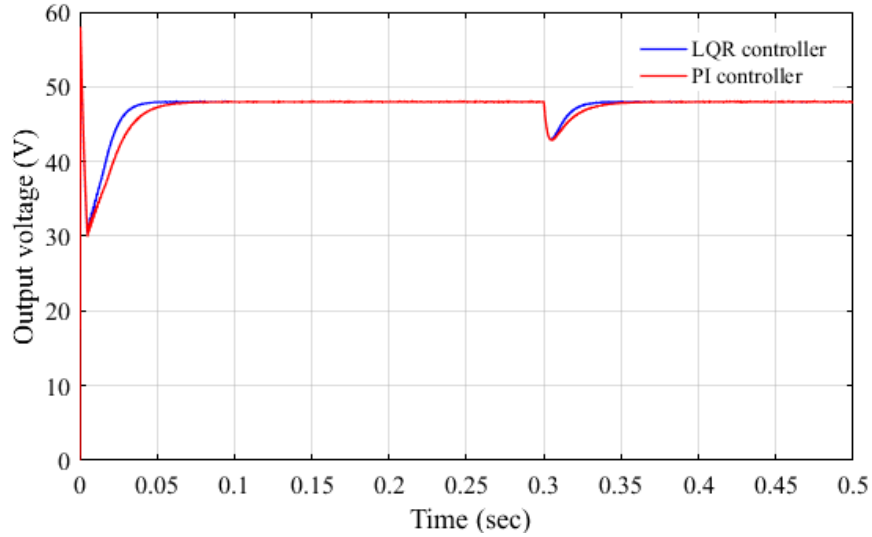


**Figure 3.11** Output voltage response boost converter of the LQR controller and PI controller.

### 3.3.3 FFT analysis:

FFT response of the LQR controlled nanogrid bus voltage still shows harmonics which has profound peak at 580Hz. In a DC circuit, total harmonic distortion (THD) should ideally be close to zero. However, in this case, THD is observed due to an intentionally introduced sinusoidal disturbance at the source-side converter. Although both THD values are small, with the PI controller yielding 0.41% and the LQR controller reducing it to 0.24%, the latter demonstrates superior performance in mitigating the effects of this disturbance, further validating the effectiveness of the LQR controller.

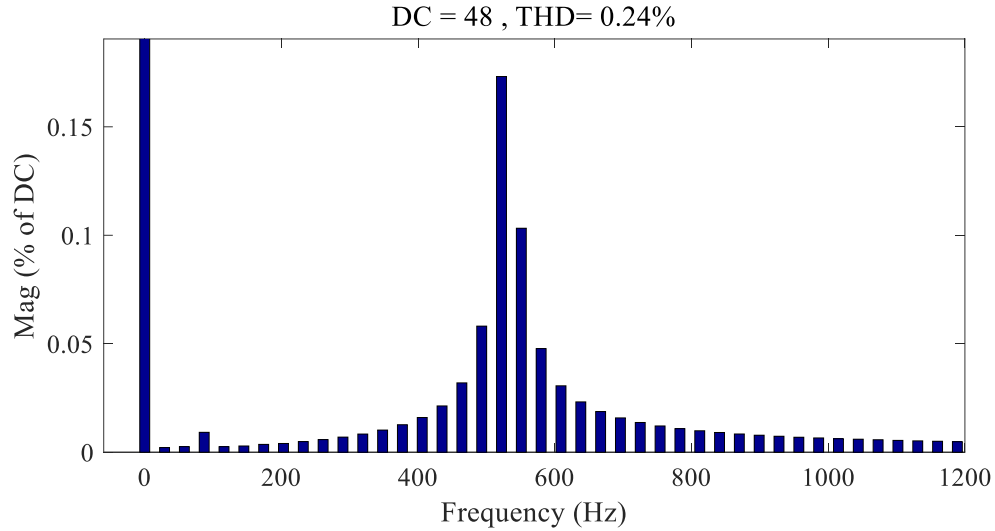


**Figure 3.12** FFT analysis of the bus voltage under with LQR controller.

### 3.4 Conclusions

The modular DC nanogrid can serve as a flexible solution for current and future solar-powered devices. The key innovation lies in the energy management system (EMS), utilizing parametric controls and selecting optimal operating modes based on the DC bus voltage and battery SOC. The model facilitates easy integration of new PV panels and loads while maintaining the bus voltage at a stable 48V. Additionally, the comprehensive stability analysis ensures reliable system performance. Moreover, an LQR controller enhances stability and minimizes harmonics, successfully reducing total harmonic distortion (THD) to 0.24%. The nanogrid enables a personalized, generic model for various applications, such as off-grid isolated houses, businesses, camps, expedition vehicles, radar stations, and cellular towers. The potential of this open-source solar-powered nanogrid extends to re-evaluating electrical technologies for isolated communities where traditional electrical service is unreliable or missing. The DC nanogrid holds promise for widespread adoption, enhancing access to sustainable and efficient energy solutions.

## Chapter 4

### 4 Hardware experimental setup and results

For designing the nanogrid hardware, all the converter circuits were first finalized. Subsequently, all the converters and the controllers were implemented on a protoboard to assess the system's feasibility and facilitate the controller design process. After successful implementation, a functional modular hardware setup for the DC nanogrid was developed and PCBs for all the converters were designed. Additionally, the EMS and central processing unit were implemented. All units, including the PV, battery, and load converters, were connected to the bus bar system, and the communication connections were established. The first functional version of the DC nanogrid was thus created. The detailed design process is elaborated in the following sections.

#### 4.1 Introduction

The feasibility of solar DC nanogrid has already been established, with most of the components of nanogrid being well-defined. The converter technologies, maximum power point tracker (MPPT), and battery charge controller technologies are well-established products that are used in conventional solar PV nanogrid systems. But these systems are designed for use in AC off grid/microgrid systems, and as a result, DC converter-based designs at the system level require personnel with high technical knowledge for proper design, connection, and integration of all components [32]. They are not readily available in the market for nanogrid use. The hardware implementation of DC nanogrid is challenging for the average user because it requires extensive technical expertise to ensure the safe and proper operation of all components, including converters, controllers, energy storage systems, and monitoring devices [115]. This raises costs and limits wide acceptance of a proven technology.

To address this issue, a novel modular version of the DC nanogrid has been designed here to be installed at consumer premises in device form, operating as a plug-and-play device that can be customized according to consumer requirements. The design follows open hardware best practices to ensure maximum accessibility [116], [117]. Earlier, the

architecture, controller design, stability analysis, and a novel energy management system (EMS) of modular DC nano grid were proposed [118] and here this research introduces the first hardware setup of a modular, plug-and-play open source nanogrid device, operable with minimal technical expertise, akin to other consumer electronics available in the market. This modular DC nanogrid can be easily customized according to consumers' power requirements, enabling the supply of various voltage levels to accommodate different device voltage needs. All designs utilize open-source hardware and software, ensuring accessibility for users worldwide. The step-by-step design process of the converter, controller, data logger, and assembly of the complete system is provided. A time-domain simulation and stability analysis of the designed system were conducted in MATLAB/Simulink. Subsequently, the connection and disconnection of a 30W load were observed to assess the stability of the designed hardware. The results are presented and discussed in the context of transforming the nanogrid from a distribution network or system to a device makes it suitable for various user-specific applications, such as remotely supplying power to camp vehicles, campsites, emergency vehicles like ambulances, and small houses lacking grid electricity.

## 4.2 Materials and Methods

### 4.2.1 System architecture

In the nanogrid architecture shown in Figure 4.1, a PV converter connects the PV system to the DC bus. Additionally, bidirectional battery converters and load converters link lithium-ion (Li-ion) batteries and various loads to the grid. Among the low voltage levels (12V to 100V), 48V is identified as the optimal choice for cost and performance. The nanogrid design is scalable; additional PV modules and interface converters can be added to the bus to increase generation capacity. Similarly, extra batteries can be integrated using additional battery converters to support increased loads or storage needs. The EMS can manage variations in DC load and weather conditions, enhancing the system's modularity and adaptability.

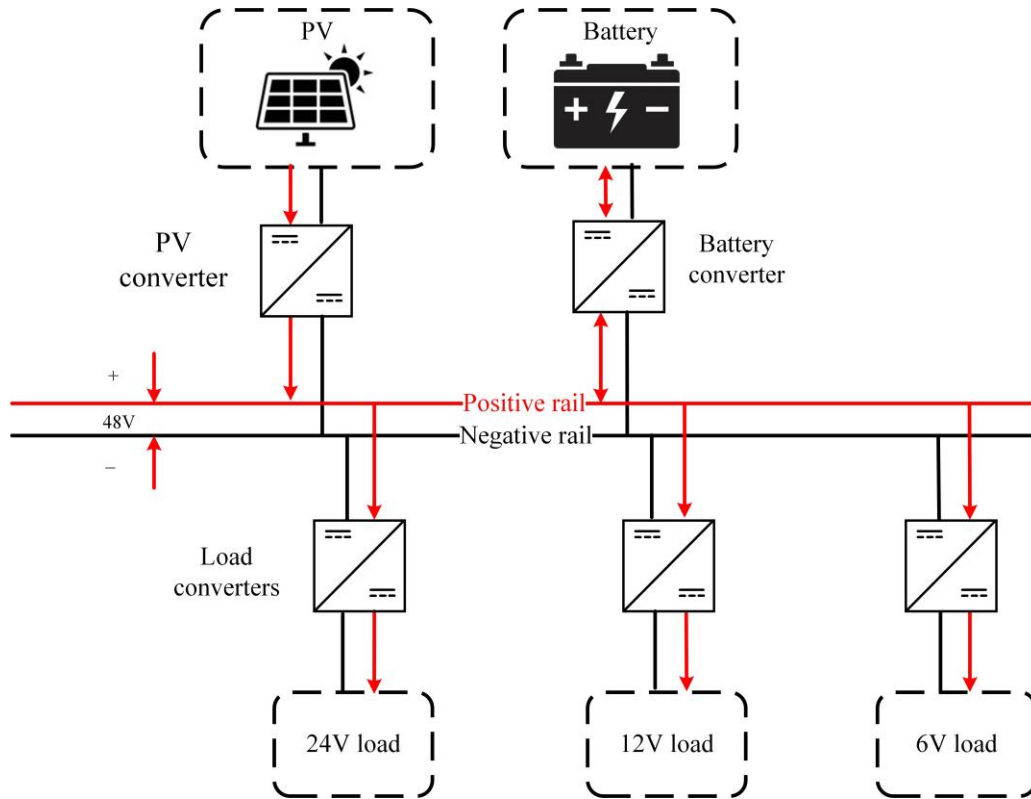


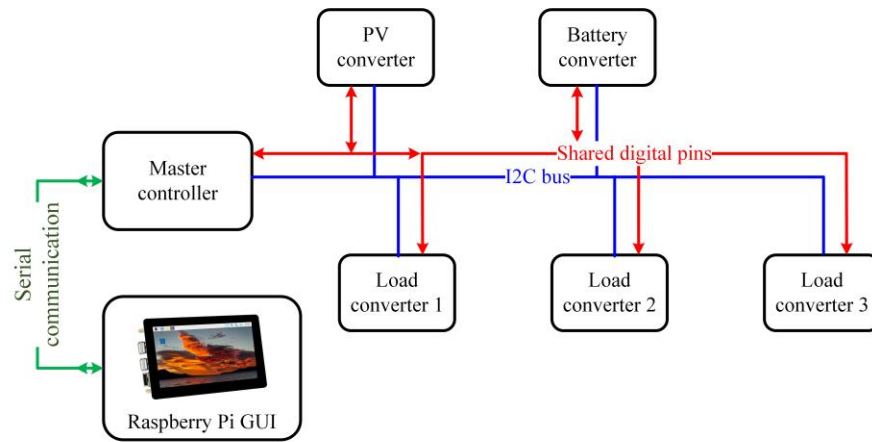
**Figure 4.1.** Architecture of DC Nano grid.

In the nanogrid, the battery discharges only in power deficit mode, defined by a bus voltage below 48V. The controller compares the bus voltage to a reference value, initiating battery discharge to raise the bus voltage to 48V. In power surplus mode when bus voltage is above 48V, the controller lowers the bus voltage to reference 48V and initiate battery charging. Three different levels of load can be served using a step-down load converter, and loads rated at 48V can be directly connected to the bus, as the bus voltage remains stable.

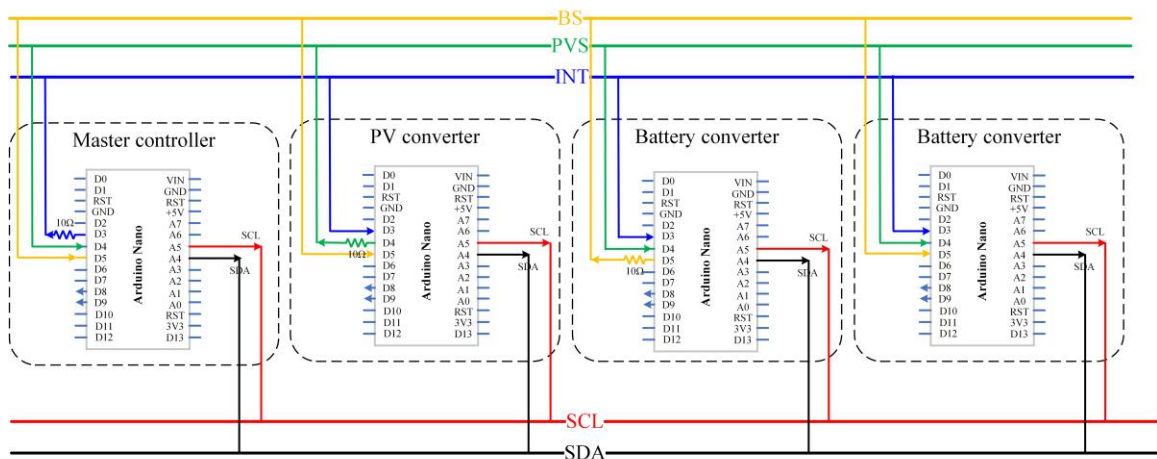
#### 4.2.2 Control strategy

The nanogrid controller coordinates various power sources to achieve optimal power flow. The Energy Management System (EMS) proposed in [118] maintains this coordination and dispatches the required power levels demanded by the load. Various control strategies can be implemented, broadly classified into centralized, decentralized, and hybrid control topologies [119].

In the centralized control method, a central controller manages the power, voltage, and load of the nanogrid using data from various sources and loads, communicated through a network, with all units in the nanogrid directly interfacing with the central controller. This central controller makes decisions based on information collected from sensors attached to all sources and loads via communication channels. While this strategy is fast and precise, it has a significant drawback: a single communication link failure can lead to total grid failure [120]. In contrast, the decentralized control scheme has each unit in the nanogrid collect local information from sources or loads through individual sensors. This approach is more robust and reliable as it avoids costly communication links [121]. Coordination between units, fault management, and overall system data monitoring, however, become more challenging [122]. Hybrid distributed control combines elements of both distributed and decentralized control. In the hybrid topology, converters in the nanogrid communicate with each other to create a cohesive control strategy and share information with the central master controller. Local control decisions are made by local controllers, while the central master controller oversees the entire system and makes broader decisions. This approach enhances system reliability by eliminating dependence on a dedicated communication link all the time and makes the system more resistant to failures.



(a)



(b)

**Figure 4.2.** Control strategy (a) Hybrid control model of modular DC nano grid and (b) Detail connection diagram

In this modular open-source DC nanogrid system, a hybrid control technique is used to implement the EMS. Converters manage source and load level control, while a dedicated central controller coordinates each unit shown in Figure 4.2. Communication between the units and the central controller occurs through two methods. Critical information is shared via the digital pins of the Arduino microcontroller, with specific pins dedicated to the PV converter and the battery converter to indicate their modes, and another for the master controller to manage all units. Additionally, the master controller connects to all converters using an I<sub>2</sub>C path, allowing the central controller to collect local information cyclically and

to interrupt, control, or send commands to each converter as needed [123]. This hybrid approach delivers a powerful and fast control system with enhanced resilience to failure.

### 4.2.3 Controllers design

#### 4.2.3.1 PV controller design

Based on the battery charging status and state of charge (SOC), the PV controller operates in two different modes. When the battery is in a constant current charging state and connected to the system, the PV controller operates in MPPT mode. In this mode, the controller maximizes the input power from the PV using an MPPT algorithm implemented through PWM control, while the battery regulates the bus voltage. When the battery is nearly charged and in a constant voltage charging state, where the charging current depends only on the battery SOC, or when the battery is fully discharged and the PV is connected to the system, the PV switches to bus control mode. In this mode, the converter maintains the bus voltage at a defined 48V using a PI controller. The schematic diagram of this PV controller is given in Figure 4.3.

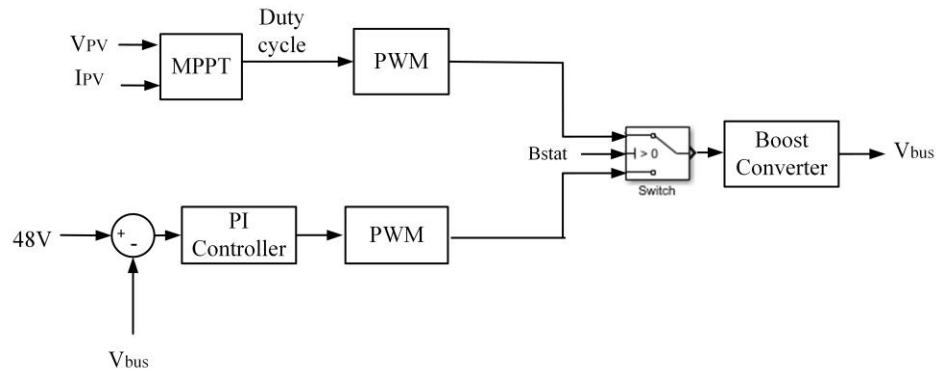


**Figure 4.3.** PV controller for boost converter.

Generally, the cost of commercial MPPT devices is significantly higher than solar charge controllers, making them less accessible and affordable for users [124]. Previous work has shown a successful strategy for accelerating innovation and lowering hardware costs is to use an open source design [125], [126]. Previous studies have argued open source design should be applied to PV systems and components to reduce costs [127]. Following that theory, to help make small solar PV systems more economically accessible and easier

inclusion in the DC bus an efficient MPPT PV converter is designed. There has been some open-source hardware development in the electronics of PV systems [128], [129], which began with the design of smart monitoring system for different PV applications and majority of these system used Arduino microcontrollers for conditioning and processing the output signals of the sensors and it was flexible, modular, and scalable, and of low cost [130]. A prototype of an MPPT using the microcontroller PIC16F877A was designed for 10W power, which is very low power and not suitable for most applications or commercial use [131]. In this design the P&O method is used due to less complexity and comparatively faster tracking capability. Many modified versions of P&O have been developed, which use converter duty cycle as the perturbed signal or adaptive perturbation values [132]. The fundamental concept of the P&O algorithm is to adjust the perturbation amplitude according to the present operational conditions. In the case of the PV controller in DC nano grid it takes the PV voltage and current as an input and generates the optimal duty cycle for the converter.

#### **4.2.3.2 Battery controller design for bidirectional converter**

The battery controller determines the charging and discharging modes based on the bus voltage and the SOC of the battery. Any surplus energy in the grid increases the bus voltage, indicating a charging state, and vice versa. The SOC or battery voltage indicates the charging state. Depending on this, the battery can be charged in constant current mode or constant voltage mode.

#### **4.2.3.3 Load controller design**

The load controller regulates the output voltage to a specific level using a PI controller. The controller compares the reference voltage with the actual output voltage and adjusts the duty cycle accordingly. Additionally, the load controller can disconnect any load upon receiving instructions from the master controller, based on the priority of the specific load.

#### **4.2.4 Converter design**

Three different converter topologies are used in this research to design the modular DC nano grid system with a bus voltage of 48V. The boost converter topology is utilized as the

PV converter, with the maximum PV input voltage kept below 48V, preferably between 15-40V. The maximum charging current capacity is chosen to be 16.66A, allowing for the connection of up to 800W of PV panels to the system using a single boost converter module. Multiple such modules can be used in a single system to scale up the PV power.

For charging and discharging the battery, a bidirectional buck-boost converter topology is employed, with the battery voltage considered to be 24V. Given that the lower voltage side is the battery side and allowing a maximum current of 16.67A, up to 400W of power can be charged or discharged using a single battery module in the system.

Lastly, a buck converter topology is used for loads of 24V, 12V, and 6V, with each rated for a maximum of 400W, 200W, and 100W, respectively, within the system. Ensuring that the bus voltage is stable at 48V allows for loads rated at 48V to be connected directly to the bus without any intermediary converters. The specifications of these modules, along with the PV, battery, and load ratings, are included in Table 4.1.

**Table 4.1.** System specifications.

Parameters	PV module	Battery module	Load module
Converter type	Boost converter	Bidirectional converter	Buck converter
Converter power rating (W)	800W	400W	400W (24V), 200W (12V), and 100W (6V)
Input voltage range (V)	15-40V	20-29.4 V (24V battery)	48V
Maximum input current (A)	20A	16.67A	(8.33 A, 4.17 A, 2.08 A)
Output current (A)	16.67A	8.33A	16.67A
Switching frequency (kHz)	50 kHz	50 kHz	50 kHz

The components of the converter and the controller parameters are calculated and listed in Table 4.2. Components are chosen to exceed their critical ratings and are matched to the nearest common inductor and capacitor values. Based on these parameters, an open-source hardware nanogrid is designed and licensed under GNU GPL v3, CERN OHL v2, and OSF. All code, GUI, 3D-printed parts, and converter PCBs are uploaded to an open-source repository [133].

**Table 4.2.** Converter components and controller parameters calculation

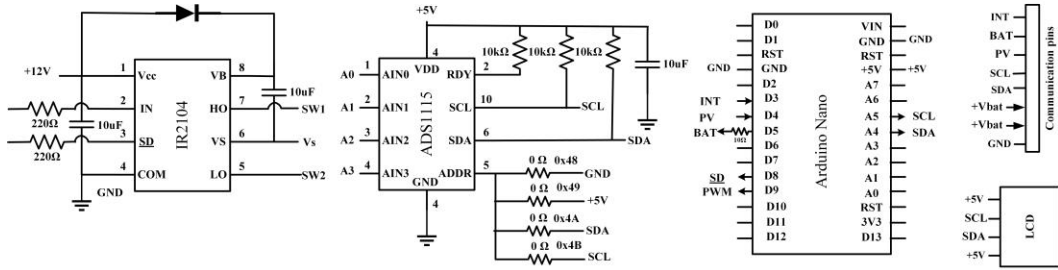
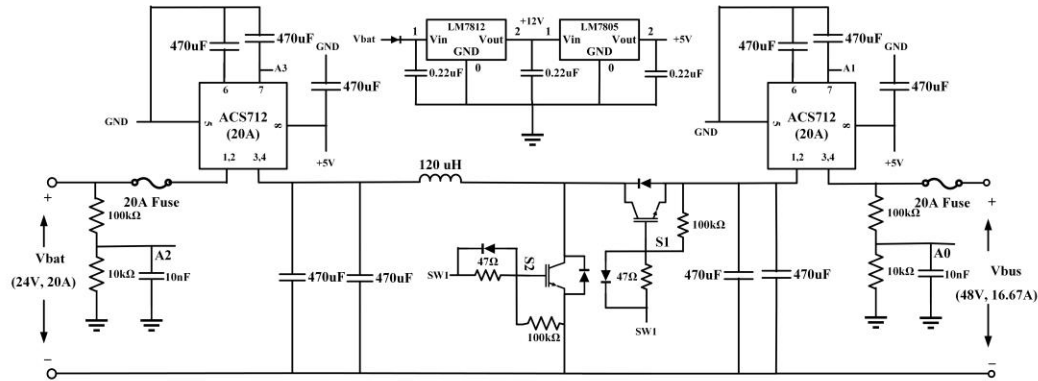
Parameter	Boost Converter	Bidirectional converter	Buck converter (24V)	Buck converter (12V)	Buck converter (6V)
Critical Inductance	$L_1=45 \mu\text{H}$	$L_2= 115.2 \mu\text{H}$	$L_3=57.58 \mu\text{H}$	$L_4=43.18 \mu\text{H}$	$L_5=25.2 \mu\text{H}$
Critical Capacitance	$C_1= 260 \mu\text{F}$	$C_2= 217.01 \mu\text{F}$ , $C_3= 173.6 \mu\text{F}$	$C_4= 43.41 \mu\text{F}$	$C_5= 86.83 \mu\text{F}$	$C_6= 173.61 \mu\text{F}$
Selected Inductance	$L_1=47 \mu\text{H}$ (20A)	$L_2= 120 \mu\text{H}$ (16.67A)	$L_3=68 \mu\text{H}$ (16.67A)	$L_4=47 \mu\text{H}$ (16.67A)	$L_5=33 \mu\text{H}$ (16.67A)
Selected Capacitance	$C_1= 470 \mu\text{F}$ (100V)	$C_2= 470 \mu\text{F}$ (50V) $C_3= 470 \mu\text{F}$ (100V)	$C_4= 470 \mu\text{F}$ (50V)	$C_5= 470 \mu\text{F}$ (50V)	$C_6= 470 \mu\text{F}$ (50V)
Proportional gain (Kp)	0.00021	Charging mode: 0.0004 Discharging mode: 0.0005	0.000451	0.000722	0.00021
Integral gain (Ki)	2.734	Charging mode: 4.78 Discharging mode: 6.01	9.52	11.01	9.35
Gain Margin (GM)	15.57dB	17.32dB, 15.3dB	14.18 dB	20.8 dB	13.85 dB
Phase Margin (PM)	$90^\circ$	$90^\circ$ , $90^\circ$	$90^\circ$	$90^\circ$	$90^\circ$

#### 4.2.5 Bidirectional Battery converter design

The bidirectional buck-boost converter is designed using two alternately switched MOSFETs and one reverse parallel diode to reduce stress on the lower-side MOSFET when it is switched off. The duty ratio of the switching pulse is controlled to regulate both the current and the direction of current flow. With the battery connected to the source terminal of the high-side MOSFET, an IR 2104 MOSFET driver with a bootstrap capacitor keeps the gate voltage above the battery voltage during switching. The Arduino Nano manages the switching pulse and controls the charging and discharging current by monitoring four parameters: battery voltage, battery charging current, bus voltage, and discharge current, all through a 16-bit ADS1115 analog-to-digital converter. The ADC can have four unique addresses, which allows multiple battery converters to be connected and share data using the same I<sub>2</sub>C bus.

The Arduino code limits the discharge current to the maximum allowable battery discharge rate. During charging, two modes are utilized for the lithium battery until the state of charge (SOC) reaches 95%. Initially, the controller charges the battery at the current supplied by the MPPT, provided it is below the maximum charging current of the battery. Once the

SOC is 95%, the charging mode switches to constant voltage mode, charging the battery at a constant voltage with lower current. At this point, the digital pin dedicated to the battery controller (BS) is set high, signaling the MPPT to switch from MPPT mode to bus control mode. The schematic and PCB of the bidirectional converter is shown in Figure 4.4. The assembled battery converter with components on the board are shown in Figure 4.5.



(a)



(b)

**Figure 4.4.** (a) Schematic of bidirectional converter for battery, (b) 3D assembled PCB of bidirectional converter.

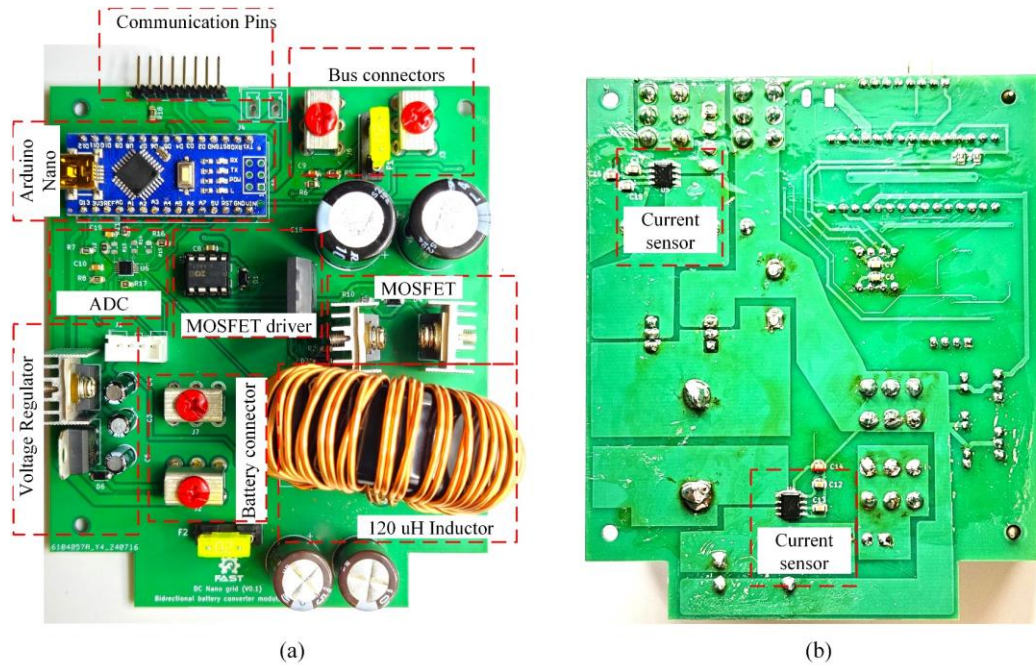
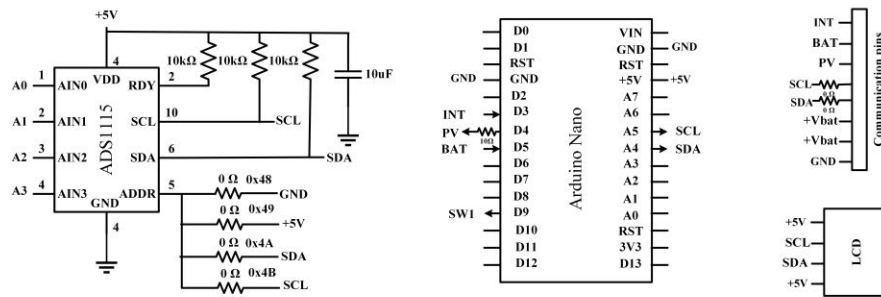
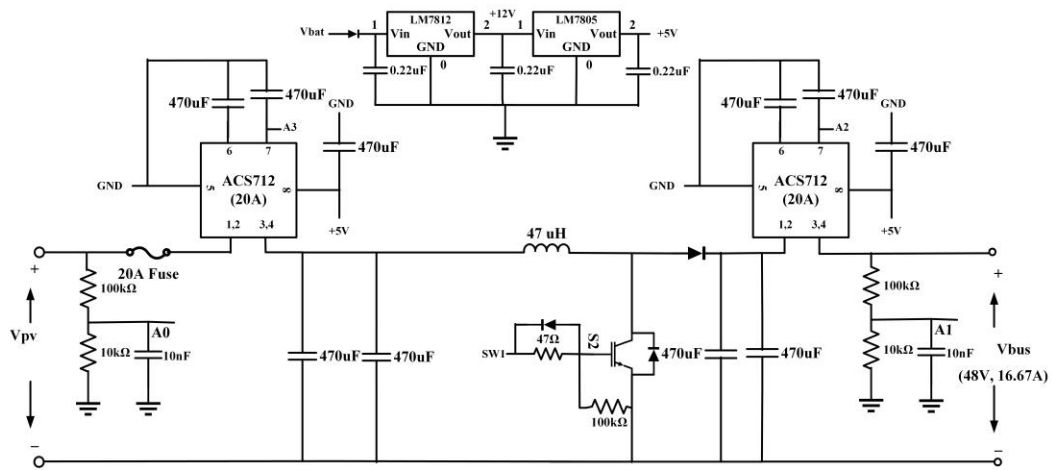


**Figure 4.5.** Assembled bidirectional battery converter

#### 4.2.6 PV Boost converter design

The boost converter for the PV system is rated at 800W, with an input voltage range of 15-40V, and it boosts the voltage to 48V. The converter is designed with one low-side MOSFET and a diode to allow current flow from the PV to the bus. The pulse generated by the Arduino Nano is sufficient to drive the MOSFET. The system measures PV voltage, PV current, bus voltage, and current supplied to the bus using an ADS1115 16-bit ADC. To avoid frequent interruptions by the master controller for data acquisition, an OLED display is connected to the PV converter to show local information, while overall critical system status is shared through the digital pin.

The PV converter operates in two different modes based on the BS signal provided by the battery. When the battery is in constant current (CC) mode, the PV operates in MPPT mode. The rest of the time, it operates in bus control mode. The components and the assembled boost converter are shown in Figure 4.7.



(a)



(b)

**Figure 4.6.** (a) Schematic of boost converter for PV, (b) 3D assembled PCB of Boost converter.

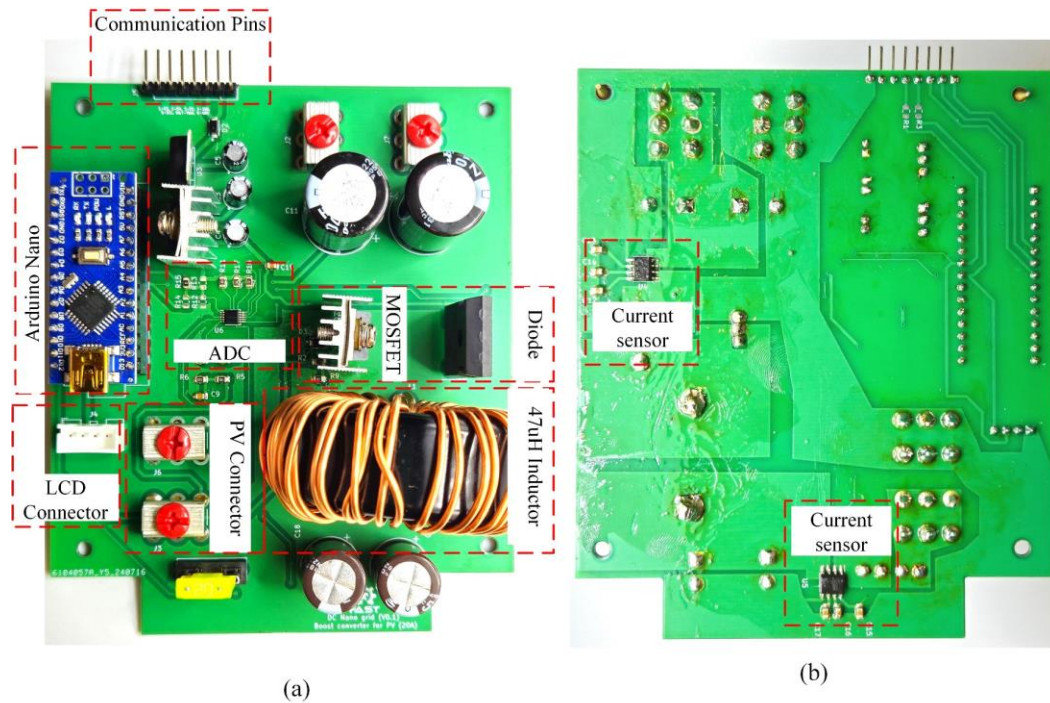


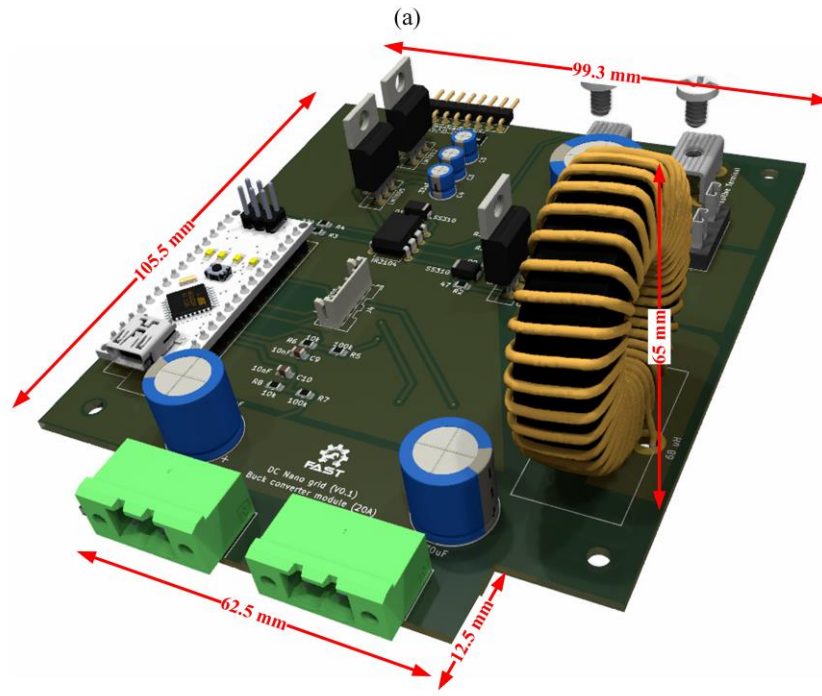
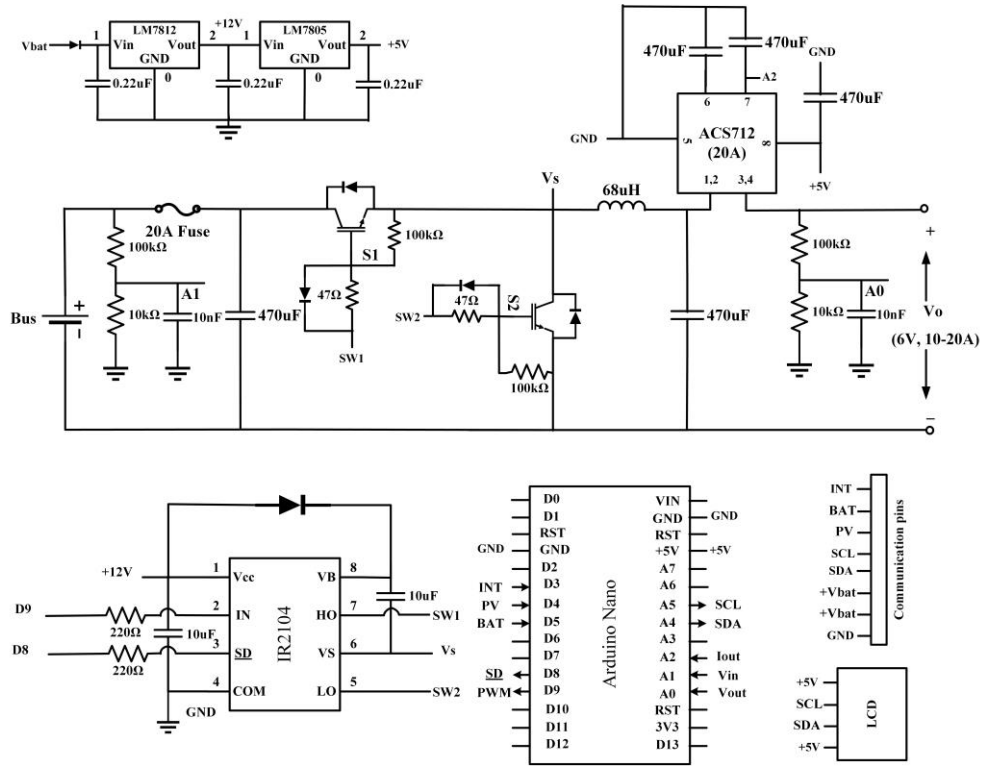
**Figure 4.7.** Assembled Boost converter for PV.

#### 4.2.7 Buck converter design

To serve loads of different voltage levels, a DC-DC converter was designed using an open-source Arduino Nano and a PI controller to regulate the output voltage according to a predefined reference. A synchronous buck converter, utilizing two CSD19533KCS MOSFETs (100V, 100A) [134], is used instead of a conventional buck converter to reduce power loss and improve efficiency, which is achieved due to the replacement of the power diode in conventional buck converter with a low-side MOSFET [135]. The IR2104 MOSFET driver IC provides complementary pulse width modulation (PWM) pulses to both the low-side and high-side MOSFETs, with a 10 $\mu$ F bootstrap capacitor included in the driver circuit.

Three different voltage level load converters can be implemented using the same PCB, requiring only the specific inductor for each converter level as previously calculated. Additionally, the master controller can stop the buck converter from supplying the load either by sending a signal through I<sup>2</sup>C or by raising the INT pin high. The Buck converter

schematic and 3D rendering are shown in Figure 4.8 and the PCBs are shown in Figure 4.9.



(b)

**Figure 4.8.** (a) Schematic of buck converter for 24V load, (b) 3D assembled PCB of Buck converter

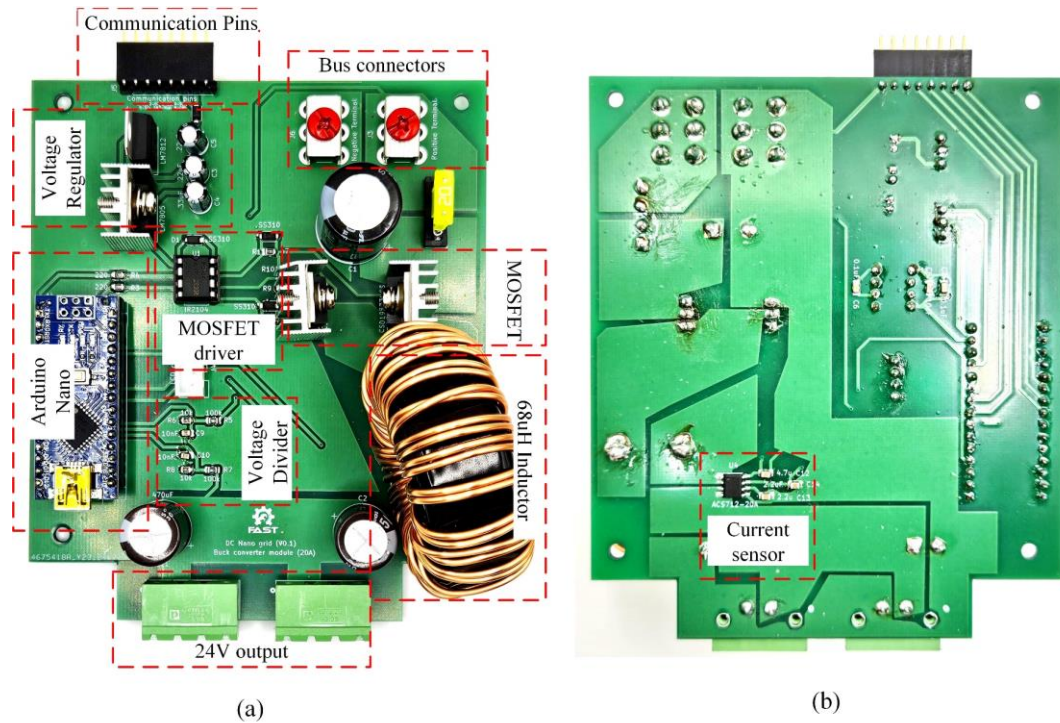


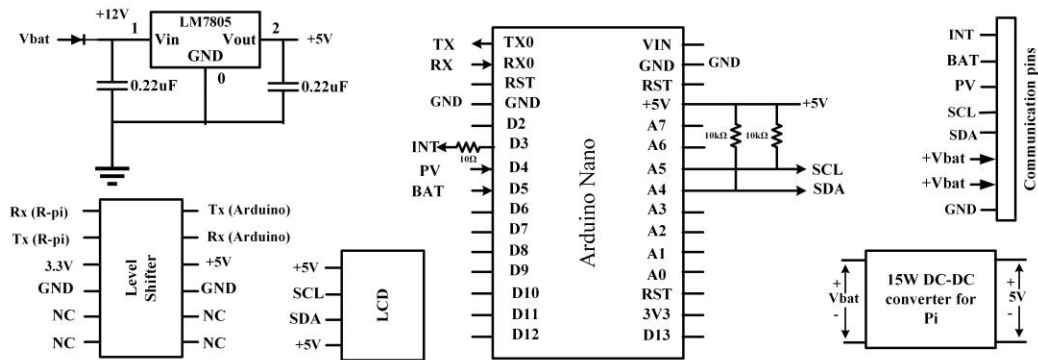
**Figure 4.9.** Buck converter PCB with components (a) front side (b) back side.

#### 4.2.8 Master Controller design

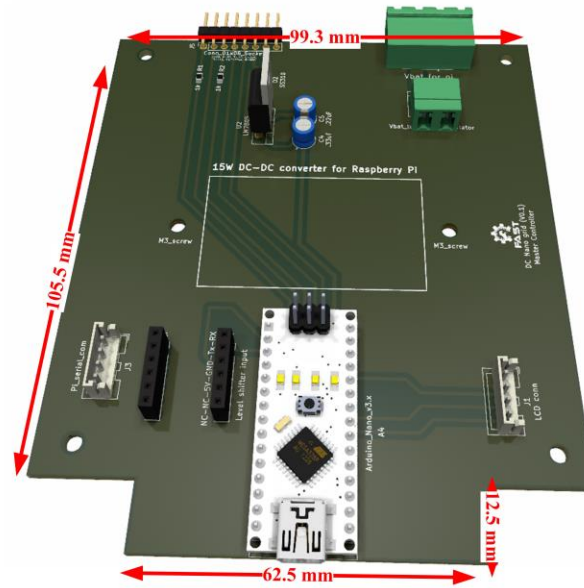
In the nanogrid system, all converters and the master controller share the same I<sub>2</sub>C bus for inter-converter communication. Both the PV and battery converters use ADS1115 ADCs for local measurements on this I<sub>2</sub>C bus also. To prevent interruptions and conflicts, the PV converter, which continuously monitors current and voltage and adjusts switch pulses in MPPT mode, is isolated from the I<sub>2</sub>C bus prioritizing local measurement. Consequently, the battery converter, load converter, and master controller use the I<sub>2</sub>C bus, while the PV converter displays its status on its own OLED.

The shared digital pins are always connected to each converter to change their mode of operation. The master controller simultaneously requests voltage, current, and battery SOC data from the battery and load converters. The corresponding converters send back the data,

which the master controller then combines sequentially and serially prints to the Raspberry Pi-based GUI and data logger.



(a)



(b)

**Figure 4.10.** (a) Schematic of Master controller, (b) 3D assembled PCB of master controller.



**Figure 4.11.** Master controller PCB layout and assembly.

#### 4.2.9 Communication bus

The communication bus comprises 8 lines used for I<sub>2</sub>C communication, shared digital pins, and power supply (+12V, GND). It features an 8-pin socket to interface with the pin headers of the converter and master controller, facilitating information exchange among the converters and the master controller. The bus is 25mm in height and is placed inside the DIN rail where the converter pin header slots in. Pin sockets are spaced 35mm apart, and two communication buses can be interconnected to cover the full length of the DIN rail shown in Figure 4.13.

**Table 4.3.** Function of each traced in the communication bus

Serial	Trace name	Function
1	PVS (D3)	PV signal from PV converter to indicate operating mode (0=MPPT, 1=Bus control)
2	BS (D4)	Battery status signal from Battery converter (0=Current control, 1=Voltage control/isolated)
3	INT (D5)	Interrupt signal by master (Normally 0)

4	SDA	Serial data line
5	SCL	Serial clock line
6	+12V	+12V supply for the control circuit
7	+12V	+12V supply for the control circuit
8	GND	Common ground

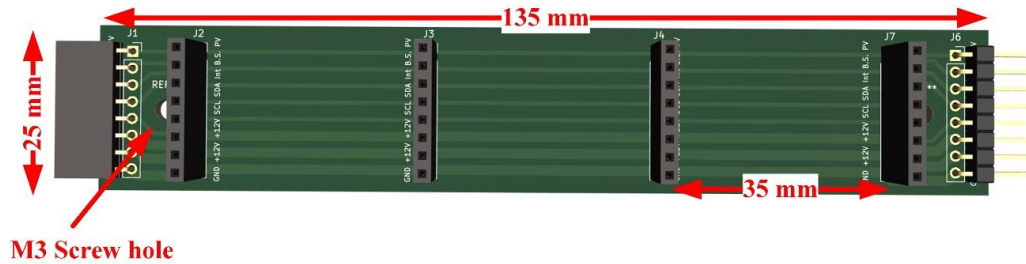


**Figure 4.12.** Schematic of Communication bus.

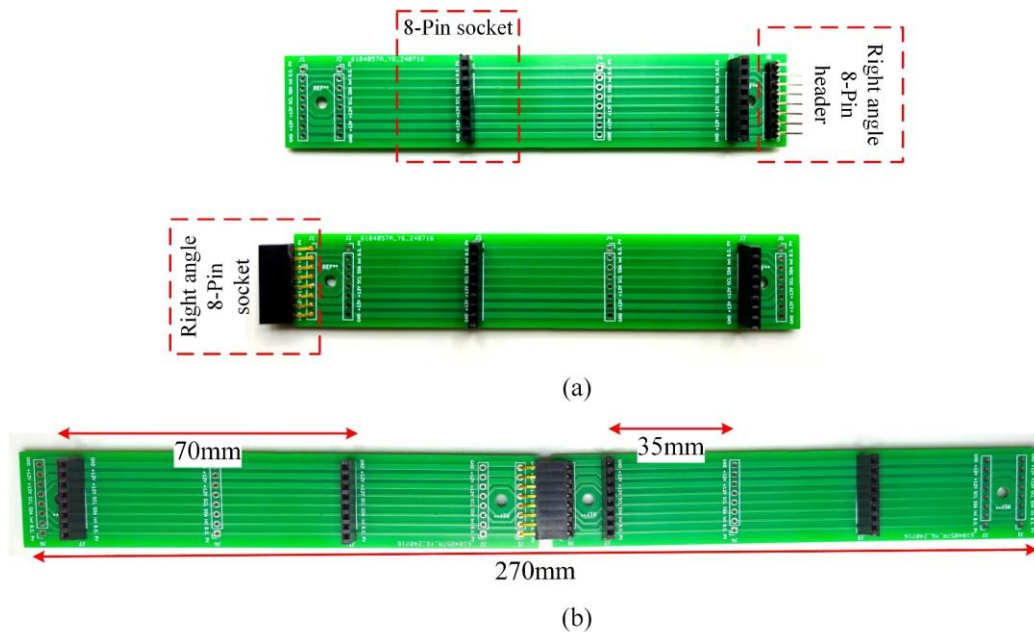


**Figure 4.13.** Assembled and extended communication bus.

#### 4.2.10 Inductor design

For designing the inductors of various converters, each handling a peak current of approximately 20-24A, the toroidal inductor core 0077443A7 from Magnetics (Pittsburgh,

PA, USA) is used. This core has an outer diameter of 46.74 mm and a width of 18.03 mm, with a relative magnetic permeability of 75 and an inductance factor of 169 nH per turn. The design parameters for the 47  $\mu\text{H}$ , 120  $\mu\text{H}$ , and 68  $\mu\text{H}$  inductors are summarized in Table 4.4.

**Table 4.4.** Design parameters of inductors.

Parameters	Boost converter	Bidirectional converter	Buck Converter 1 (24 V)
Inductor	L1=47 $\mu\text{H}$	L2= 120 $\mu\text{H}$	L3=68 $\mu\text{H}$
Current	20A	16.67A	16.67A
Peak current	24	20	20
Wire AWG	16AWG	16AWG	16AWG
Number of strands	2	2	2
Turns	23	37	28
Length	3,223 mm	5,266 mm	3,924 mm

#### 4.2.11 Bill of materials

The bill of materials for all subcomponents is listed in Appendix B. The summary of the total cost for each subsystem is shown in Table 4.5 and the total cost of the system is CAD\$380.

**Table 4.5.** Summary of total cost of the system.

Type	Cost (CAD)
Buck Converter	\$55.81
Boost converter	\$66.07
Bidirectional converter	\$76.28
Master Controller	\$28.78
Communication Bus	\$5.03
Monitoring system	\$147.52
Total	\$379.49

#### 4.2.12 Arduino codes and GUI

Each converter and the master Arduino have separate code, as detailed in Table 4.6. In addition to the pre-installed libraries in the Arduino IDE, the SSD1306 library for the OLED display and the ADS1115 library for the 16-bit ADC must also be installed. At the start of the code, the PWM switching frequency is selected, and the OLED and ADC are initialized. Except for the master controller, all Arduino code follows a similar structure: measuring circuit parameters using the ADC, averaging three consecutive measurements for accuracy, and then adjusting the PWM duty cycle based on current and voltage measurements to control the converter. When the master requests data from a converter, it interrupts the ongoing operation to transmit the local parameters in string format. Consequently, the master controller cyclically requests each converter every three seconds. Upon receiving the complete set of data from all converters in string format, the master concatenates these strings and transmits them as a single unified string, with the length corresponding to the aggregate length of the data from each individual converter.

To avoid interruption from the ADC and OLED display, the firmware must be uploaded to the Arduino before it is placed on the board for the first time. Each converter is assigned a different slave address, defined in the wire setup before initiating transmission, to communicate with the master. If more than one converter of the same type is present in the system, each must be assigned a different wire address.

**Table 4.6.** Arduino codes and GUI of the DC nano grid system are all licensed with GNU GPL v3.

Code	File type	Location of file
Boost converter code	.ino	<a href="https://osf.io/73yf5/">https://osf.io/73yf5/</a>
Buck converter code	.ino	<a href="https://osf.io/73yf5/">https://osf.io/73yf5/</a>
Bidirectional converter code	.ino	<a href="https://osf.io/73yf5/">https://osf.io/73yf5/</a>
Master controller code	.ino	<a href="https://osf.io/73yf5/">https://osf.io/73yf5/</a>
GUI for Raspberry pi	.py	<a href="https://osf.io/73yf5/">https://osf.io/73yf5/</a>

### 4.2.13 Interface and GUI

All converter controllers utilize Arduino Nano processors, and the EMS also implemented on an Arduino Nano serving as the master processor. This master processor communicates with the other Arduino Nanos within the DC nano grid using an I<sub>2</sub>C communication protocol while the master controller only communicates with Raspberry Pi using serial communication protocol. To display the status and voltage/current levels of each converter, a Raspberry Pi (Cambridge, England) with a 7-inch display has been integrated into the system as a separate module. This display module, along with the master Arduino, functions as the central control unit of the entire DC nano grid.

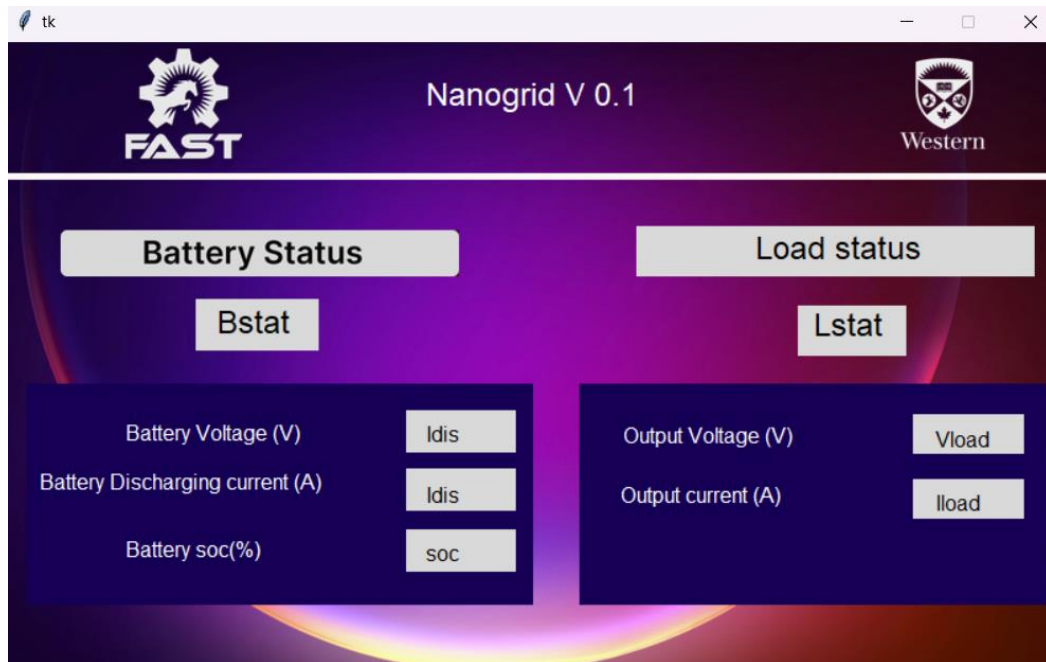


**Figure 4.14.** DC nano grid GUI for data monitoring.

The graphical user interface (GUI) for the nanogrid system operates by receiving real-time data from a master Arduino via serial communication. This data, transmitted through a USB connection at a baud rate of 9600, is processed by a Raspberry Pi running a Python script using the Tkinter library. Currently, with only the battery converter and one load converter connected, the GUI is designed to display their statuses exclusively, including battery voltage, state of charge (SoC), battery discharging current, output voltage of load converter, and output current.

The Python script continuously reads the incoming serial data in a separate thread, ensuring that the GUI remains responsive. The data is processed, and specific values are extracted and updated on the display in real-time. For instance, the battery status and load status are dynamically updated based on the current and voltage readings. The GUI, developed using Tkinter Designer, provides a user-friendly interface with clear visual indicators, making it easier to monitor the nanogrid's performance immediately. This setup enhances the reliability and efficiency of DC nanogrid system by offering real-time monitoring and control. This GUI is open source and can be modified as needed. As this is the initial version of the GUI, it can be easily modified in the future to send commands to the master Arduino for controlling the DC nanogrid.

#### 4.2.14 Step by step integration and commissioning process

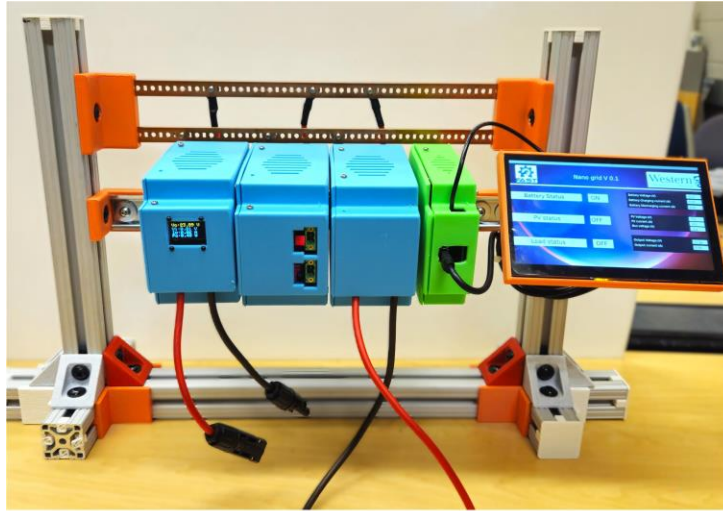
The installation process and guidelines are as follows:

- The design and assembly process of frame and the converters enclosure is given in Appendix A.
- After all the converter and the frame is designed, attach the master controller to the frame. This is the only unit that does not require connections to the bus bar, and there should only be one master controller present in a DC nano grid.
- Attach the PV and battery modules to the system one by one. For systems with multiple PV and battery modules, alternate the installation sequence between PV and battery to maintain consistent DC resistance across all modules.
- Attach the buck converter module and inverters module (if any) to the system according to the load requirements.
- Sequentially turn on all the battery switches. This action will power on the master controller and all connected modules along with the Raspberry Pi display. Next, connect the PV panels to the PV converter, and finally, connect the loads to the system.
- For shutdown, follow the reverse order of the installation process.

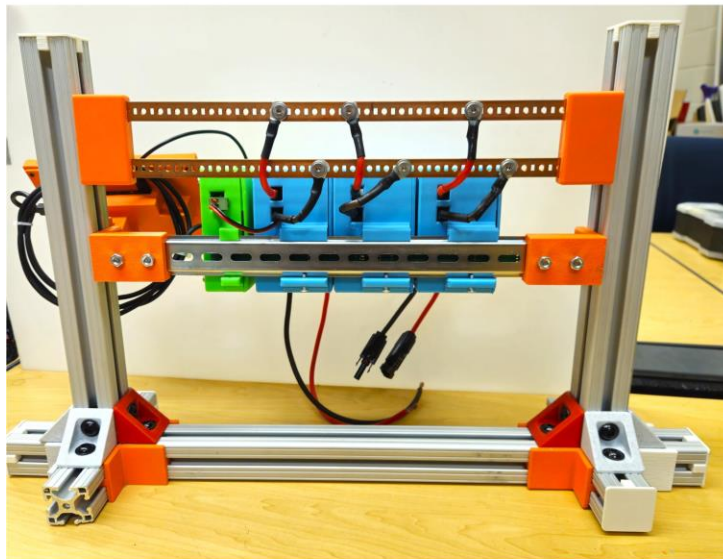
## 4.3 Final Hardware and Result

### 4.3.1 Final nanogrid hardware

The assembled nanogrid hardware is shown in Figure 4.15. The PV converter, 24V load converter, and battery controller are placed in order from the left, all housed in blue enclosures. The master controller in green enclosure is positioned on the far right, close to the Raspberry Pi display.



(a)



(b)

**Figure 4.15.** Nanogrid final hardware (a) front view (b) back view

### 4.3.2 Stability of 24V bus voltage under load disconnection

Although the simulation results and converter design parameters were based on a 48V bus voltage, testing was conducted at 24V due to limitations in testing and the frame. Since 48V is considered a hazardous DC voltage, all electrical contacts must be enclosed. However, simply changing the reference bus voltage in the code to 48V would enable the system to operate at 48V. A 30W load is connected to the system and subsequently disconnected to evaluate the stability of the supply voltage, as shown in Figure 4.16. The bus voltage remains stable during the load variation and quickly returns to the reference 24V after the disconnection.



**Figure 4.16.** The bus voltage after sudden disconnection of 30W load (0-70sec)

## 4.4 Discussion

This research differentiates itself by not extensively discussing new control mechanisms or converter designs for DC nanogrids. Instead, it focuses on the comprehensive setup of a DC nanogrid. This includes maximizing power extraction from solar PV, maintaining a stable DC bus voltage, and ensuring the proper operation of the battery system to supply power to appliances at their required voltage levels. A key aspect of its uniqueness is its modularity and the device version of the DC distribution network system. This represents the first-ever nanogrid that incorporates all the features of a complete DC nanogrid in a

modular, user-friendly, plug-and-play hardware design. It is designed to be easily assembled and operated by users, making it accessible for DIY applications [136] and enhancing its practicality and flexibility. The hardware implementation is completed using open-source design. Being opensource will allow modifications by the user such as disconnecting low-priority loads when the generation capability is inadequate [137].

Later the bus voltage stability, and the supply voltage quality of the hardware are also verified. The benefit of the open-source hardware is the adaptation of this nanogrid using material from local vendors and it gives the opportunity to modify the device quite easily according to users' requirements. Its modular design allows for easy integration into a frame or electrical box. Single households, vehicles such as ambulances, mini-clinics, and camps can be powered using the nanogrid setup, with the design facilitating easy modifications to integrate new loads and batteries. While this setup introduces a novel strategy for making PV systems modular and more accessible, further improvements in the GUI and communication system are necessary for the seamless integration of converter modules. Additionally, a better communication strategy is needed to enable the PV converter to share data with the master controller without interruption. Implementing a more advanced MPPT algorithm could also help reduce the impact of partial shading. Currently, the converters are connected to the bus bar using wires, which disrupts seamless integration, but incorporating bus bar clips will make the process easier.

## 4.5 Conclusions

The open-source modular DC nanogrid presented in this research represents the first hardware implementation of a plug-and-play device that is, easily adaptable, expandable, and customizable at different voltage and power levels. Transforming the nanogrid from a distribution network to a device makes it suitable for various user-specific applications, such as remotely supplying power to camp vehicles, campsites, emergency vehicles like ambulances, and small houses lacking grid electricity. The modular DC nanogrid includes all the features available in a DC distribution network, including intercommunication of each converter using a master-slave protocol. It also exhibits additional features such as data logging, which enhances user experience and promotes the use of DC grid systems.

This approach not only makes the system more user-friendly but also differentiates it from traditional PV systems, promoting the adoption of DC grid systems as a modular device.

The converter technologies, maximum power point tracking (MPPT), and battery charge controller technologies are well-established products which are used on conventional PV systems. The novelty and user-friendly features of the modular nanogrid system are:

**Open-Source Hardware Implementation:** Implementing these technologies using open-source hardware and then forming a nanogrid in a modular and adaptable manner is completely novel.

**Modular Device Design:** Creating the nanogrid as a device with interconnection and control techniques makes it distinct from conventional PV systems.

**User-Friendly Features:** Additional features such as data logging enhance user experience and promote the use of DC grid systems. This approach not only makes the system more user-friendly but also differentiates it from traditional PV systems, promoting the adoption of DC grid systems.

## Chapter 5

### 5 Application of OS Nanogrid in Ambulance

Medical equipment for isolated communities can be powered by modular photovoltaic (PV)-powered DC nanogrid systems by ensuring an uninterrupted power supply for mini-mobile clinics and ambulances. Given their primarily low power requirements, DC loads, and low voltage applications this is a particularly promising means to directly integrate renewable PV-electricity, which inherently generate DC power, and supplies local loads without AC conversion, thereby eliminating conversion losses and boosting efficiency [138]. There is a challenge of the various voltage requirements for different medical equipment, but a modular open source DC nanogrid has been developed that is flexible enough to adapt to various needs [139]. This study aims to i) integrate this modular DC nanogrid into ambulances, ii) analyze the estimated loads and iii) optimize the sizes of PV modules and batteries using the physical constraints of the ambulance and simulations with the Solar Alone Multi-Objective Advisor (SAMA) [140]. Based on the compatibility analysis of the ambulance with DC grid, the voltage and power levels required by the instruments inside the ambulance will be determined, and the nanogrid will be modified accordingly. In addition, the type of PV modules suitable for use on the ambulance roof will be evaluated specifically assessing the feasibility of using flexible PV modules, along with cost and installation methods. The results will be presented and discussed in the context of isolated communities.

#### 5.1 Typical load of ambulance

A reliable power supply is essential to keep critical devices operational in medical facilities and during emergencies [141]. Regardless of different types, all ambulances are equipped with some basic emergency and lifesaving instruments [142], many of which rely on a stable power supply. These include vital life-saving devices such as defibrillators, suction machines, ventilators, portable oxygen systems, nebulizers, and infusion pumps [143]. The operation and compatibility of these devices with a DC nanogrid will be summarized here. In addition, the availability of open source hardware designs [144], [117], [145] for these medical devices that could aid in optimizing designs in the future will also be summarized.

### 5.1.1 Defibrillator

Defibrillators are devices that apply an electric charge or current to the heart to restore a normal heartbeat [146]. In cases of cardiac arrest, defibrillators can help restart the heart's rhythm. Depending on the use case, a defibrillator can be classified as either a manual defibrillator or an automated external defibrillator (AED) [147]. Manual defibrillators necessitate operation by trained medical professionals within a hospital setting, whereas AEDs are commonly located in public spaces, especially in ambulances, where they can be used by individuals with limited training or experience in emergencies [148]. Modern AEDs come with internal lithium-ion batteries [149]. Manufacturers are developing cost-effective defibrillator battery management systems with clear runtime indicators to reduce unnecessary battery replacements [150]. Also, modern defibrillators are equipped with a range of advanced features, including temperature and blood pressure monitoring, pulse oximetry, and multi-lead ECG capabilities, thereby eliminating the need for a separate ECG monitor [151]. These advanced features and battery management systems make the defibrillator ideal for operation on DC voltage provided by a solar-powered nanogrid. In addition, there has been progress made in developing low-cost open source defibrillators [152], [153].

### 5.1.2 Suction unit

A suction machine, also known as an aspirator, is a medical device primarily used for removing obstructions, like mucus, saliva, blood, or secretions from a person's airway [154]. When an individual is unable to clear secretions due to a lack of consciousness or an ongoing medical procedure, suction machines help them breathe by maintaining a clear airway. Suction units generally operate on 100-240V AC, 50/60 Hz, but also have the capability to run on 12V DC batteries [155]. Most suction units work efficiently on both AC and DC power supply, with 3 hours of continuous run time at maximum vacuum on a fully-charged battery [156]. Additionally, it can be equipped with a 12V DC power cord to connect directly to the vehicle's DC power outlet [157]. Thus, suction machines are also compatible with DC nanogrids. Although there are open source aspirators developed [158], more work is needed to adapt and apply them to medical systems.

### 5.1.3 Ventilators

A ventilator is an advanced life support machine used in ambulances when a patient's condition requires mechanical assistance to breathe [159]. Normally, ambulance ventilators typically operate on 100-240V AC, 50/60 Hz, and have an inbuilt lithium battery backup [160]. 10-30V DC batteries are usually used to power ventilators that are used in ambulances [161]. Also, they often have built-in inverters that convert this DC power to the necessary AC voltage, making them compatible with the DC nanogrid. It should be noted that during [162] and directly after the COVID-19 pandemic a wide range of open source ventilators [163], [164], [165] were developed that could be easily reconfigured to work with the DC nanogrid.

### 5.1.4 Portable Oxygen Concentrators (POCs)

Portable oxygen concentrators (POC) are designed to provide a continuous supply of oxygen to patients with respiratory conditions [166]. Most models offer adjustable flow settings, allowing paramedics to adjust the flow rate based on the patient's needs. POCs are particularly useful in mobile environments, such as ambulances, due to their in-built battery storage [167]. Batteries were designed and tested for longevity with some models offering up to 4.5 hours of continuous operation on a single charge [168] and are thus also compatible with a DC nanogrid. Additional work is needed in the area of open source POCs [169].

### 5.1.5 Nebulizer

Nebulizer turns liquid medicine into a mist which is then inhaled through a mouthpiece or a mask [170]. This is particularly useful for treating respiratory conditions such as asthma, chronic obstructive pulmonary disease (COPD), and other airway disorders [171]. While standard nebulizers are generally designed for home use and require AC power, portable or battery-operated nebulizers are preferred in ambulances due to their flexibility and independence from vehicle power sources. The portable nebulizer comes with an inbuilt battery and the battery is rechargeable which gives the option to provide up to 30 treatments (120 minutes of use) between each charge [172]. The portable ones generally also come

with DC adapter to directly plug with DC voltage sources or batteries [173], thus making them compatible with DC nanogrids, but open source options are needed.

### 5.1.6 Infusion Pump

Infusion pumps are found in ambulances, particularly those equipped for advanced life support (ALS). They are medical devices that delivers fluids, such as nutrients and medications, into a patient's body in controlled amounts [174]. Similar to other equipment in the ambulance, infusion pumps are equipped with built-in batteries that ensure continuous power supply [175]. Additionally, manufacturers are actively developing low-voltage DC-DC converters to directly power these devices from the ambulance's DC power outlet, minimizing the risk of power failure [176]. It should be noted that there are many open source designs for precision pumps [177], [178] and some have been adapted to medical applications [179], [180], [181].

### 5.1.7 Summary of emergency equipment’s power requirements

The DC power compatibility analysis confirms that all emergency equipment can be made to function with DC power sources. While hospital emergency equipment is usually connected to AC outlets, ambulances, being mobile and not stationary, DC power is more suitable for their operation. Additionally, emergency equipment includes built-in batteries that are charged using DC power, ensuring reliable operation. Consequently, a solar DC nanogrid emerges as an ideal solution for powering ambulances, offering a sustainable and efficient energy option.

Based on the typical energy demands of an ambulance, excluding locomotion, lighting and air conditioning, the total energy consumption for the equipment operating with full backup for 4-10 hours is determined and summarized in Table 5.1. This operation time can be extended with the use of a larger battery and additional PV modules.

Table 5.1 Typical loads of equipment inside an ambulance

Instrument	Model	Compatible with DC	Battery Specification	Energy required	Backup	Instrument power rating	Ref.
Defibrillator	Lifepak 15	Yes	11.1V, 5.7Ah	63 Whr	6hr	10W	[182]

Suction unit	Laerdal Suction Unit (LSU)	Yes	12V, 2 Ah,	24 Whr	4hr	6W	[157]
Ventilators	Newport HT70	Yes	14.4V	50-150 Whr	10 hr.	5-15W	[183]
Portable Oxygen Concentrator (POC)	Inogen G5	Yes	14.4V	100 Whr	6.5 hr.	15W	[167]
Nebulizer	DeVilbiss 6910 P-DR	Yes	12V, 1.5Ah	18 Whr	45 mins	25W	[184]
Infusion Pump	CADD-Solis	Yes	7.2V, 2.75Ah,	20 Whr	10 hr	2W	[185]
Total				375 Whr		60-75W	

## 5.2 PV installation capacity and Load estimation

### 5.2.1 Maximum PV installation capacity

For any vehicle, the maximum capacity of PV installation depends on the surface area of the vehicle. Thus, even if a given amount energy is required the area available on an ambulance in a given location may not be able to provide it. To determine the area constraint a typical ambulance by Mercedes Benz ABL [186] is used as shown in Figure 5.1. The maximum surface area is 20.5m<sup>2</sup>, allowing for up to 4 kW of PV installation assuming PV modules of 19.5 % efficiency [187] .

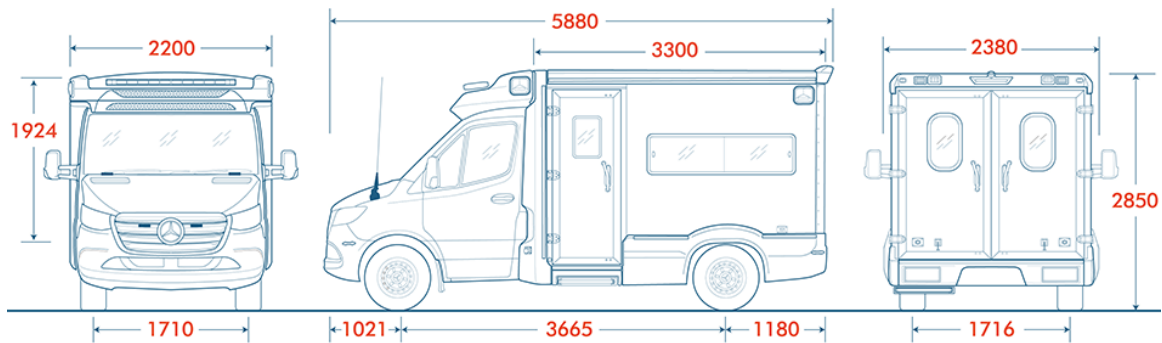


**Figure 5.1** External dimensions of Mercedes Benz ABL-XLT-SL Ambulance [186].

Fortunately, the energy load inside the ambulance is relatively low compared to the maximum available surface area for installing PV panels, only the roof of the ambulance, which has an area of approximately 8m<sup>2</sup>, needs to be considered. This permits a theoretical maximum of a maximum of 1.53 kW of PV modules shown in Table 5.2.

**Table 5.2** Area of surface of an Ambulance available for PV installation

	Area m <sup>2</sup>	PV installing capacity (195 W/m <sup>2</sup> )[187]
Roof surface area:	3300mm × 2380mm= 7854000 mm <sup>2</sup> (7.854m <sup>2</sup> )	1,530W
One side surface area	3300mm × 1924 mm =6349200 mm <sup>2</sup> (6.35m <sup>2</sup> )	-

Two sides surface area	$2 \times 6.35\text{m}^2 = 12.7 \text{ m}^2$	2,476W
Total		4,006 W

## 5.2.2 Selection of PV panels

In the world of commercial PV panels, two primary categories emerge based on their structural properties: rigid and flexible panels. Each type has unique advantages, making them suitable for different applications and environments.

### 5.2.2.1 Rigid PV Panels

Rigid PV modules can be categorized as monocrystalline silicon (c-Si), polycrystalline silicon (p-Si), thin film such as cadmium telluride (CdTe), copper indium gallium selenide (CIGS), and amorphous silicon (a-Si:H) [188]. Such PV are distinguished by their rigid and durable construction, which necessitates robust mounting systems for installation. While their resilience is advantageous, it increases installation complexity, weight and cost, particularly when integrating them onto the roof of an ambulance. The structural integrity of the ambulance roof must be considered to accommodate this integration effectively. In addition, they are heavier than flexible panels, which would slightly reduce fuel efficiency [189].

### 5.2.2.2 Flexible PV Panels

Flexible PV modules, such as thin-film panels, marine PV, very thin silicon wafer PV and certain building-integrated photovoltaics (BIPV), offer versatility and adaptability for a variety of surfaces and unconventional installations. These panels are usually constructed from materials like a-Si:H, CdTe, or CIGS and typically have a slightly lower efficiency [190]. Their flexibility enables installation on curved or irregular surfaces, making them suitable for applications where traditional rigid panels are impractical. In addition, recent advancements in solar panel technology have also introduced high-efficiency flexible panels based on c-Si, which match the performance of rigid panels while providing additional benefits [191]. Their lightweight and flexible nature allows for easy installation using adhesive mounting methods, minimizing installation and racking costs and reducing

stress on the structural integrity of the roof making it more suitable for ambulance application.

### 5.2.2.3 Comparison

A direct comparison between the installation of rigid and flexible panels is made here. For this comparison, the 395W HiKu6 solar panel from Canadian Solar (rigid) [187] and the 175W RNG-175DB-H [192] solar panel from Renogy (flexible) are evaluated. Although it should be pointed out that the functional properties of these modules are generic and could be applied to any other suppliers. The racking cost for solar panel installation on the roof is considered at CAD\$1.00/Watt [193]. While the maximum number of panels which can be installed is shown in Figure 5.2 and summarized in Table 5.3.

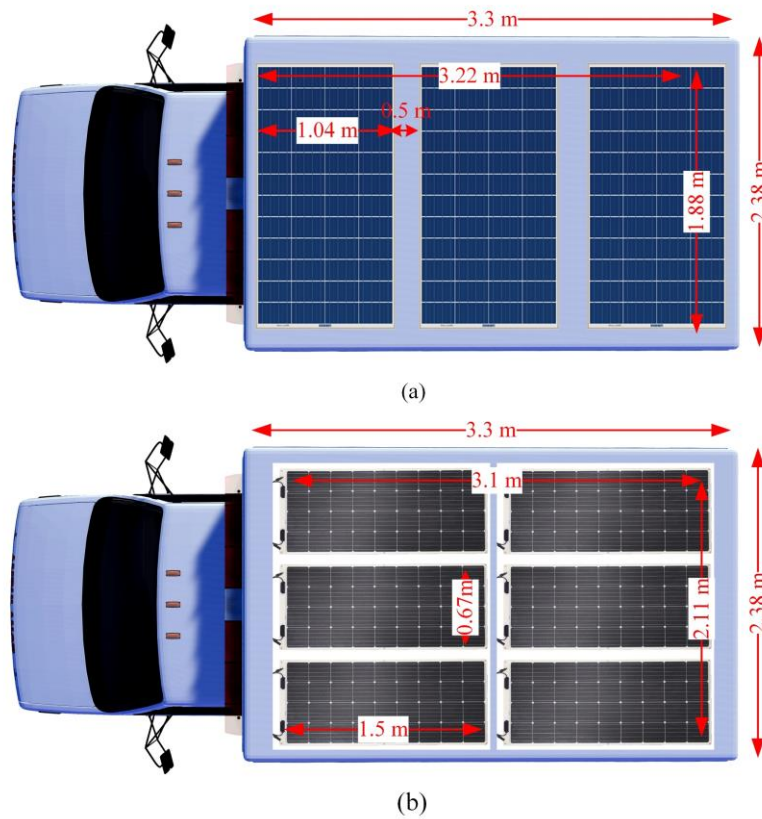


**Figure 5.2** Top view of ambulance with PV panels placement

**Table 5.3** Comparison between rigid panel vs flexible panel for Ambulance

Feature	Rigid panel	Flexible panel
---------	-------------	----------------

Model	HiKu6 Solar Panel 395W	RNG-175DB-H
Manufacturer	Canadian Solar	Renogy
Size	1722×1134×35 (in mm)	1504 x 673 x 2 mm
Total number of panels	3	6
Total power	1,185 W	1,050 W
Total weight	4 x 22.4kg=89.6 kg	6 x 2.8kg =16.8 kg
Panel Cost	3 x \$268.60 = CAD\$805.80	CAD \$2,100
Racking system cost	CAD \$1,185 (Approx.)	CAD \$150 (Approx)
Total hardware cost	CAD \$1,990	CAD \$2,250
Roof reinforcement	Required	Not required

As flexible modules are relatively new and have lower demand compared to rigid PV modules, their cost is generally higher on a \$/W basis. When considering the overall system cost, including racking and reinforcement, the expenses are comparable as shown in Table 3. The cost of racking for a roof is considerably higher than installing flexible panels with adhesive to the surface. Additionally, flexible panels offer the advantage of reduced weight.

### 5.2.3 Annual load assumed of an ambulance

Typical loads connected to an ambulance are calculated around 50-70W, which consumes a total of 375Whr energy per day and provides backup between 4-10hr depending on device. Considering all of them having 10hr back up, would result in around 500Whr energy consumption while the hourly load is 50W for all the devices. An 8,760 hourly data has been prepared considering the medical instrument inside the ambulance charges and consumes power at constant rate of 50W for 10 hrs., from 8AM -6PM. The result of the PV and battery sizing calculations described above resulted in a total of 182.5kWhr of energy required yearly. The monthly loads for the ambulance, based on previous considerations, are shown in Figure 5.3. Although the daily loads are assumed to be equal, the variation in monthly is due to the differing total number of days in each month.

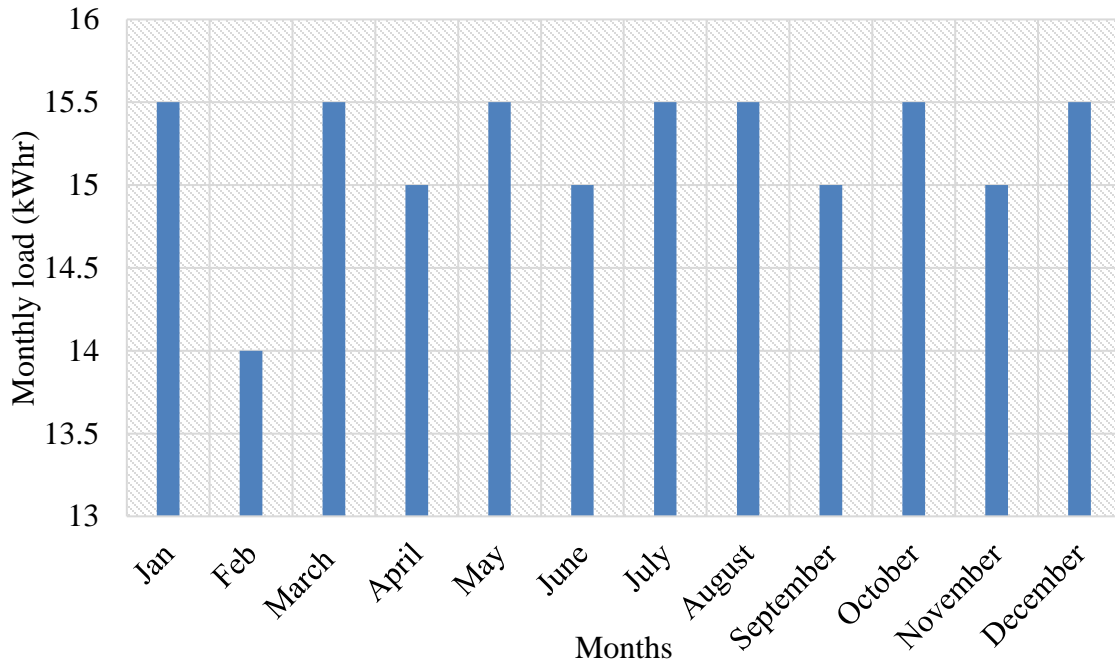


**Figure 5.3** Monthly load assumed of an ambulance.

#### 5.2.4 Simulation of PV and battery

Using SAMA [140], an open-source PV system optimization software, multiple PV and battery configuration cases were obtained for two locations: Addis Ababa, Ethiopia, and London, Ontario, with a roof tilt angle of 0 degrees. The system employs 175W PV panels by Renogy and a 1 kWh (24V, 50A) LiFePO<sub>4</sub> batteries. London, Ontario, with its winter-dominated climate, experiences lower annual PV energy generation and thus represents a stress-test for the system is case 1 and 2. Addis Ababa, with its favorable solar irradiance profile, is identified as a potential site for deploying a PV-powered ambulance along with the humanitarian need of deployment of ambulance is case 3 and 4. For optimization, four scenarios were considered based on location and the number of PV panels. The system's net present cost (NPC) was calculated, factoring in the PV installation cost of CAD \$2,750/kW, which include the Flexible PV panel cost and installation cost (\$2250/kW) and cost of the DC nanogrid (\$500 CAD/kW) and the battery cost of CAD \$700/kWh [194]. The optimization parameters are detailed in Table 5.4.

**Table 5.4.** Optimizing PV systems parameters.

Parameters	Value
PV panel specification	175W
PV derating factor	90%
Battery specification	1kW (24V,50Ah)
Total load	182.5kWhr
Lifetime	15 years
Tilt angle	0 degree
Location 1	London, Ontario
Location 2	Addis Ababa
PV installation cost	CAD \$2,745/kW
Battery cost	CAD \$700/kWhr

The sizes of PV and battery along with number of converter modules requirement, wiring and installation plan has already been mentioned in the previous sections. Now in the result section impact of shading of moving vehicle on PV power generation and comparison of PV power generation depending on the mobility of the ambulance will be discussed. The hardware of the nano grid has been implemented and will be tested to validate the stability of supply voltage due to load change in the nano grid.

### 5.2.5 Modification of Nanogrid for ambulance applications

The PV modules are to be installed on the roof of the ambulance, while the converters for the nanogrid can be safely housed in an electrical box as show in Figure 5.4. A Raspberry Pi screen [195] will be placed on the front of the electrical box for monitoring purposes. The optimized system requires 700W of PV modules and two 12V, 50Ah batteries. This setup includes one battery converter module, one PV converter module, and multiple converters to supply 6V and 12V to the ambulance's instruments, as most of the loads range from 6V to 14V. The wiring diagram of the system and the components are showing in Figure 5.5.

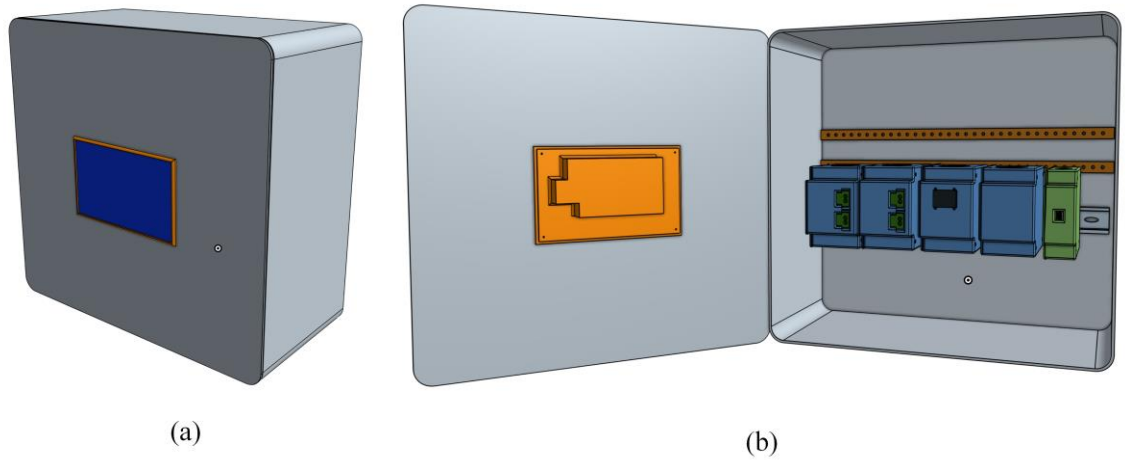


**Figure 5.4** DC nanogrid in electrical box for the ambulance.

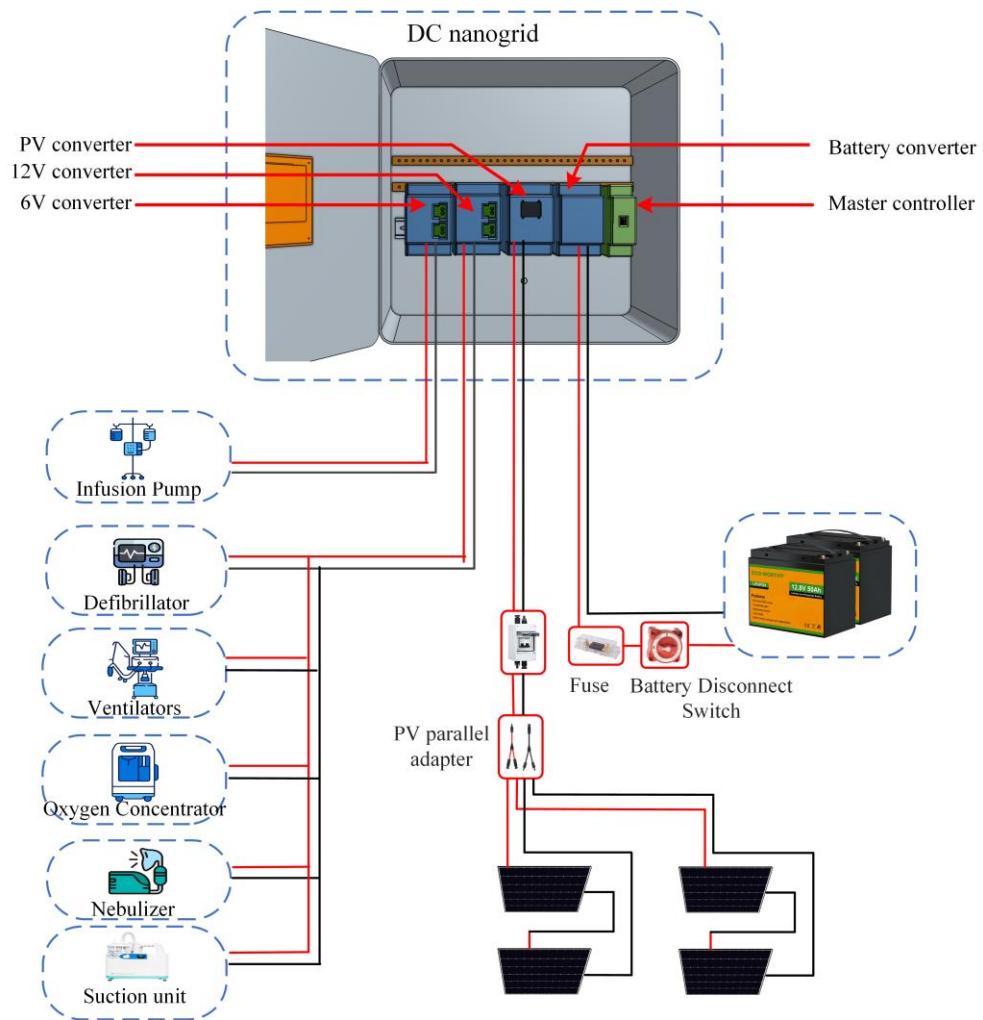


**Figure 5.5** Electrical wiring of an ambulance.

## 5.3 Results

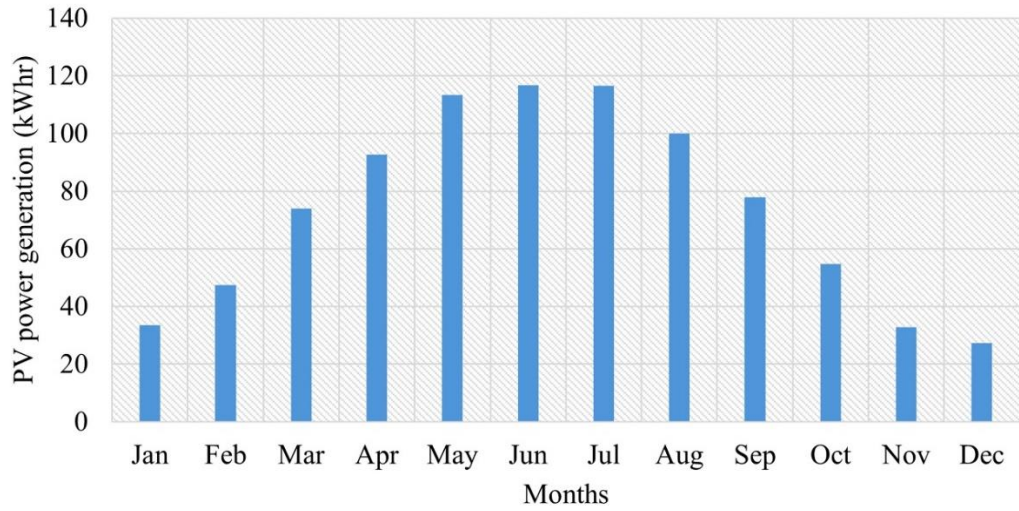
### 5.3.1 PV optimization for the location of London and Addis Ababa

The first two cases focus on London, Ontario, while the other two examine the more favorable PV installation location of Addis Ababa. A comparative study was conducted to identify the optimal scenarios for each location, based on minimizing PV power wastage. All results are summarized in Table 5.5.

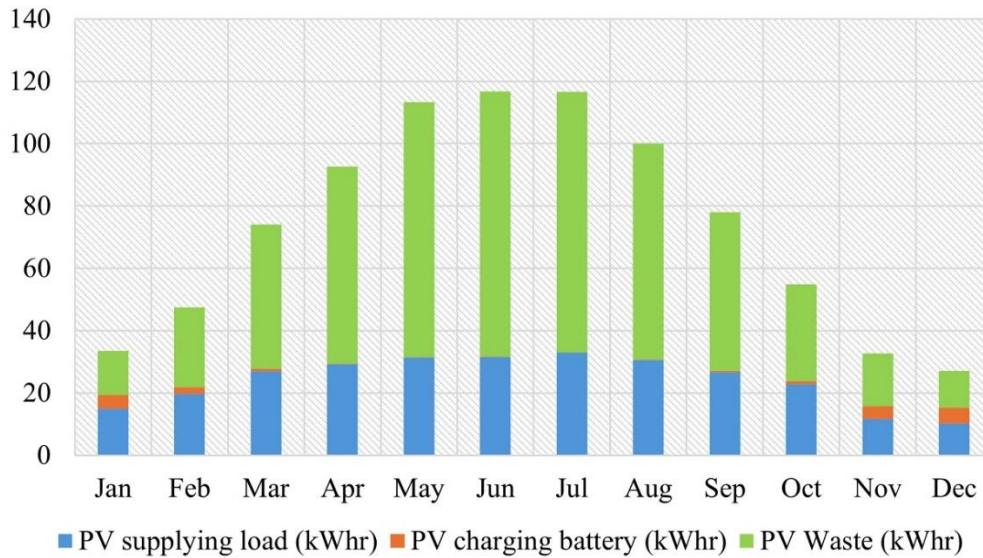
**Table 5.5** Comparison PV system optimization between different cases

Location	London, Ontario, Canada		Addis Ababa, Ethiopia	
Total load served	182.5kWhr		182.5 kWhr	
Cases	Case 1	Case 2	Case 3	Case 4
Optimum PV power	0.7 kW	0.525 kW	0.35kW	0.175kW
Number of PV panel (175W)	4	3	2	1
Optimal battery capacity	1kWhr	2kWhr	1kWhr	2kWhr
NPC (CAD)	\$3,112	\$3820	\$2145	\$2865
PV energy	887 kWhr	658 kWhr	660 kWhr	330 kWhr
PV energy wasted	700 kWhr (79%)	470 kWhr (71%)	478 kWhr (72%)	145 kWhr (44%)

In case 1 for the location of London, Ontario, the optimized result for the PV system was obtained setup consists of four 175W PV panels and two 12V, 50Ah batteries. Where the system's net present cost (NPC) is CAD \$3,112 and it generates a total PV power output of 887 kWh annually, with no AC grid or diesel generator (DG) backup power required shown in Figure 5.6. The annual load served load is 182 kWh and resulting in an excess electricity generation of 700 kWh (79% of total PV power) indicating that more loads such as lighting and cooling/heating also can be operated along with the medical equipment.



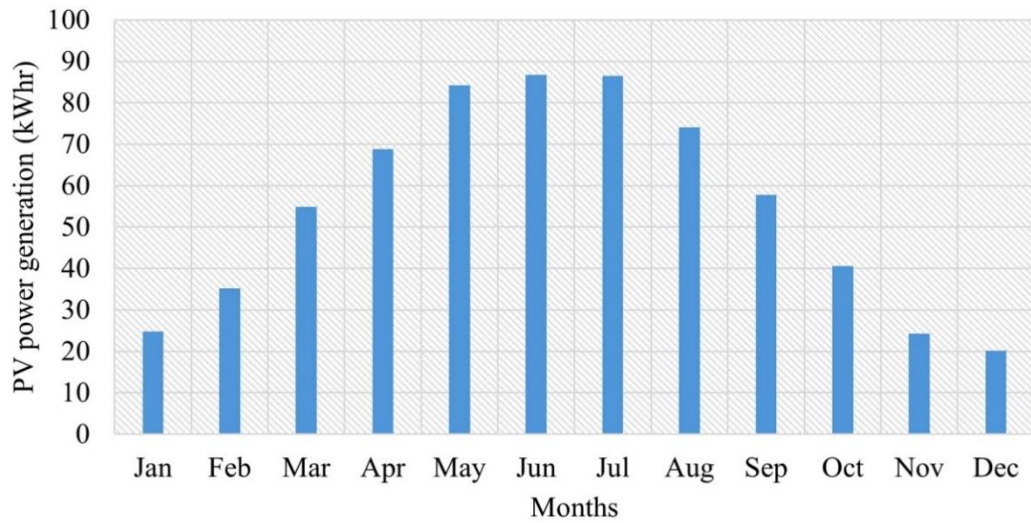
(a)



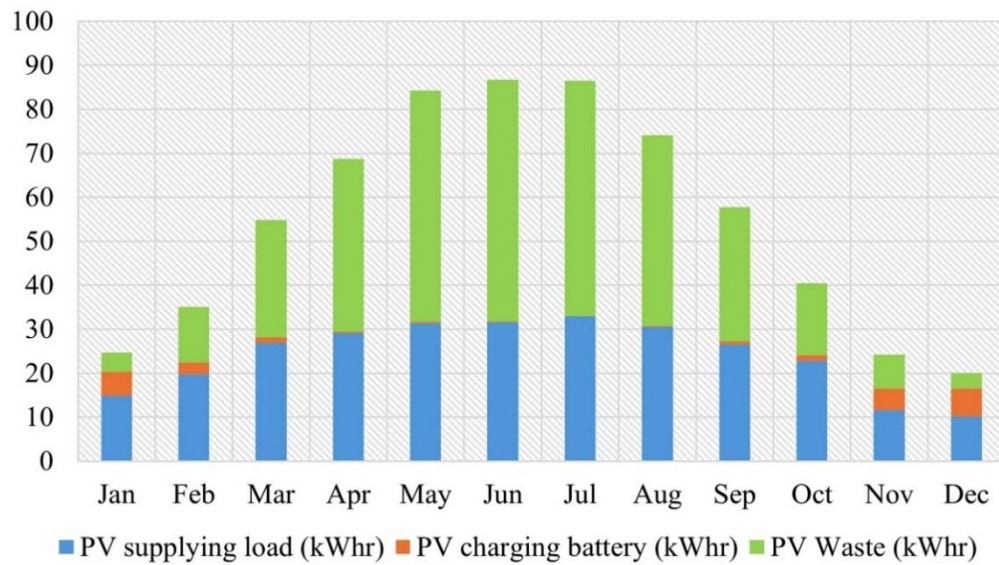
(b)

**Figure 5.6.** Optimized PV and battery performance for London, Ontario (Case 1).

To better utilize PV energy and minimize excess power, additional battery storage can be installed instead of opting for a 700W panel. Based on SAMA optimization, the system should use a 525W PV panel and a 2kWh battery considered as case 2. Where the net present cost of the system is CAD \$3820. And the setup consists of three 175W PV panels and four 12V, 50Ah batteries. The system generates a total PV power output of 658 kWh annually shown in Figure 5.7. The annual load served load is 182 kWh and results in an excess electricity generation of 470 kWh (71% of total PV power).



(a)



(b)

**Figure 5.7.** PV and battery performance with three PV panels and 2kW battery in London, ON (Case 2).

Two more cases have been obtained for the location of Addis Ababa, Ethiopia, and compared with the location of London, Ontario. Based on the irradiance profile of Addis Ababa, a 200W module paired with a 1 kWh battery would be sufficient to meet the load. However, since a 175W panel was selected for this study, two scenarios were: one with a 350W setup (two 175W) shown in Figure 5.8 and another one with only one 175W panel.

Given the consistently high solar irradiance in Addis Ababa, optimization results indicate that a single Renogy 175W module gives better results to meet the load demands throughout the year, when paired with a large 2 kWh battery bank. This configuration minimizes PV power wastage to 145kWhr (44% of total annual PV energy) shown in Figure 5.9. Additional annual performance plots, including the hourly power ratings for the PV system, battery, and load, are presented in Figure 5.10. The variation in the battery's state of charge (SOC) is illustrated in Figure 5.11, summarizing the battery charging cycles.

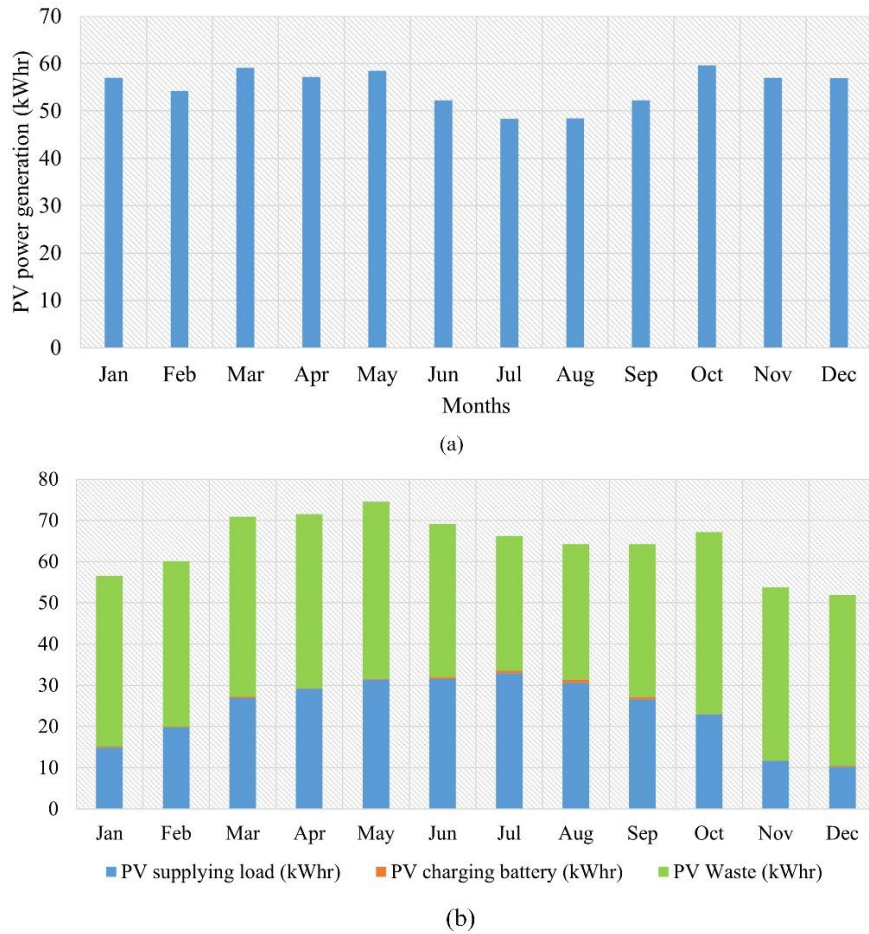
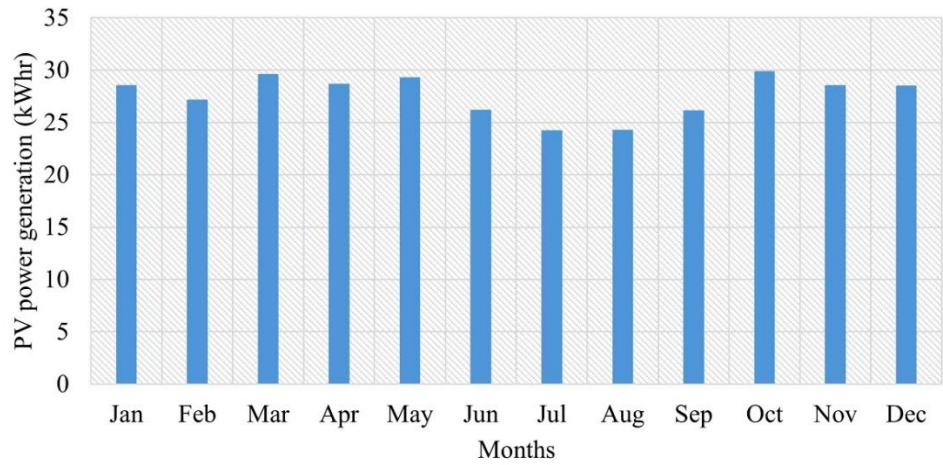
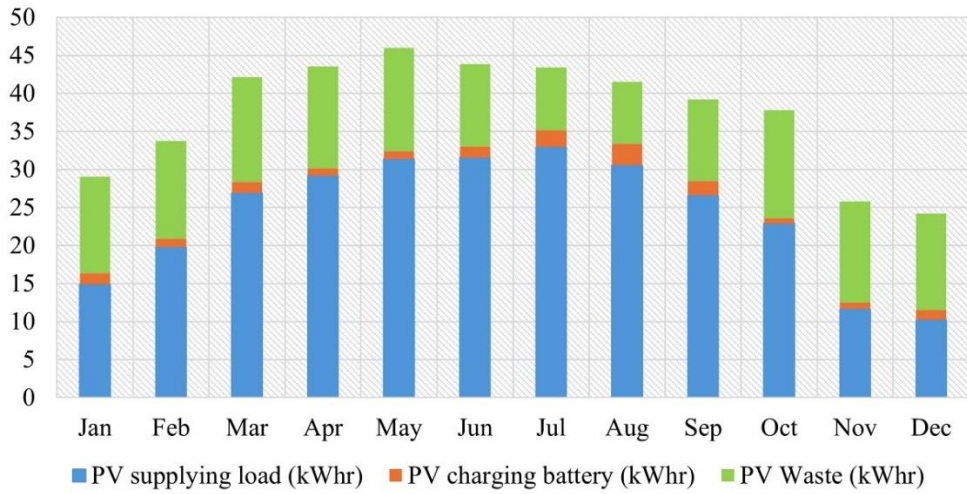


**Figure 5.8.** PV and battery performance with 350 W of PV and 1kW battery for Addis Ababa (Case 3).



(a)



(b)

**Figure 5.9.** PV and battery performance with 175W of PV and 2kW battery for Addis Ababa (Case 4).

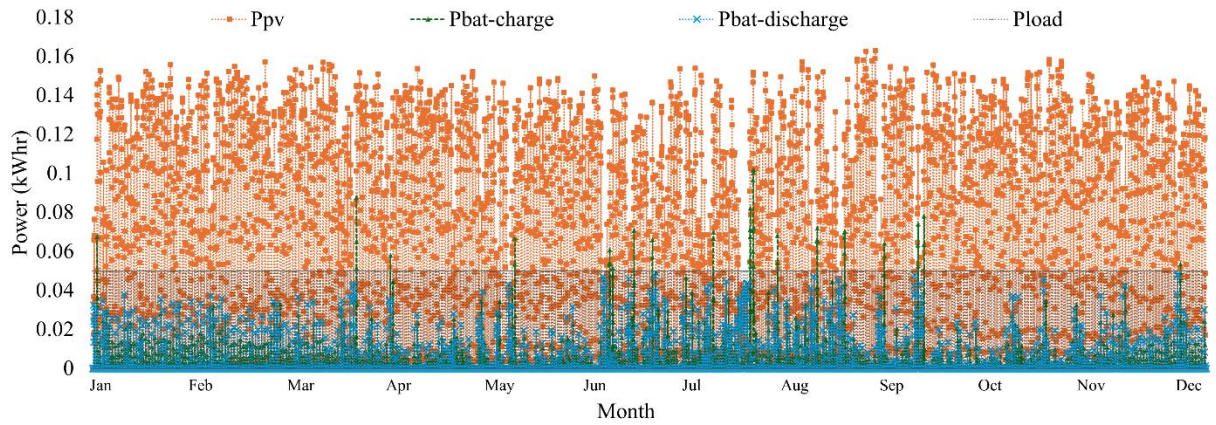


**Figure 5.10.** Hourly PV, load and battery charging/discharging power for case 4 in Addis Ababa.

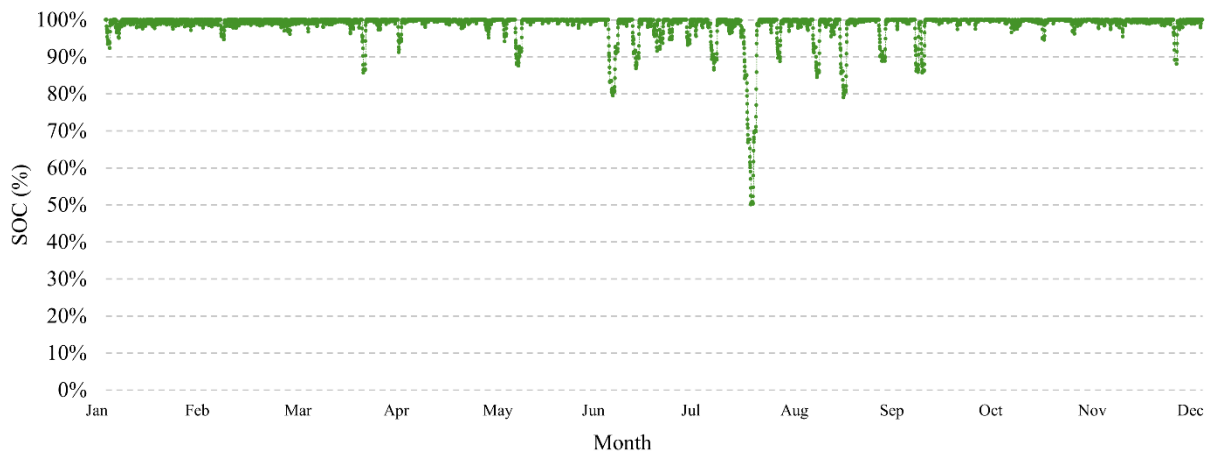


**Figure 5.11.** Battery state of charge hourly for case 4 in Addis Ababa.

### 5.3.2 Final assembled DC nanogrid for Ambulance

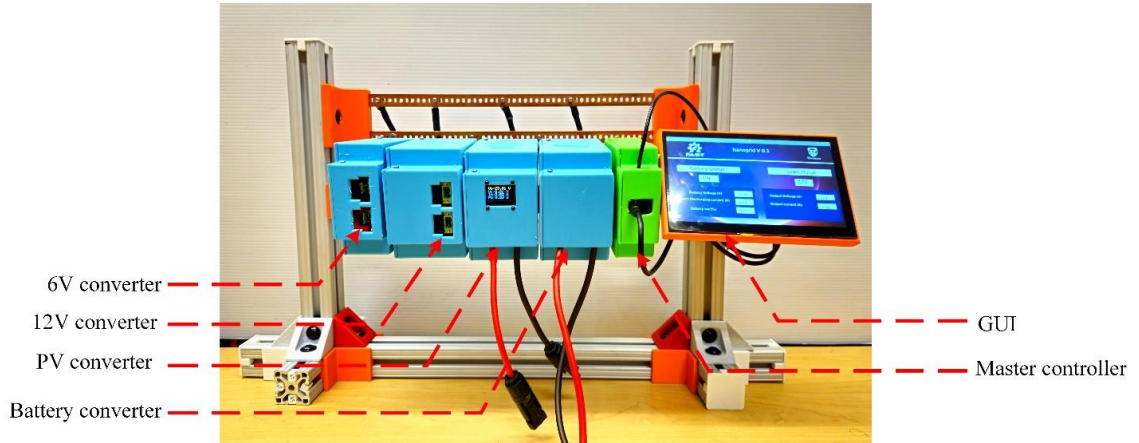


**Figure 5.12.** Hardware of nanogrid for ambulance.

### 5.3.3 Load converters performance under load change

With a 24V bus voltage, the nanogrid can support 6V, 12V, and 24V loads with the hardware shown in Figure 5.12. Two buck converters are connected to the bus bar to supply the required voltages. The system's voltage characteristics were analyzed using an oscilloscope, with load variations applied to the 6V converter (Figure 5.13) and the 12V converter (Figure 5.14), while monitoring the bus voltage. During testing, a new load was introduced and then disconnected after 30 seconds to observe the DC nanogrid's performance. Results indicate that the bus and output voltages drop slightly when a load is

added but quickly stabilize at their respective levels (24V, 12V, and 6V). This confirms that the system is capable of reliably supplying DC loads at the required voltage levels.



**Figure 5.13.** Bus voltage and 6V converter voltage variation due to load change (0-70sec)



**Figure 5.14.** Bus voltage and 12V converter voltage variation due to load change (0-70sec)

## 5.4 Discussion

To power ambulances and mini clinics, a DC nanogrid offers the advantages of modularity, adaptability, and wide accessibility. Simple modifications within the vehicle make the nanogrid suitable for this application. The system can also support future loads, battery backups, and PV installations. Deploying this type of ambulance or mini-clinic equipped

with a PV power system can ensure uninterrupted electricity for healthcare services, especially in areas with limited or no electricity access. This off-grid solution facilitates the establishment of remote healthcare services and camps, enabling reliable healthcare delivery in underserved regions. Also, in response to power outages and natural disasters, deploying renewable-powered vehicles or camps is crucial. For example, the 2015 earthquake in Nepal highlighted this need when widespread power outages and the destruction of 446 public health facilities, including 5 hospitals, severely impacted healthcare delivery, resulting in 9,000 deaths and over 23,000 injuries [196]. Remote areas, already lacking adequate services, were particularly vulnerable. The situation underscored the importance of alternative power sources like generators and sustainable batteries, with solar power emerging as a viable solution for maintaining essential healthcare services in such critical situations

Previous initiatives have aimed to deliver off-grid, reliable power to mini-clinics and healthcare camps. In rural Morocco, a hybrid power system incorporating a diesel generator, PV system, and battery storage was simulated to assess its feasibility for powering off-grid healthcare centers. Moreover, PV hybrid power systems are proposed as essential for mobile medical units or field hospitals, particularly during pandemics, ensuring consistent healthcare delivery in disaster-affected or remote areas [197].

The proposed DC nanogrid for ambulances and remote healthcare camps not only supports renewable clean energy but also offers a modular, plug-and-play design, making it ideal for quick deployment and installation. The availability of flexible PV panels enhances the compatibility of the DC nanogrid with existing ambulances, eliminating the need for any modifications to the vehicles. The PV optimization for an assumed annual load of 182.5 kWh considered four different scenarios across two locations: London, Canada, and Addis Ababa, Ethiopia. Due to the higher average solar flux in Addis Ababa, only one PV panel is sufficient to support the required load, while at least three PV panels are needed in London. With maximum roof installation capacity of 1050 kW, this suggests that additional loads within the ambulance, such as cooling/heating and lighting, can be supported in both London and Addis Ababa by installing more PV panels and batteries based on the updated load profile. The connection and load requirements for these additional systems are an

opportunity for future work where further research could explore load calculations and their integration with an expanded DC nanogrid system.

While the ambulance is moving or parked in shaded areas can lead to lower-than-estimated PV power generation, which is arbitrary and difficult to predict accurately. Mini clinics and camps that provide emergency or temporary medical services throughout the day, however, can fully benefit by strategically placing the vehicle or camp under direct sunlight. Additionally, excess PV power, ranging from 40-80%, can help compensate for this variability or energy loss due to the unpredictability of PV generation in a moving vehicle or mini clinic. Furthermore, the nanogrid system within the ambulance is capable of handling loads at 6V, 12V, and 24V. If any other voltage levels are required, a buck converter should be assembled with inductor size of closest voltage level, and the code must be adjusted to select the appropriate reference voltage. For any existing AC loads in the system, an inverter module compatible with the nanogrid should be designed to support those AC loads.

The PV system optimization and performance comparison between London, a developed location with advanced emergency healthcare facilities and Addis Ababa a developing region with unreliable emergency healthcare, not only underscores the urgent need to improve emergency healthcare services in countries like Ethiopia but also demonstrates that the higher solar irradiance and superior PV performance in Addis Ababa, Ethiopia further validate the viability of the proposed PV-powered ambulance utilizing a nanogrid as a practical solution.

## Chapter 6

### 6 Conclusions and Future scope

This thesis presents a modular nanogrid for the first time, aimed at reducing complexity in PV system installation and conversion, and enhancing accessibility for lower power applications. It explores its use in ambulances and mini clinics. This chapter will discuss additional applications, modifications, and future for the nanogrid in the following sections.

#### 6.1 Conclusions

The aim of this project was to make PV systems more accessible to the general users and simplify their installation. The DC nanogrid was identified as a promising structure for a modular PV system. A detailed study of the architecture and converter topology suitable for a DC nanogrid was conducted, followed by the development of a novel energy management system through simulation and mathematical modeling. Initially, a protoboard version of the nanogrid was developed, which evolved and eventually led to the creation of a final version. This final version included PV power harvesting, bidirectional battery charging/discharging, system monitoring, and data logging. All these developments have been made open-source, with PCB designs, 3-D printed parts, and code available in an open-source repository.

This modular system enables an average user to plug and play the nanogrid system in any electrical panel with additional protection equipment such as fuses and circuit breakers when connecting the PV and battery to the system. The number of converters required will depend on the size of the battery, PV, and load. The system's best feature, however, is its ability to accommodate additional load, PV, or battery with the existing DC bus and communication system. New types of converters, such as adjustable DC-DC converters and inverters, can also be integrated with the same bus system, enhancing its adaptability. The need for an accessible PV system has been long overdue, and this system meets expectations of modularity and adaptability. Additionally, the DC nanogrid could be a viable solution for powering single households, expedition vehicles, and laboratory power

supplies that are off grid. Further research can make this system a promising alternative to conventional PV systems.

## 6.2 Thesis contributions

This work introduces a modular photovoltaic system architecture that is both adaptable and adjustable, along with a new energy management system (EMS) to control the overall operation of the nanogrid. It also demonstrates how a DC nanogrid can serve as a general solution for various application-specific requirements.

This is the first modular PV hardware system utilizing nanogrid architecture that integrates PV, battery, and load, while also establishing a communication framework to manage the flow of information and commands.

Additionally, the project addresses the urgent need for reliable electricity in emergency healthcare systems in Africa and South Asia, analyzing the potential applications of nanogrid systems and providing viable solutions.

### 6.2.1 Publications from this thesis

M. M. Rahman and J. Pearce, “Modular Open Source Solar Photovoltaic-Powered DC Nanogrids with Efficient Energy Management System,” *Solar Energy and Sustainable Development Journal*, vol. 13, no. 1, Art. no. 1, Feb. 2024, doi: 10.51646/jsesd.v13i1.169.

M. M. Rahman, S Khan and J. Pearce, “Open-source Hardware Design of Modular Solar DC Nanogrid,” (to be published).

M. M. Rahman, S Khan, KS Hayibo and J. Pearce, “An Application of a Modular Open-Source Solar Photovoltaic-Powered DC Nanogrid to Ambulances,” (to be published)

## 6.3 Future scope

In the current version of the nanogrid, two minor modifications can be made. First, the PV converter communication is currently isolated, and it uses its own display to show the status. There is already a facility that allows the PV converter to be connected to the same I<sup>2</sup>C bus, however. This connection is currently avoided due to potential interruptions

caused by the master controller and other ADCs connected to the I<sub>2</sub>C bus. The second modification involves developing a more interactive GUI, which would allow sending commands and setting parameters and operation modes using the display which would make it more user friendly.

Although the integration plan and feasibility analysis for powering an ambulance using a DC nanogrid have been conducted, most of the existing loads considered here are designed to run on DC. Due to the prevalence of existing AC instruments, however, a plan to convert these loads to function with a DC supply needs to be assessed.

Even in small-scale systems, there may be loads that are only AC compatible or not yet made DC compatible. For these applications, an inverter module connected to the 48V bus is required. An open-source inverter developed in [135] can be modified and utilized in nanogrid applications. The necessary modifications include making it compatible with 48V and extracting the inverter's status through the same communication bus.

The open-source DC nanogrid can also be utilized to create battery charging kiosks in off-grid communities, providing battery charging facilities at various voltage levels. Customers could swap their discharged electric vehicle batteries for charged ones at these kiosks. The batteries in the kiosks would be charged during the day using PV power, reducing dependency on the grid, especially for nighttime charging. This approach would optimize the utilization of PV energy.

## References

- [1] J. Schonbergerschonberger, R. Duke, and S. D. Round, "DC-Bus Signaling: A Distributed Control Strategy for a Hybrid Renewable Nanogrid," *IEEE Transactions on Industrial Electronics*, vol. 53, no. 5, pp. 1453–1460, Oct. 2006, doi: 10.1109/TIE.2006.882012.
- [2] M. C. Kinn, "Proposed components for the design of a smart nano-grid for a domestic electrical system that operates at below 50V DC," in *2011 2nd IEEE PES International Conference and Exhibition on Innovative Smart Grid Technologies*, Dec. 2011, pp. 1–7. doi: 10.1109/ISGTEurope.2011.6162674.
- [3] S. Nag, R. Adda, O. Ray, and S. Mishra, *Current-Fed Switched Inverter based hybrid topology for DC Nanogrid application*. 2013, p. 7151. doi: 10.1109/IECON.2013.6700320.
- [4] H. Gelani, F. Dastgeer, M. Nasir, S. Khan, and J. Guerrero, "AC vs. DC Distribution Efficiency: Are We on the Right Path?," *Energies*, vol. 14, p. 4039, Jul. 2021, doi: 10.3390/en14134039.
- [5] D. Boroyevich, I. Cvetkovic, D. Dong, R. Burgos, F. Wang, and F. Lee, "Future electronic power distribution systems a contemplative view," *2010 12th International Conference on Optimization of Electrical and Electronic Equipment*, pp. 1369–1380, May 2010, doi: 10.1109/OPTIM.2010.5510477.
- [6] M. M. H. Sajeeb, A. Rahman, and S. Arif, "Feasibility analysis of solar DC Nano grid for off grid rural Bangladesh," in *2015 3rd International Conference on Green Energy and Technology (ICGET)*, Sep. 2015, pp. 1–5. doi: 10.1109/ICGET.2015.7315109.
- [7] M. R. Khan and E. D. Brown, "DC nanogrids: A low cost PV based solution for livelihood enhancement for rural Bangladesh," in *2014 3rd International Conference on the Developments in Renewable Energy Technology (ICDRET)*, May 2014, pp. 1–5. doi: 10.1109/ICDRET.2014.6861687.
- [8] S. Mishra and O. Ray, "Advances in nanogrid technology and its integration into rural electrification in India," in *2014 International Power Electronics Conference (IPEC-Hiroshima 2014 - ECCE ASIA)*, May 2014, pp. 2707–2713. doi: 10.1109/IPEC.2014.6869973.
- [9] B. Tudu, K. K. Mandal, and N. Chakraborty, "Optimal design and development of PV-wind-battery based nano-grid system: A field-on-laboratory demonstration," *Front. Energy*, vol. 13, no. 2, pp. 269–283, Jun. 2019, doi: 10.1007/s11708-018-0573-z.
- [10] E. Hamatwi, I. E. Davidson, J. Agee, and G. Venayagamoorthy, "Model of a hybrid distributed generation system for a DC nano-grid," in *2016 Clemson University*

- Power Systems Conference (PSC)*, Mar. 2016, pp. 1–8. doi: 10.1109/PSC.2016.7462851.
- [11] A. T. Dahiru and C. W. Tan, “Optimal sizing and techno-economic analysis of grid-connected nanogrid for tropical climates of the Savannah,” *Sustainable Cities and Society*, vol. 52, p. 101824, Jan. 2020, doi: 10.1016/j.scs.2019.101824.
- [12] D. Dong, I. Cvetkovic, D. Boroyevich, W. Zhang, R. Wang, and P. Mattavelli, “Grid-Interface Bidirectional Converter for Residential DC Distribution Systems—Part One: High-Density Two-Stage Topology,” *IEEE Transactions on Power Electronics*, vol. 28, no. 4, pp. 1655–1666, Apr. 2013, doi: 10.1109/TPEL.2012.2212462.
- [13] V. Sudev and S. Parvathy, “Switched boost inverter based Dc nanogrid with battery and bi-directional converter,” in *2014 International Conference on Circuits, Power and Computing Technologies [ICCPCT-2014]*, Mar. 2014, pp. 461–467. doi: 10.1109/ICCPCT.2014.7054920.
- [14] S. I. Ganesan, D. Pattabiraman, R. K. Govindarajan, M. Rajan, and C. Nagamani, “Control Scheme for a Bidirectional Converter in a Self-Sustaining Low-Voltage DC Nanogrid,” *IEEE Transactions on Industrial Electronics*, vol. 62, no. 10, pp. 6317–6326, Oct. 2015, doi: 10.1109/TIE.2015.2424192.
- [15] H. H. Sathler, L. H. Sathler, F. L. F. Marcelino, T. R. de Oliveira, S. I. Seleme, and P. F. D. Garcia, “A comparative efficiency study on bidirectional grid interface converters applied to low power DC nanogrids,” in *2017 Brazilian Power Electronics Conference (COBEP)*, Nov. 2017, pp. 1–6. doi: 10.1109/COBEP.2017.8257219.
- [16] F. Queiroz, P. Praça, A. Freitas, and F. Antunes, “High-Gain Bidirectional DC-DC Converter for Battery Charging in DC Nanogrid of Residential Prosumer,” in *2019 IEEE 15th Brazilian Power Electronics Conference and 5th IEEE Southern Power Electronics Conference (COBEP/SPEC)*, Dec. 2019, pp. 1–6. doi: 10.1109/COBEP/SPEC44138.2019.9065631.
- [17] P. C. D. Goud and R. Gupta, “Solar PV based nanogrid integrated with battery energy storage to supply hybrid residential loads using single-stage hybrid converter,” *IET Energy Systems Integration*, vol. 2, no. 2, pp. 161–169, 2020, doi: 10.1049/iet-esi.2019.0030.
- [18] A. R. Saxena and A. Kulshreshtha, “A fourth-order bidirectional DC–DC converter for interfacing battery in a solar -photovoltaic-fed low-voltage residential DC nanogrid: Design and analysis,” *International Journal of Circuit Theory and Applications*, vol. 49, no. 7, pp. 1932–1958, 2021, doi: 10.1002/cta.3016.

- [19] N. J. Bodele and P. S. Kulkarni, “Modular battery-integrated bidirectional single-stage DC–DC converter for solar PV based DC Nano-grid application,” *Solar Energy*, vol. 259, pp. 1–14, Jul. 2023, doi: 10.1016/j.solener.2023.04.040.
- [20] M. H. Shwehdi and S. R. Mohamed, “Proposed smart DC nano-grid for green buildings — A reflective view,” in *2014 International Conference on Renewable Energy Research and Application (ICRERA)*, Oct. 2014, pp. 765–769. doi: 10.1109/ICRERA.2014.7016488.
- [21] T. Taufik and M. Muscarella, “Development of DC house prototypes as demonstration sites for an alternate solution to rural electrification,” in *2016 6th International Annual Engineering Seminar (InAES)*, Aug. 2016, pp. 262–265. doi: 10.1109/INAES.2016.7821945.
- [22] S. S. Nag, S. Mandal, and S. Mishra, “Solar PV based DC power supply for rural homes with analog, multiplier-less MPPT controller,” in *IECON 2017 - 43rd Annual Conference of the IEEE Industrial Electronics Society*, Oct. 2017, pp. 2689–2694. doi: 10.1109/IECON.2017.8216452.
- [23] S. C. Joseph, S. Ashok, and P. R. Dhanesh, “Low voltage direct current(LVDC) nanogrid for home application,” in *2017 IEEE Region 10 Symposium (TENSYMP)*, Jul. 2017, pp. 1–5. doi: 10.1109/TENCONSpring.2017.8069993.
- [24] I. Cvetkovic *et al.*, “Future home DC-based renewable energy nanoGrid system,” in *Proceedings of the 2010 Conference on Grand Challenges in Modeling & Simulation*, in GCMS '10. Vista, CA: Society for Modeling & Simulation International, Jul. 2010, pp. 337–343.
- [25] Ó. Lucía, I. Cvetkovic, H. Sarnago, D. Boroyevich, P. Mattavelli, and F. C. Lee, “Design of Home Appliances for a DC-Based Nanogrid System: An Induction Range Study Case,” *IEEE Journal of Emerging and Selected Topics in Power Electronics*, vol. 1, no. 4, pp. 315–326, Dec. 2013, doi: 10.1109/JESTPE.2013.2283224.
- [26] I. Cvetkovic *et al.*, “A testbed for experimental validation of a low-voltage DC nanogrid for buildings,” in *2012 15th International Power Electronics and Motion Control Conference (EPE/PEMC)*, Sep. 2012, p. LS7c.5-1-LS7c.5-8. doi: 10.1109/EPEPEMC.2012.6397514.
- [27] T.-F. Wu, Y.-K. Chen, G.-R. Yu, and Y.-C. Chang, “Design and development of dc-distributed system with grid connection for residential applications,” in *8th International Conference on Power Electronics - ECCE Asia*, May 2011, pp. 235–241. doi: 10.1109/ICPE.2011.5944591.
- [28] D. Nilsson and A. Sannino, “Load modelling for steady-state and transient analysis of low-voltage dc systems,” in *Conference Record of the 2004 IEEE Industry Applications Conference, 2004. 39th IAS Annual Meeting.*, Oct. 2004, pp. 774–780 vol.2. doi: 10.1109/IAS.2004.1348502.

- [29] M. A. Cordova-Fajardo and E. S. Tututi, “Incorporating home appliances into a DC home nanogrid,” *J. Phys.: Conf. Ser.*, vol. 1221, no. 1, p. 012048, Jun. 2019, doi: 10.1088/1742-6596/1221/1/012048.
- [30] S. Moussa, M. J.-B. Ghorbal, and I. Slama-Belkhodja, “Bus voltage level choice for standalone residential DC nanogrid,” *Sustainable Cities and Society*, vol. 46, p. 101431, Apr. 2019, doi: 10.1016/j.scs.2019.101431.
- [31] M. Mottaghi, M. Rahman, A. Kulkarni, and J. M. Pearce, “AC/off-grid photovoltaic powered open-source ball mill,” *HardwareX*, vol. 14, p. e00423, Jun. 2023, doi: 10.1016/j.ohx.2023.e00423.
- [32] M. M. Rahman, G. Antonini, and J. Pearce, “Open-Source DC-DC Converter Enabling Direct Integration of Solar Photovoltaics with Anion Exchange Membrane Electrolyzer for Green Hydrogen Production,” Jul. 22, 2024, *Preprints: 2024071698*. doi: 10.20944/preprints202407.1698.v1.
- [33] M. M. Rahman and J. M. Pearce, “Open-source portable solar power supply unit for plasma generator,” Jan. 2024, Accessed: Jan. 08, 2024. [Online]. Available: <https://osf.io/nksef/>
- [34] N. Pulsiri, R. Vatananan-Thesenvitz, T. Sirisamutr, and P. Wachiradilok, “Save Lives: A Review of Ambulance Technologies in Pre-Hospital Emergency Medical Services,” in *2019 Portland International Conference on Management of Engineering and Technology (PICMET)*, Aug. 2019, pp. 1–10. doi: 10.23919/PICMET.2019.8893973.
- [35] I. Kant, *Foundations of the Metaphysics of Morals: And What is Enlightenment?* Liberal Arts Press, 1959.
- [36] The World Bank, “Saving One Life Every 30 Minutes,” World Bank. Accessed: Aug. 05, 2024. [Online]. Available: <https://www.worldbank.org/en/news/feature/2014/03/10/saving-one-life-every-30-minutes>
- [37] T. D. Rea, M. S. Eisenberg, L. L. Culley, and L. Becker, “Dispatcher-assisted cardiopulmonary resuscitation and survival in cardiac arrest,” *Circulation*, vol. 104, no. 21, pp. 2513–2516, Nov. 2001, doi: 10.1161/hc4601.099468.
- [38] D. P. Zipes, “Saving Time Saves Lives,” *Circulation*, vol. 104, no. 21, pp. 2506–2508, Nov. 2001, doi: 10.1161/circ.104.21.2506.
- [39] M. S. Varghese, E. Pérez, and A. L. Schwarz, “A Systems Engineering Approach to Designing a Mobile Assessment Clinic for Patients in Need of Assistive Technology,” *IISE Annual Conference. Proceedings*, pp. 1166–1171, 2019.
- [40] R. Tarek, A. Anjum, M. A. Hoque, and A. Azad, “Solar electric ambulance van unfolding medical emergencies of rural Bangladesh,” in *2016 IEEE Global*

- Humanitarian Technology Conference (GHTC)*, Oct. 2016, pp. 514–519. doi: 10.1109/GHTC.2016.7857328.
- [41] Y. B. Aemro, P. Moura, and A. T. de Almeida, “Energy access during and post-COVID-19 pandemic in sub-Saharan countries: the case of Ethiopia,” *Environ Dev Sustain*, vol. 25, no. 2, pp. 1236–1257, Feb. 2023, doi: 10.1007/s10668-021-02090-9.
- [42] M. Moner-Girona, G. Kakoulaki, G. Falchetta, D. J. Weiss, and N. Taylor, “Achieving universal electrification of rural healthcare facilities in sub-Saharan Africa with decentralized renewable energy technologies,” *Joule*, vol. 5, no. 10, pp. 2687–2714, Oct. 2021, doi: 10.1016/j.joule.2021.09.010.
- [43] WHO, “Strategic Roadmap on Health and Energy.” Accessed: Aug. 02, 2024. [Online]. Available: <https://www.who.int/initiatives/health-and-energy-platform-of-action/high-level-coalition-on-health-and-energy/strategic-roadmap-on-health-and-energy>
- [44] M. Mango, J. A. Casey, and D. Hernández, “Resilient Power: A home-based electricity generation and storage solution for the medically vulnerable during climate-induced power outages,” *Futures*, vol. 128, p. 102707, Apr. 2021, doi: 10.1016/j.futures.2021.102707.
- [45] E. Zio and R. B. Duffey, “Chapter 12 - The risk of the electrical power grid due to natural hazards and recovery challenge following disasters and record floods: What next?,” in *Climate Change and Extreme Events*, A. Fares, Ed., Elsevier, 2021, pp. 215–238. doi: 10.1016/B978-0-12-822700-8.00008-1.
- [46] H. T. Debas, P. Donkor, A. Gawande, D. T. Jamison, M. E. Kruk, and C. N. Mock, Eds., *Essential Surgery: Disease Control Priorities, Third Edition (Volume 1)*. Washington (DC): The International Bank for Reconstruction and Development / The World Bank, 2015. Accessed: Aug. 05, 2024. [Online]. Available: <http://www.ncbi.nlm.nih.gov/books/NBK333500/>
- [47] “Take Action for the Sustainable Development Goals - United Nations Sustainable Development.” Accessed: Nov. 08, 2022. [Online]. Available: <https://www.un.org/sustainabledevelopment/sustainable-development-goals/>
- [48] “Report: Universal Access to Sustainable Energy Will Remain Elusive Without Addressing Inequalities,” World Bank. Accessed: Nov. 08, 2022. [Online]. Available: <https://www.worldbank.org/en/news/press-release/2021/06/07/report-universal-access-to-sustainable-energy-will-remain-elusive-without-addressing-inequalities>
- [49] J. Ayaburi, M. Bazilian, J. Kincer, and T. Moss, “Measuring ‘Reasonably Reliable’ access to electricity services,” *The Electricity Journal*, vol. 33, no. 7, p. 106828, Aug. 2020, doi: 10.1016/j.tej.2020.106828.

- [50] S. Szabó, K. Bódis, T. Huld, and M. Moner-Girona, “Energy solutions in rural Africa: mapping electrification costs of distributed solar and diesel generation versus grid extension\*,” *Environ. Res. Lett.*, vol. 6, no. 3, p. 034002, Jul. 2011, doi: 10.1088/1748-9326/6/3/034002.
- [51] D. Palit and K. R. Bandyopadhyay, “Rural electricity access in South Asia: Is grid extension the remedy? A critical review,” *Renewable and Sustainable Energy Reviews*, vol. 60, pp. 1505–1515, Jul. 2016, doi: 10.1016/j.rser.2016.03.034.
- [52] M. Kintner-Meyer, K. Schneider, and R. Pratt, “Impacts Assessment of Plug-In Hybrid Vehicles on Electric Utilities And Regional U.S. Power Grids Part 1: Technical Analysis,” p. 20, *Pacific Northwest National Laboratory* (2007).
- [53] C. F. Yu, W. G. J. H. M. van Sark, and E. A. Alsema, “Unraveling the photovoltaic technology learning curve by incorporation of input price changes and scale effects,” *Renewable and Sustainable Energy Reviews*, vol. 15, no. 1, pp. 324–337, Jan. 2011, doi: 10.1016/j.rser.2010.09.001.
- [54] A. M. Elshurafa, S. R. Albardi, S. Bigerna, and C. A. Bollino, “Estimating the learning curve of solar PV balance-of-system for over 20 countries: Implications and policy recommendations,” *Journal of Cleaner Production*, vol. 196, pp. 122–134, Sep. 2018, doi: 10.1016/j.jclepro.2018.06.016.
- [55] M. Kamran *et al.*, “Solar Photovoltaic Grid Parity: A Review of Issues, Challenges and Status of Different PV Markets,” *International Journal of Renewable Energy Research (IJRER)*, vol. 9, no. 1, Art. no. 1, Mar. 2019.
- [56] A. A. Adesanya and J. M. Pearce, “Economic viability of captive off-grid solar photovoltaic and diesel hybrid energy systems for the Nigerian private sector,” *Renewable and Sustainable Energy Reviews*, vol. 114, p. 109348, Oct. 2019, doi: 10.1016/j.rser.2019.109348.
- [57] A. M. Ershad, F. Ueckerdt, R. C. Pietzcker, A. Giannousakis, and G. Luderer, “A further decline in battery storage costs can pave the way for a solar PV-dominated Indian power system,” *Renewable and Sustainable Energy Transition*, vol. 1, p. 100006, Aug. 2021, doi: 10.1016/j.rset.2021.100006.
- [58] N. M. Kumar, A. K. Singh, and K. V. K. Reddy, “Fossil Fuel to Solar Power: A Sustainable Technical Design for Street Lighting in Fugar City, Nigeria,” *Procedia Computer Science*, vol. 93, pp. 956–966, Jan. 2016, doi: 10.1016/j.procs.2016.07.284.
- [59] P. Primiceri and P. Visconti, “Solar-Powered Led-Based Lighting Facilities: An Overview on Recent Technologies and Embedded Iot Devices to Obtain Wireless Control, Energy Savings and Quick Maintenance,” *Journal of Engineering and Applied Sciences ARPAN*, vol. 12, no. 1, p. 11, 2017.

- [60] M. Dallard, A. Forest, and A. Shabani, "Design of a portable smart connected solar-powered charger for consumer electronics," in *2017 IEEE 30th Canadian Conference on Electrical and Computer Engineering (CCECE)*, Apr. 2017, pp. 1–4. doi: 10.1109/CCECE.2017.7946781.
- [61] A. Verma, B. Singh, A. Chandra, and K. Al-Haddad, "An Implementation of Solar PV Array Based Multifunctional EV Charger," in *2018 IEEE Transportation Electrification Conference and Expo (ITEC)*, Jun. 2018, pp. 531–536. doi: 10.1109/ITEC.2018.8450191.
- [62] M. R. Qtaishat and F. Banat, "Desalination by solar powered membrane distillation systems," *Desalination*, vol. 308, pp. 186–197, Jan. 2013, doi: 10.1016/j.desal.2012.01.021.
- [63] S. McCarney, J. Robertson, J. Arnaud, K. Lorenson, and J. Lloyd, "Using solar-powered refrigeration for vaccine storage where other sources of reliable electricity are inadequate or costly," *Vaccine*, vol. 31, no. 51, pp. 6050–6057, Dec. 2013, doi: 10.1016/j.vaccine.2013.07.076.
- [64] I. Daut, M. Adzrie, M. Irwanto, P. Ibrahim, and M. Fitra, "Solar Powered Air Conditioning System," *Energy Procedia*, vol. 36, pp. 444–453, Jan. 2013, doi: 10.1016/j.egypro.2013.07.050.
- [65] B. Singh, A. K. Mishra, and R. Kumar, "Solar Powered Water Pumping System Employing Switched Reluctance Motor Drive," *IEEE Transactions on Industry Applications*, vol. 52, no. 5, pp. 3949–3957, Sep. 2016, doi: 10.1109/TIA.2016.2564945.
- [66] A. W. Kiprono and A. I. Llario, *Solar pumping for water supply: harnessing solar power in humanitarian and development contexts*. Warwickshire, UK: Practical Action Publishing Ltd, 2020.
- [67] A. Jahid, Md. S. Hossain, Md. K. H. Monju, Md. F. Rahman, and Md. F. Hossain, "Techno-Economic and Energy Efficiency Analysis of Optimal Power Supply Solutions for Green Cellular Base Stations," *IEEE Access*, vol. 8, pp. 43776–43795, 2020, doi: 10.1109/ACCESS.2020.2973130.
- [68] S. Zhong, P. Rakhe, and J. M. Pearce, "Energy Payback Time of a Solar Photovoltaic Powered Waste Plastic Recyclebot System," *Recycling*, vol. 2, no. 2, Art. no. 2, Jun. 2017, doi: 10.3390/recycling2020010.
- [69] D. L. King, A. Babasola, J. Rozario, and J. M. Pearce, "Mobile Open-Source Solar-Powered 3-D Printers for Distributed Manufacturing in Off-Grid Communities," *Challenges in Sustainability*, vol. 2, no. 1, Art. no. 1, Oct. 2014, doi: 10.12924/cis2014.02010018.

- [70] J. Gwamuri, D. Franco, K. Y. Khan, L. Gauchia, and J. M. Pearce, “High-Efficiency Solar-Powered 3-D Printers for Sustainable Development,” *Machines*, vol. 4, no. 1, Art. no. 1, Mar. 2016, doi: 10.3390/machines4010003.
- [71] L. Grafman and J. M. Pearce, *To catch the sun*. Humboldt State Press, 2021.
- [72] S. Khan and Md. M. Rahman, “Design and Simulation of Solar DC Nano Grid System from Bangladesh Perspective,” in *2021 International Conference on Automation, Control and Mechatronics for Industry 4.0 (ACMI)*, Jul. 2021, pp. 1–6. doi: 10.1109/ACMI53878.2021.9528159.
- [73] R. M. Pindoriya, N. M. Pindoriya, and S. Rajendran, “Simulation of DC/DC converter for DC nano-grid integrated with solar PV generation,” in *2015 IEEE Innovative Smart Grid Technologies - Asia (ISGT ASIA)*, Nov. 2015, pp. 1–6. doi: 10.1109/ISGT-Asia.2015.7387065.
- [74] S. Moussa, M. J.-B. Ghorbal, and I. Slama-Belkhdja, “Bus voltage level choice for standalone residential DC nanogrid,” *Sustainable Cities and Society*, vol. 46, p. 101431, Apr. 2019, doi: 10.1016/j.scs.2019.101431.
- [75] J. M. Pearce and M. M. Rahman, “Modular Open Source Solar Photovoltaic-Powered DC Nanogrids with Efficient Energy Management System,” Dec. 2022, Accessed: Dec. 27, 2022. [Online]. Available: <https://osf.io/sv84n/>
- [76] “The GNU General Public License v3.0 - GNU Project - Free Software Foundation.” Accessed: Dec. 27, 2022. [Online]. Available: <https://www.gnu.org/licenses/gpl-3.0.en.html>
- [77] J. Arancio, M. Morales Tirado, and J. Pearce, “Equitable Research Capacity Towards the Sustainable Development Goals: The Case for Open Science Hardware,” *JSPG*, vol. 21, no. 02, Dec. 2022, doi: 10.38126/JSPG210202.
- [78] S. Chopra and S. D. Dexter, *The Promise of Free and Open Source Software*. New York: Routledge, 2007. doi: 10.4324/9780203942147.
- [79] A. J. Buitenhuis and J. M. Pearce, “Open-source development of solar photovoltaic technology,” *Energy for Sustainable Development*, vol. 16, no. 3, pp. 379–388, Sep. 2012, doi: 10.1016/j.esd.2012.06.006.
- [80] J. M. Pearce, “The case for open source appropriate technology,” *Environ Dev Sustain*, vol. 14, no. 3, pp. 425–431, Jun. 2012, doi: 10.1007/s10668-012-9337-9.
- [81] B. Indu Rani, G. Saravana Ilango, and C. Nagamani, “Control Strategy for Power Flow Management in a PV System Supplying DC Loads,” *IEEE Transactions on Industrial Electronics*, vol. 60, no. 8, pp. 3185–3194, Aug. 2013, doi: 10.1109/TIE.2012.2203772.

- [82] Y. Zhang, H. J. Jia, and L. Guo, "Energy management strategy of islanded microgrid based on power flow control," in *2012 IEEE PES Innovative Smart Grid Technologies (ISGT)*, Jan. 2012, pp. 1–8. doi: 10.1109/ISGT.2012.6175644.
- [83] K. Gowtham, C. V. Sivaramadurai, P. Hariprasath, and B. Indurani, "A Management of power flow for DC Microgrid with Solar and Wind Energy Sources," in *2018 International Conference on Computer Communication and Informatics (ICCCI)*, Jan. 2018, pp. 1–5. doi: 10.1109/ICCCI.2018.8441324.
- [84] Z. Yi, W. Dong, and A. H. Etemadi, "A Unified Control and Power Management Scheme for PV-Battery-Based Hybrid Microgrids for Both Grid-Connected and Islanded Modes," *IEEE Transactions on Smart Grid*, vol. 9, no. 6, pp. 5975–5985, Nov. 2018, doi: 10.1109/TSG.2017.2700332.
- [85] L. Xu and D. Chen, "Control and Operation of a DC Microgrid With Variable Generation and Energy Storage," *IEEE Transactions on Power Delivery*, vol. 26, no. 4, pp. 2513–2522, Oct. 2011, doi: 10.1109/TPWRD.2011.2158456.
- [86] H. Fan, W. Yu, and S. Xia, "Review of Control Strategies for DC Nano-Grid," *Front. Energy Res.*, vol. 9, Mar. 2021, doi: 10.3389/fenrg.2021.644926.
- [87] N. Kondrath, "Bidirectional DC-DC converter topologies and control strategies for interfacing energy storage systems in microgrids: An overview," in *2017 IEEE International Conference on Smart Energy Grid Engineering (SEGE)*, Aug. 2017, pp. 341–345. doi: 10.1109/SEGE.2017.8052822.
- [88] M. I. Hlal, V. K. Ramachandaramurthy, A. Sarhan, A. Pouryekta, and U. Subramaniam, "Optimum battery depth of discharge for off-grid solar PV/battery system," *Journal of Energy Storage*, vol. 26, p. 100999, Dec. 2019, doi: 10.1016/j.est.2019.100999.
- [89] I.-K. Won, D.-Y. Kim, J.-H. Hwang, J.-H. Lee, and C.-Y. Won, "Lifetime management method of Lithium-ion battery for energy storage system," in *2015 18th International Conference on Electrical Machines and Systems (ICEMS)*, Oct. 2015, pp. 1375–1380. doi: 10.1109/ICEMS.2015.7385253.
- [90] M. Parandhaman, L. T. S. Annambhotla, and P. Parthiban, "Hardware Prototype for Portable Automatic MPPT Solar Charger Using Buck Converter and PSO Technique," in *2022 IEEE Delhi Section Conference (DELCON)*, Feb. 2022, pp. 1–6. doi: 10.1109/DELCON54057.2022.9764362.
- [91] "Design of Maximum Power Point Tracking Photovoltaic System Based on Incremental Conductance Algorithm using Arduino Uno and Boost Converter," *Applied Technology and Computing Science Journal*, vol. 4, no. 2, pp. 101–112, 2022, doi: <https://doi.org/10.33086/atcsj.v4i2.2450>.

- [92] A. K. Podder, N. K. Roy, and H. R. Pota, "MPPT methods for solar PV systems: a critical review based on tracking nature," *IET Renewable Power Generation*, vol. 13, no. 10, pp. 1615–1632, 2019, doi: 10.1049/iet-rpg.2018.5946.
- [93] Fangrui Liu, Shanxu Duan, Fei Liu, Bangyin Liu, and Yong Kang, "A Variable Step Size INC MPPT Method for PV Systems," *IEEE Trans. Ind. Electron.*, vol. 55, no. 7, pp. 2622–2628, Jul. 2008, doi: 10.1109/TIE.2008.920550.
- [94] N. Karami, N. Moubayed, and R. Outbib, "General review and classification of different MPPT Techniques," *Renewable and Sustainable Energy Reviews*, vol. 68, pp. 1–18, Feb. 2017, doi: 10.1016/j.rser.2016.09.132.
- [95] Md. M. Rahman and M. S. Islam, "Artificial Neural Network Based Maximum Power Point Tracking of a Photovoltaic System," in *2019 3rd International Conference on Electrical, Computer & Telecommunication Engineering (ICECTE)*, Dec. 2019, pp. 117–120. doi: 10.1109/ICECTE48615.2019.9303531.
- [96] Md. M. Rahman and Md. S. Islam, "PSO and ANN Based Hybrid MPPT Algorithm for Photovoltaic Array under Partial Shading Condition," *Eng. int. (Dhaka)*, vol. 8, no. 1, pp. 9–24, Apr. 2020, doi: 10.18034/ei.v8i1.481.
- [97] A. Mohapatra, B. Nayak, P. Das, and K. B. Mohanty, "A review on MPPT techniques of PV system under partial shading condition," *Renewable and Sustainable Energy Reviews*, vol. 80, pp. 854–867, Dec. 2017, doi: 10.1016/j.rser.2017.05.083.
- [98] M. Yaichi, M.-K. Fella, and A. Mammeri, "A Neural Network Based MPPT Technique Controller for Photovoltaic Pumping System," *International Journal of Power Electronics and Drive Systems (IJPEDS)*, vol. 4, no. 2, Art. no. 2, Jun. 2014.
- [99] K. Y. Yap, C. R. Sarimuthu, and J. M.-Y. Lim, "Artificial Intelligence Based MPPT Techniques for Solar Power System: A review," *Journal of Modern Power Systems and Clean Energy*, vol. 8, no. 6, pp. 1043–1059, Nov. 2020, doi: 10.35833/MPCE.2020.000159.
- [100] F. Liu, Y. Kang, Y. Zhang, and S. Duan, "Comparison of P& hill climbing MPPT methods for grid-connected PV converter," in *2008 3rd IEEE Conference on Industrial Electronics and Applications*, Jun. 2008, pp. 804–807. doi: 10.1109/ICIEA.2008.4582626.
- [101] M. M. Ur Rehman, F. Zhang, R. Zane, and D. Maksimovic, "Control of bidirectional DC/DC converters in reconfigurable, modular battery systems," in *2017 IEEE Applied Power Electronics Conference and Exposition (APEC)*, Mar. 2017, pp. 1277–1283. doi: 10.1109/APEC.2017.7930860.
- [102] R. Li and F. Shi, "Control and Optimization of Residential Photovoltaic Power Generation System With High Efficiency Isolated Bidirectional DC–DC Converter," *IEEE Access*, vol. 7, pp. 116107–116122, 2019, doi: 10.1109/ACCESS.2019.2935344.

- [103] P. Murugesan, P. W. David, P. Murugesan, and P. Periyasamy, “Battery based mismatch reduction technique for partial shaded solar PV system,” *Energy*, vol. 272, p. 127063, Jun. 2023, doi: 10.1016/j.energy.2023.127063.
- [104] R. W. Erickson and D. Maksimovic, *Fundamentals of Power Electronics*. Springer Science & Business Media, 2007.
- [105] M. Amin and M. Molinas, “Non-parametric Impedance based Stability and Controller Bandwidth Extraction from Impedance Measurements of HVDC-connected Wind Farms,” Apr. 16, 2017, *arXiv*: arXiv:1704.04800. doi: 10.48550/arXiv.1704.04800.
- [106] M. Amin and M. Molinas, “Small-Signal Stability Assessment of Power Electronics Based Power Systems: A Discussion of Impedance- and Eigenvalue-Based Methods,” *IEEE Transactions on Industry Applications*, vol. 53, no. 5, pp. 5014–5030, Sep. 2017, doi: 10.1109/TIA.2017.2712692.
- [107] M. Habibullah, M. Nadarajah, R. Sharma, and R. Shah, “A Comprehensive Stability Analysis of Multi-Converter-Based DC Microgrids,” *Emerging Power Converters for Renewable Energy and Electric Vehicles*, 2021, pp. 281–314. doi: 10.1201/9781003058472-8.
- [108] M. Habibullah, N. Mithulanathan, F. Zare, and R. Sharma, “Impact of Control Systems on Power Quality at Common DC Bus in DC Grid,” in *2019 IEEE PES GTD Grand International Conference and Exposition Asia (GTD Asia)*, Mar. 2019, pp. 411–416. doi: 10.1109/GTDAsia.2019.8715875.
- [109] X. Feng, J. Liu, and F. C. Lee, “Impedance specifications for stable DC distributed power systems,” *IEEE Transactions on Power Electronics*, vol. 17, no. 2, pp. 157–162, Mar. 2002, doi: 10.1109/63.988825.
- [110] R. Ahmadi, D. Paschedag, and M. Ferdowsi, “Closed-loop input and output impedances of DC-DC switching converters operating in voltage and current mode control,” in *IECON 2010 - 36th Annual Conference on IEEE Industrial Electronics Society*, Nov. 2010, pp. 2311–2316. doi: 10.1109/IECON.2010.5675123.
- [111] M. Habibullah, K. N. Bhukkittipich, N. Mithulanathan, R. Sharma, and F. Zare, “Damping oscillation and removing resonance in a RE based DC microgrids,” *IEEE Access*, vol. 9, pp. 163516–163525, 2021.
- [112] M. Habibullah, N. Mithulanathan, F. Zare, and D. S. Alkaran, “Investigation of power oscillation at common DC bus in DC grid,” in *2019 IEEE International Conference on Industrial Technology (ICIT)*, Feb. 2019, pp. 1695–1700. doi: 10.1109/ICIT.2019.8843694.
- [113] A. Brahimi, D. Kerdoun, and A. Boumassata, “Boost Converter Control using LQR and P&O Technique for Maximum Power Point Tracking,” in *2022 19th*

*International Multi-Conference on Systems, Signals & Devices (SSD)*, May 2022, pp. 1998–2003. doi: 10.1109/SSD54932.2022.9955798.

- [114] K. K. Patri and S. Samanta, “State feedback with integral control for boost converter & its microcontroller implementation,” in *2018 IEEMA Engineer Infinite Conference (eTechNxt)*, Mar. 2018, pp. 1–5. doi: 10.1109/ETECHNXT.2018.8385374.
- [115] S. Gadzanku, A. Kramer, and B. Smith, “An Updated Review of the Solar PV Installation Workforce Literature,” 2023, doi: 10.2172/1971876.
- [116] A. M. Chagas, “Haves and have nots must find a better way: The case for open scientific hardware,” *PLOS Biology*, vol. 16, no. 9, p. e3000014.
- [117] A. Gibb, *Building Open Source Hardware: DIY Manufacturing for Hackers and Makers*. Addison-Wesley Professional, 2014.
- [118] M. M. Rahman and J. Pearce, “Modular Open Source Solar Photovoltaic-Powered DC Nanogrids with Efficient Energy Management System,” *Solar Energy and Sustainable Development Journal*, vol. 13, no. 1, Art. no. 1, Feb. 2024, doi: 10.51646/jsesd.v13i1.169.
- [119] D. Burmester, R. Rayudu, W. Seah, and D. Akinyele, “A review of nanogrid topologies and technologies,” *Renewable and Sustainable Energy Reviews*, vol. 67, pp. 760–775, Jan. 2017, doi: 10.1016/j.rser.2016.09.073.
- [120] P. Cairoli, I. Kondratiev, and R. A. Dougal, “Controlled power sequencing for fault protection in DC nanogrids,” in *2011 International Conference on Clean Electrical Power (ICCEP)*, Jun. 2011, pp. 730–737. doi: 10.1109/ICCEP.2011.6036384.
- [121] M. S. Sadabadi, A. Karimi, and H. Karimi, “Fixed-order decentralized/distributed control of islanded inverter-interfaced microgrids,” *Control Engineering Practice*, vol. 45, pp. 174–193, Dec. 2015, doi: 10.1016/j.conengprac.2015.09.003.
- [122] M. Uddin, H. Mo, D. Dong, S. Elsayah, J. Zhu, and J. M. Guerrero, “Microgrids: A review, outstanding issues and future trends,” *Energy Strategy Reviews*, vol. 49, p. 101127, Sep. 2023, doi: 10.1016/j.esr.2023.101127.
- [123] S. Oberloier, N. G. Whisman, F. Hafting, and J. M. Pearce, “Open source framework for a Broadly Expandable and Reconfigurable data acquisition and automation device (BREAD),” *HardwareX*, vol. 15, p. e00467, Sep. 2023, doi: 10.1016/j.ohx.2023.e00467.
- [124] F. Schmid and F. Behrendt, “Optimal sizing of Solar Home Systems: Charge controller technology and its influence on system design,” *Sustainable Energy Technologies and Assessments*, vol. 45, p. 101198, Jun. 2021, doi: 10.1016/j.seta.2021.101198.

- [125] J. M. Pearce, *Open-Source Lab: How to Build Your Own Hardware and Reduce Research Costs*. Elsevier, 2013.
- [126] J. M. Pearce, “Cut costs with open-source hardware,” *Nature*, vol. 505, no. 7485, Art. no. 7485, Jan. 2014, doi: 10.1038/505618d.
- [127] A. J. Buitenhuis and J. M. Pearce, “Open-source development of solar photovoltaic technology,” *Energy for Sustainable Development*, vol. 16, no. 3, pp. 379–388, Sep. 2012, doi: 10.1016/j.esd.2012.06.006.
- [128] P. de Arquer Fernández, M. Á. Fernández Fernández, J. L. Carús Candás, and P. Arboleya Arboleya, “An IoT open source platform for photovoltaic plants supervision,” *International Journal of Electrical Power & Energy Systems*, vol. 125, p. 106540, Feb. 2021, doi: 10.1016/j.ijepes.2020.106540.
- [129] I. González, J. M. Portalo, and A. J. Calderón, “Configurable IoT Open-Source Hardware and Software I-V Curve Tracer for Photovoltaic Generators,” *Sensors*, vol. 21, no. 22, Art. no. 22, Jan. 2021, doi: 10.3390/s21227650.
- [130] J. M. Portalo, I. González, and A. J. Calderón, “Monitoring System for Tracking a PV Generator in an Experimental Smart Microgrid: An Open-Source Solution,” *Sustainability*, vol. 13, no. 15, Art. no. 15, Jan. 2021, doi: 10.3390/su13158182.
- [131] R. Santhosh, S. U. Sabareesh, R. Aswin, and R. Mahalakshmi, “Hardware Design of PIC Microcontroller based Charge controller and MPPT for the Standalone PV-Battery charging System,” in *2021 International Conference on Recent Trends on Electronics, Information, Communication & Technology (RTEICT)*, Aug. 2021, pp. 172–175. doi: 10.1109/RTEICT52294.2021.9573523.
- [132] M. L. Kathe, A. B. Makokha, S. O. Zachary, and M. S. Adaramola, “A Comprehensive Review of Maximum Power Point Tracking (MPPT) Techniques Used in Solar PV Systems,” *Energies*, vol. 16, no. 5, Art. no. 5, Jan. 2023, doi: 10.3390/en16052206.
- [133] M. M. Rahman, S. Khan, and J. M. Pearce, “Open source modular DC nano grid hardware designs.” Accessed: Jul. 23, 2024. [Online]. Available: <https://osf.io/73yf5/>
- [134] “CSD19533KCS data sheet, product information and support | TI.com.” Accessed: Jul. 24, 2024. [Online]. Available: <https://www.ti.com/product/CSD19533KCS?>
- [135] Z. Iqbal, U. Nasir, M. T. Rasheed, and K. Munir, “A comparative analysis of synchronous buck, isolated buck and buck converter,” in *2015 IEEE 15th International Conference on Environment and Electrical Engineering (EEEIC)*, Jun. 2015, pp. 992–996. doi: 10.1109/EEEIC.2015.7165299.
- [136] L. Grafman, J. M. Pearce, P. Droz, and H. Louie, *To Catch the Sun: Inspiring stories of communities coming together to harness their own solar energy, and how you can do it too!* Arcata: Humboldt State University Press, 2021.

- [137] A. R. Kalair, N. Abas, Q. U. Hasan, M. Seyedmahmoudian, and N. Khan, “Demand side management in hybrid rooftop photovoltaic integrated smart nano grid,” *Journal of Cleaner Production*, vol. 258, p. 120747, Jun. 2020, doi: 10.1016/j.jclepro.2020.120747.
- [138] Y. Yerasimou, M. Kynigos, V. Efthymiou, and G. E. Georghiou, “Design of a Smart Nanogrid for Increasing Energy Efficiency of Buildings,” *Energies*, vol. 14, no. 12, Art. no. 12, Jan. 2021, doi: 10.3390/en14123683.
- [139] M. M. Rahman, S. Khan, and J. M. Pearce, “Open-source Hardware Design of Modular Solar DC Nanogrid,” Aug. 02, 2024, *Preprints: 2024080085*. doi: 10.20944/preprints202408.0085.v1.
- [140] S. Ali Sadat, J. Takahashi, and J. M. Pearce, “A Free and open-source microgrid optimization tool: SAMA the solar alone Multi-Objective Advisor,” *Energy Conversion and Management*, vol. 298, p. 117686, Dec. 2023, doi: 10.1016/j.enconman.2023.117686.
- [141] J. Liu, L. Jian, W. Wang, Z. Qiu, J. Zhang, and P. Dastbaz, “The role of energy storage systems in resilience enhancement of health care centers with critical loads,” *Journal of Energy Storage*, vol. 33, p. 102086, Jan. 2021, doi: 10.1016/j.est.2020.102086.
- [142] Heal Middle East, “Top 10 Equipment to Include in Your Ambulance.” Accessed: Aug. 06, 2024. [Online]. Available: <https://healmiddleeast.com/top-10-equipment-to-include-in-your-ambulance/>
- [143] Alberta Government, “Standards of ambulance equipment and supplies - Open Government.” Accessed: Aug. 06, 2024. [Online]. Available: <https://open.alberta.ca/publications/standards-of-ambulance-equipment-and-supplies>
- [144] J. M. Pearce, “Building Research Equipment with Free, Open-Source Hardware,” *Science*, vol. 337, no. 6100, pp. 1303–1304, Sep. 2012, doi: 10.1126/science.1228183.
- [145] S. Oberloier and J. M. Pearce, “General Design Procedure for Free and Open-Source Hardware for Scientific Equipment,” *Designs*, vol. 2, no. 1, Art. no. 1, Mar. 2018, doi: 10.3390/designs2010002.
- [146] NHLBI, NIH, “Defibrillators - What are Defibrillators?” Accessed: Aug. 06, 2024. [Online]. Available: <https://www.nhlbi.nih.gov/health/defibrillators>
- [147] J. Tough and L. Berry, “Elective and emergency defibrillation,” *Nursing Standard (through 2013)*, vol. 22, no. 38, pp. 49–56; quiz 58, 60, Jun. 2008.

- [148] C. Go, “Difference Between Full Auto, Semi-Auto, & Manual Defibrillators,” First Response Safety Training. Accessed: Jul. 24, 2024. [Online]. Available: <https://www.firstresponsecpr.com/blog/semi-auto-and-manual-defibrillators/>
- [149] AED USA, “Defibrillator Battery Maintenance Guide.” Accessed: Aug. 06, 2024. [Online]. Available: <https://www.aedusa.com/knowledge/learn-to-maintain-your-defibrillator-battery-what-you-need-to-know/>
- [150] ZOLL Medical Corporation, “Manual Defibrillator and Monitors for ALS.” Accessed: Aug. 06, 2024. [Online]. Available: <https://www.zoll.com/products/defibrillators>
- [151] Raúl J. Gazmuri, “Defibrillator/Monitors for ICU and Hospital Use,” *ICU Management & Practice*. Accessed: Aug. 06, 2024. [Online]. Available: <https://healthmanagement.org/c/icu/Issuearticle/defibrillator-monitors-for-icu-and-hospital-use>
- [152] S. R. Díaz, D. B. Rodriguez, and A. M. Gonzalez-Vargas, “Low-cost, open source defibrillation analyzer for educational purposes,” in *2021 IEEE 2nd International Congress of Biomedical Engineering and Bioengineering (CI-IB&BI)*, Oct. 2021, pp. 1–4. doi: 10.1109/CI-IBBI54220.2021.9626084.
- [153] J. Ferretti, L. Di Pietro, and C. De Maria, “Open-source automated external defibrillator,” *HardwareX*, vol. 2, pp. 61–70, Oct. 2017, doi: 10.1016/j.ohx.2017.09.001.
- [154] ZOLL Medical Corporation, “What Is a Suction Machine?” Accessed: Aug. 06, 2024. [Online]. Available: <https://www.zoll.com/resources/what-is-a-suction-machine>
- [155] Sunset Healthcare Solutions, “SU100DC Portable AC/DC Suction Machine,” Sunset Healthcare Solutions. Accessed: Aug. 06, 2024. [Online]. Available: <https://sunsethcs.com/product/su100dc-portable-ac-dc-suction-machine/>
- [156] Allied Medical LLC, “Gomco® OptiVac® AC/DC Portable Suction Unit – Allied Medical LLC.” Accessed: Aug. 06, 2024. [Online]. Available: <https://alliedmedicalllc.com/en-us/product/gomco-optimvac-ac-dc-portable-suction-unit/>
- [157] Laerdal Medical, “Laerdal Suction Unit (LSU),” Laerdal Medical. Accessed: Aug. 06, 2024. [Online]. Available: <https://laerdal.com/us/products/medical-devices/airway-management/laerdal-suction-unit-lsu/>
- [158] T.-C. Ha, M. Morgan, and A. Schambach, “HYKYHT: A versatile, affordable, and open-source 3D-printed liquid aspiration system,” *HardwareX*, vol. 17, p. e00509, Mar. 2024, doi: 10.1016/j.ohx.2024.e00509.

- [159] I. Iamkit, T. Singhnoo, T. Chaiyana, P. Boonkrong, J. Prinyakupt, and K. Roongprasert, "Designing Ambulatory Ventilator for Ambulance Department and Homecare in Thailand," in *2023 15th Biomedical Engineering International Conference (BMEiCON)*, Oct. 2023, pp. 1–5. doi: 10.1109/BMEiCON60347.2023.10322030.
- [160] Medion Healthcare, "Transport Ventilator for Ambulance." Accessed: Aug. 06, 2024. [Online]. Available: <https://medion.co.in/transport-ventilator.php>
- [161] Wall Industries, "Power Supply Solutions for Mechanical Ventilator Machines," Wall Industries. Accessed: Aug. 06, 2024. [Online]. Available: <https://www.wallindustries.com/powering-mechanical-ventilators/>
- [162] J. M. Pearce, "A review of open source ventilators for COVID-19 and future pandemics," Apr. 30, 2020, *F1000Research*: 9:218. doi: 10.12688/f1000research.22942.2.
- [163] T. Abuzairi, A. Irfan, and Basari, "COVENT-Tester: A low-cost, open source ventilator tester," *HardwareX*, vol. 9, p. e00196, Apr. 2021, doi: 10.1016/j.ohx.2021.e00196.
- [164] A. Petsiuk, N. G. Tanikella, S. Dertinger, A. Pringle, S. Oberloier, and J. M. Pearce, "Partially RepRapable automated open source bag valve mask-based ventilator," *HardwareX*, vol. 8, p. e00131, Oct. 2020, doi: 10.1016/j.ohx.2020.e00131.
- [165] O. Garmendia *et al.*, "Low-cost, easy-to-build noninvasive pressure support ventilator for under-resourced regions: open source hardware description, performance and feasibility testing," *European Respiratory Journal*, vol. 55, no. 6, Jun. 2020, doi: 10.1183/13993003.00846-2020.
- [166] American Lung Association, "Getting Started with a Portable Oxygen Concentrator." Accessed: Aug. 06, 2024. [Online]. Available: <https://www.lung.org/lung-health-diseases/lung-procedures-and-tests/oxygen-therapy/getting-started-portable-oxygen-concentrator>
- [167] Oxygen Concentrator Store, "Inogen One G5 Portable Concentrator." Accessed: Aug. 06, 2024. [Online]. Available: <https://www.oxygenconcentratorstore.com/inogen-one-g5/>
- [168] Philips, "COPD Respiratory Medical Supplies," Philips. Accessed: Aug. 06, 2024. [Online]. Available: <https://www.usa.philips.com/c-e/breathe-easier.html>
- [169] Janesh S, Gowtham P, Pooja R, Ajibala G, R. PS, and U. K, "Designing and Development of Respiratory Ailment System for a Rapidly Deployable Emergency Ventilator," in *2023 International Conference on Intelligent Technologies for Sustainable Electric and Communications Systems (iTech SECOM)*, Dec. 2023, pp. 567–572. doi: 10.1109/iTechSECOM59882.2023.10435142.

- [170] O. Nerbrink and M. Dahlback, “Basic Nebulizer Function,” *Journal of Aerosol Medicine*, vol. 7, no. s1, p. S-7, Jan. 1994, doi: 10.1089/jam.1994.7.Suppl\_1.S-7.
- [171] Medical News Today, “What a nebulizer is and how to use it.” Accessed: Aug. 06, 2024. [Online]. Available: <https://www.medicalnewstoday.com/articles/324947>
- [172] Philips, “Asthma Management | InnoSpire Go,” Philips. Accessed: Aug. 06, 2024. [Online]. Available: <https://www.usa.philips.com/c-e/hs/respiratory-care/innospire-go.html>
- [173] Oxygen Concentrator Supplies, “Buy Nebulizer Batteries and Power Supplies,” [oxygenconcentratorsupplies.com](https://www.oxygenconcentratorsupplies.com). Accessed: Aug. 06, 2024. [Online]. Available: <https://www.oxygenconcentratorsupplies.com/nebulizers/batteries-and-power-supplies>
- [174] Jenny del Carmen Arcentales Herrera, A. Santa Cruz Belela-Anacleto, M. L. G. Pedreira, and D. M. Kusahara, “Influence of transport conditions on infusion pumps performance and triggering alarms: A simulation-based research,” *International Emergency Nursing*, vol. 62, p. 101144, May 2022, doi: 10.1016/j.ienj.2022.101144.
- [175] Baxter, “The Novum IQ Large volume pump.” Accessed: Aug. 06, 2024. [Online]. Available: [https://www.baxterglobal.com/LP\\_US\\_NovumIQ\\_LVP\\_Launch/](https://www.baxterglobal.com/LP_US_NovumIQ_LVP_Launch/)
- [176] Advanced Energy, “Infusion Pumps.” Accessed: Aug. 06, 2024. [Online]. Available: <https://www.advancedenergy.com/en-us/applications/medical/patient-monitoring/infusion-pumps/>
- [177] B. Wijnen, E. J. Hunt, G. C. Anzalone, and J. M. Pearce, “Open-Source Syringe Pump Library,” *PLOS ONE*, vol. 9, no. 9, p. e107216, Sep. 2014, doi: 10.1371/journal.pone.0107216.
- [178] C. Bresch, D. Hély, S. Chollet, and R. Lysecky, “SecPump: A Connected Open-Source Infusion Pump for Security Research Purposes,” *IEEE Embedded Systems Letters*, vol. 13, no. 1, pp. 21–24, Mar. 2021, doi: 10.1109/LES.2020.2979595.
- [179] J. Hatcliff, B. Larson, T. Carpenter, P. Jones, Y. Zhang, and J. Jorgens, “The open PCA pump project: an exemplar open source medical device as a community resource,” *SIGBED Rev.*, vol. 16, no. 2, pp. 8–13, Aug. 2019, doi: 10.1145/3357495.3357496.
- [180] B. R. Larson, J. Hatcliff, and P. Chalin, “Open source Patient-Controlled Analgesic pump requirements documentation,” in *2013 5th International Workshop on Software Engineering in Health Care (SEHC)*, May 2013, pp. 28–34. doi: 10.1109/SEHC.2013.6602474.
- [181] M. Payne *et al.*, “Design of an open source ultra low cost insulin pump,” *HardwareX*, vol. 12, p. e00375, Oct. 2022, doi: 10.1016/j.ohx.2022.e00375.

- [182] Soma Tech Intl, “Lifepak 15 Defibrillator,” Soma Tech Intl’s Blog. Accessed: Aug. 06, 2024. [Online]. Available: <https://www.somatechnology.com/defibrillators/physio-control-lifepak-15/>
- [183] Medtronic, “Newport™ HT70 Plus Ventilator | Medtronic.” Accessed: Aug. 06, 2024. [Online]. Available: <https://www.medtronic.com/covidien/en-us/products/mechanical-ventilation/newport-ht70-plus-ventilator.html>
- [184] American Discount, “DeVilbiss Traveler Portable Nebulizer w/ Battery 6910P-DR,” American Discount Home Medical. Accessed: Aug. 06, 2024. [Online]. Available: <https://www.home-med-equip.com/catalog/devilbiss-traveler-portable-nebulizer-w-battery-6910p-dr.html>
- [185] ICU Medical, “CADD-Solis™ Infusion System.” Accessed: Aug. 06, 2024. [Online]. Available: <https://www.icumed.com/products/infusion-therapy/infusion-pumps-and-software/cadd-ambulatory-pumps/cadd-solis-infusion-system/>
- [186] Benz Ambulance, “ABL-XLT-SL BENZ,” RICOH THETA. Accessed: Aug. 06, 2024. [Online]. Available: <https://carryboyambulance.com/box-body/abl-xlt-sl/>
- [187] Canadian Solar, “HiKu6.” Accessed: Aug. 06, 2024. [Online]. Available: <https://www.canadiansolar.com/hiku6/>
- [188] M. H. Shubbak, “Advances in solar photovoltaics: Technology review and patent trends,” *Renewable and Sustainable Energy Reviews*, vol. 115, p. 109383, Nov. 2019, doi: 10.1016/j.rser.2019.109383.
- [189] F. A. Tiano, G. Rizzo, M. Marino, and A. Monetti, “Evaluation of the potential of solar photovoltaic panels installed on vehicle body including temperature effect on efficiency,” *eTransportation*, vol. 5, p. 100067, Aug. 2020, doi: 10.1016/j.etrans.2020.100067.
- [190] R. Dallaev, T. Pisarenko, N. Papež, and V. Holcman, “Overview of the Current State of Flexible Solar Panels and Photovoltaic Materials,” *Materials*, vol. 16, no. 17, Art. no. 17, Jan. 2023, doi: 10.3390/ma16175839.
- [191] X. Li, P. Li, Z. Wu, D. Luo, H.-Y. Yu, and Z.-H. Lu, “Review and perspective of materials for flexible solar cells,” *Materials Reports: Energy*, vol. 1, no. 1, p. 100001, Feb. 2021, doi: 10.1016/j.matre.2020.09.001.
- [192] Renogy Solar, “Renogy 1750W 12 Volt Flexible Solar Panel.” Accessed: Aug. 06, 2024. [Online]. Available: <https://ca.renogy.com/350w-2pcs-175-watt-12-volt-flexible-monocrystalline-solar-panels/>
- [193] Greentech Renewables, “Solar PV Racking Options - Comparison Chart.” Accessed: Aug. 06, 2024. [Online]. Available: <https://www.greentechrenewables.com/article/solar-pv-racking-options-comparison-chart>

- [194] ECO-WORTHY, “ECO-WORTHY Lithium Iron Phosphate Battery,” eco-worthy-ca. Accessed: Aug. 24, 2024. [Online]. Available: <https://ca.eco-worthy.com/products/lifepo4-12v-50ah-lithium-iron-phosphate-battery>
- [195] Amazon, “Freenove 5 Inch Touchscreen Monitor for Raspberry Pi 4B.” Accessed: Aug. 06, 2024. [Online]. Available: <https://www.amazon.ca/Freenove-Touchscreen-Raspberry-Capacitive-Driver-Free/dp/B0B44VZTRG>
- [196] B. Adhikari *et al.*, “Earthquakes, Fuel Crisis, Power Outages, and Health Care in Nepal: Implications for the Future,” *Disaster Medicine and Public Health Preparedness*, vol. 11, no. 5, pp. 625–632, Oct. 2017, doi: 10.1017/dmp.2016.195.
- [197] B. Nourdine and A. Saad, “Hybrid System for Powering Moroccan Healthcare Centers in Remote Rural Areas,” *J. Electr. Eng. Technol.*, vol. 16, no. 2, pp. 809–820, Mar. 2021, doi: 10.1007/s42835-020-00643-y.
- [198] R. Jones *et al.*, “RepRap – the replicating rapid prototyper,” *Robotica*, vol. 29, no. 1, pp. 177–191, Jan. 2011, doi: 10.1017/S026357471000069X.
- [199] E. Sells, S. Bailard, Z. Smith, A. Bowyer, and V. Olliver, “RepRap: The Replicating Rapid Prototyper: Maximizing Customizability by Breeding the Means of Production,” in *Handbook of Research in Mass Customization and Personalization*, World Scientific Publishing Company, 2009, pp. 568–580. doi: 10.1142/9789814280280\_0028.

## Appendices

### Appendix A: Integration of converters

To house the converters and to interconnect them, an open-source frame is designed to facilitate modular plugging of the converters onto the frame's DIN rail. A display with a Raspberry Pi is used for data monitoring and logging. The converters and the master controller are also housed in an enclosure. Both the converters and the frame support the installation of the system.

#### A.1. DC nano grid frame design

The parts required for assembling the frame are listed in Table A.1 along with the open-source repository of the files. All custom components can be 3-D printed on a RepRap class-[198], [199] open source 3-D printer. Components were printed using polylactic acid (PLA) filament in Prusa MK3 print using print settings given in Table A.2.

**Table A.1.** 3D printed parts required for assembly of the frame of the DC nano grid all licensed with CERN OHL-S 2.0.

Parts name	Quantity	File type	Location of file
Sliding corner bracket	8	STEP/stl	<a href="https://osf.io/73yf5/">https://osf.io/73yf5/</a>
Corner bracket	8	STEP/stl	<a href="https://osf.io/73yf5/">https://osf.io/73yf5/</a>
Holder for DIN rail	2	STEP/stl	<a href="https://osf.io/73yf5/">https://osf.io/73yf5/</a>
Holder for bus bar	2	STEP/stl	<a href="https://osf.io/73yf5/">https://osf.io/73yf5/</a>
Case for display	1	STEP/stl	<a href="https://osf.io/73yf5/">https://osf.io/73yf5/</a>
Encloser for Raspberry pi	1	STEP/stl	<a href="https://osf.io/73yf5/">https://osf.io/73yf5/</a>
Raspberry pi holder	1	STEP/stl	<a href="https://osf.io/73yf5/">https://osf.io/73yf5/</a>

The printing parameters are summarized in Table A.2 and can be printed on any RepRap class 3-D printer.

**Table A.2.** 3-D printing parameters.

Parameter	Value
-----------	-------

Filament	PLA
Layer Height	0.3 mm
Initial Layer Height	0.2 mm
Infill Density	15 %
Printing Temperature	210 °C
Build Plate Temperature	60 °C
Print Speed	60 mm/s
Travel Speed	175 mm/s

The frame is designed as an alternative to placing all components inside an electrical box. The parts needed are shown in Figure A.1. It will hold three converters and a master controller box, with dimensions of 420mm in length and 390mm in height. These dimensions can be adjusted as needed. Two pieces of 350mm aluminum extrusion bars serve as stands. To support them, three pieces of 80mm long aluminum extrusion are used per stand, totaling six pieces. A 420mm long aluminum extrusion bar connects the two stands together. Two 410mm bus bars cut from a 1m long bus bar. And a 410mm long DIN rail to accommodate the converters. Four types of corner brackets and holders are used in this design process, as detailed in Table A.1, also the design steps are mentioned in Figure A.2. A case and holder are also made for the display connected to the Raspberry Pi 4b for data monitoring and connected to one of the bars of the frame.

To assemble the frame for accommodating the DIN rail, bus bars, and monitoring system, following steps are followed:

- The stands were assembled using the 350mm aluminum extrusions and 80mm support pieces first.
- The 420mm aluminum extrusion was attached to the stands to form the frame.
- The 410mm bus bars and DIN rail were installed within the frame.
- A case and holder for the display connected to the Raspberry Pi 4b for data monitoring were created and attached to one of the bars of the frame.

Figure A.2 (a-g) provides detailed design steps and the types of corner brackets and holders used, and Figure A.3 shows the assembled frame.

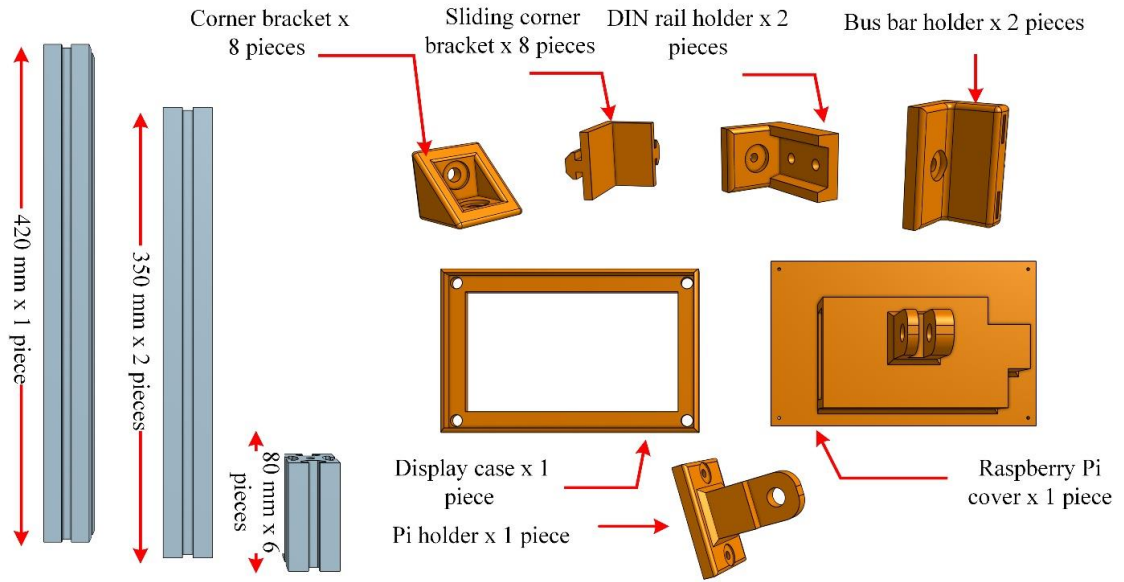


**Figure A.1.** Parts required for assembly of frame.

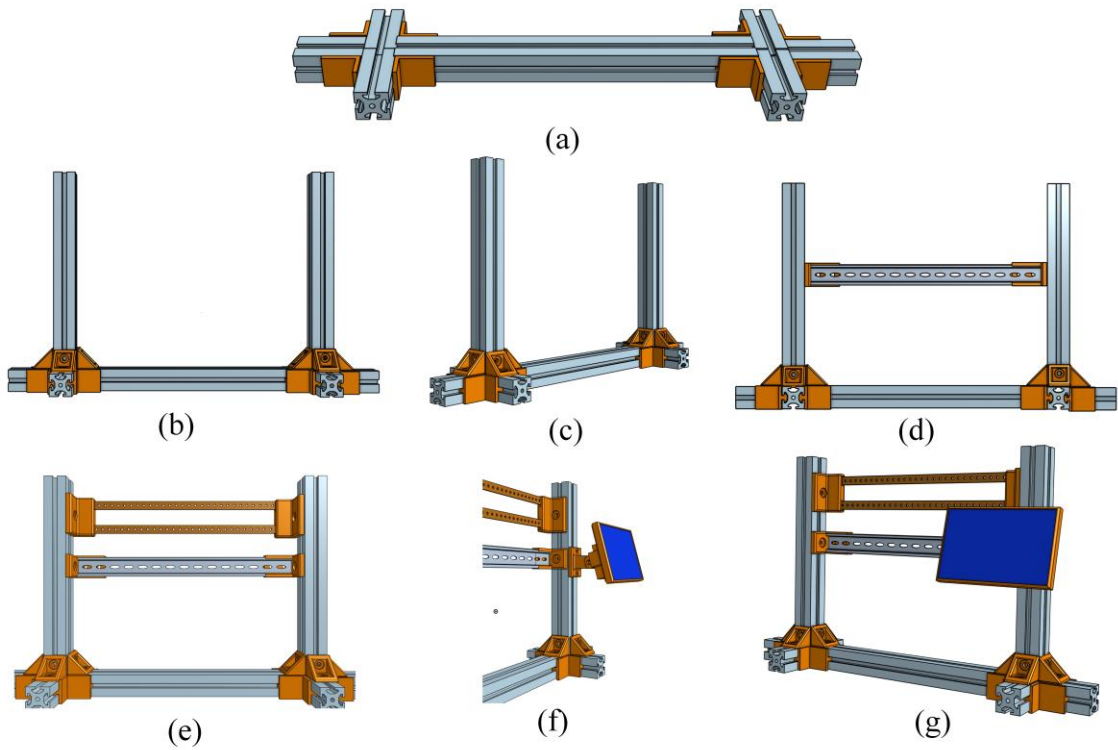


**Figure A.2.** Assembly process of the frame.

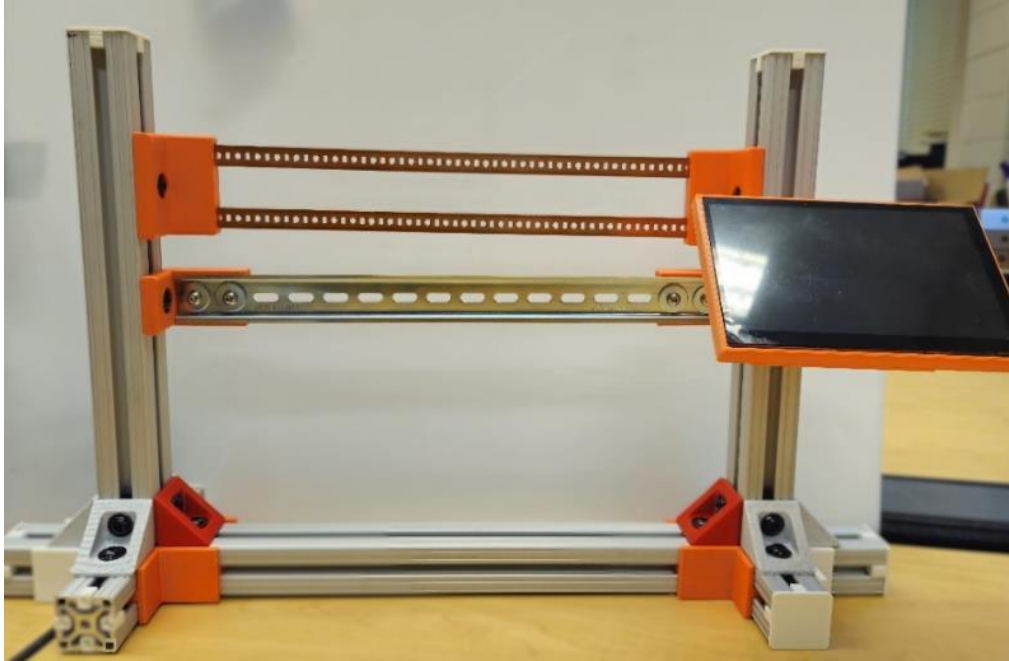


**Figure A.3.** Assembled frame.

## A.2. Converters encloser design

Each converter and master controller have an enclosure that is adequately ventilated. The enclosures are designed with the same shape, but their widths vary based on the converter module, as not all converters have the same width or features. Each module has a clip to connect to the DIN rail, with pockets for passing wires to the bus bar and communication ports. The front panel of the enclosure features different elements based on the module: the Boost converter has its own display, and the master controller has a port to connect the USB from the Raspberry Pi for serial data sharing and power supply. The STEP and STL files for all the enclosures are available in the repository listed in the following Figure A.3. Rendered images of the master controller are shown in Figure A.4. All the enclosures were printed using a 0.6mm nozzle at a 0.3mm layer height with 15% infill, utilizing PLA filament.

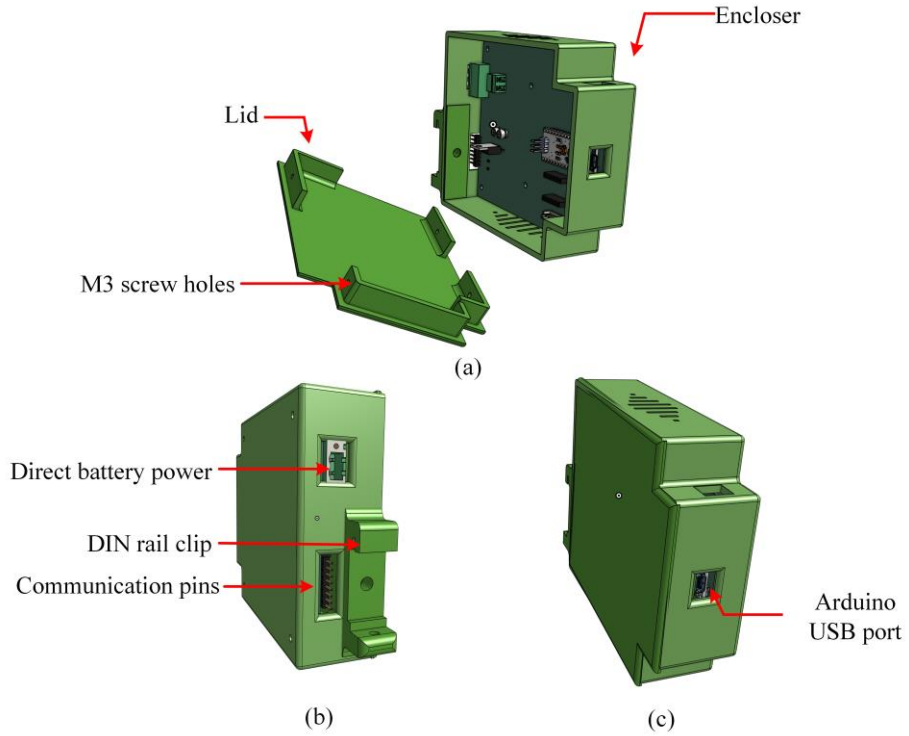


**Figure A.4.** Rendered 3D image of master controller enclosure

**Table A.3.** 3D printed parts required for assembly of converters and master controller all licensed with CERN OHL-S 2.0.

Parts name	Quantity	File type	Location of file
Buck converter enclosure	1	STEP/stl	<a href="https://osf.io/73yf5/">https://osf.io/73yf5/</a>
Buck converter lid	1	STEP/stl	<a href="https://osf.io/73yf5/">https://osf.io/73yf5/</a>
Boost converter enclosure	1	STEP/stl	<a href="https://osf.io/73yf5/">https://osf.io/73yf5/</a>
Boost converter lid	1	STEP/stl	<a href="https://osf.io/73yf5/">https://osf.io/73yf5/</a>
Bidirectional converter enclosure	1	STEP/stl	<a href="https://osf.io/73yf5/">https://osf.io/73yf5/</a>
Bidirectional converter lid	1	STEP/stl	<a href="https://osf.io/73yf5/">https://osf.io/73yf5/</a>
Master controller enclosure	1	STEP/stl	<a href="https://osf.io/73yf5/">https://osf.io/73yf5/</a>
Master controller lid	1	STEP/stl	<a href="https://osf.io/73yf5/">https://osf.io/73yf5/</a>

### A.3 Final assembly

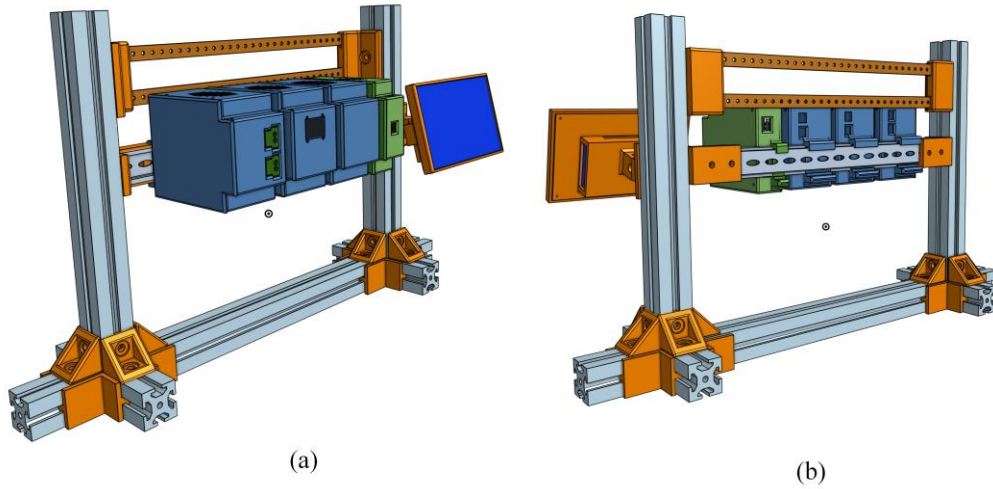


**Figure A.5.** Rendered 3D image of final assembly of Nano grid.

After the enclosures are printed, the PCBs are placed inside, and the wiring is completed, the communication pins are attached to the communication bus in all the converters before placing them on the DIN rail. Once the converters are secured in the DIN rails, the necessary connections between all the positive and negative terminals of the converters and the corresponding bus bar are made. The battery converter also has a direct battery power supply port to the master, designated for the Raspberry Pi converter. After all the interconnections are completed, the power supply and USB connection between the master Arduino and Raspberry Pi are established.

## Appendix B: Bill of materials of DC nanogrid hardware

### Bill of material of buck converter

Designator	Value	Qty	Cost per unit	Total cost	Source of materials
A4	Arduino Nano	1	\$10.66	\$10.66	<a href="https://www.amazon.ca/ELEGOO-Arduino-ATmega328P-Without-Compatible/dp/B0713XK923/?th=1">https://www.amazon.ca/ELEGOO-Arduino-ATmega328P-Without-Compatible/dp/B0713XK923/?th=1</a>
C1	Cap 470uF, 100V	1	\$1.57	\$1.57	<a href="https://www.digikey.ca/en/products/detail/rubycon/100ZLH470MEFC16X31-5/3564548">https://www.digikey.ca/en/products/detail/rubycon/100ZLH470MEFC16X31-5/3564548</a>
C2, C11	Cap 470uF, 50V	2	\$0.98	\$1.95	<a href="https://www.digikey.ca/en/products/detail/nichicon/UPW1H471MHD/589652">https://www.digikey.ca/en/products/detail/nichicon/UPW1H471MHD/589652</a>
C3, C5	Cap .22uF, 50V	1	\$0.26	\$0.26	<a href="https://www.digikey.ca/en/products/detail/nichicon/UPV1HR22MDD/588837">https://www.digikey.ca/en/products/detail/nichicon/UPV1HR22MDD/588837</a>
C4	Cap.33uF, 50V	2	\$0.26	\$0.51	<a href="https://www.digikey.ca/en/products/detail/nichicon/UPV2AR33MDD/588879">https://www.digikey.ca/en/products/detail/nichicon/UPV2AR33MDD/588879</a>
C6, C7	0.1uF, 0805 SMD	2	\$0.04	\$0.08	<a href="https://www.digikey.ca/en/products/detail/samsung-electro-mechanics/CL21B104KCFNNNE/5961324?">https://www.digikey.ca/en/products/detail/samsung-electro-mechanics/CL21B104KCFNNNE/5961324?</a>
C8	10uF,0805 SMD	1	\$0.06	\$0.06	<a href="https://www.digikey.ca/en/products/detail/samsung-electro-mechanics/CL21A106KOQNNNE/3886754">https://www.digikey.ca/en/products/detail/samsung-electro-mechanics/CL21A106KOQNNNE/3886754</a>
C9, C10	10nF,0805 SMD	2	\$0.10	\$0.21	<a href="https://www.digikey.ca/en/products/detail/kemet/C0805X103K1RAC3316/10315780">https://www.digikey.ca/en/products/detail/kemet/C0805X103K1RAC3316/10315780</a>
C12	4.7u,0805 SMD	1	\$0.06	\$0.06	<a href="https://www.digikey.ca/en/products/detail/samsung-electro-mechanics/CL21A475KAQNNNE/3886902">https://www.digikey.ca/en/products/detail/samsung-electro-mechanics/CL21A475KAQNNNE/3886902</a>
C13, C14	2.2u 0805 SMD	1	\$0.19	\$0.19	<a href="https://www.digikey.ca/en/products/detail/samsung-electro-mechanics/CL21B225KAFNFNE/3888611">https://www.digikey.ca/en/products/detail/samsung-electro-mechanics/CL21B225KAFNFNE/3888611</a>
D1, D2, D3, D4	SS310 0805 SMD	4	\$0.74	\$2.94	<a href="https://www.digikey.ca/en/products/detail/onsemi/S310FA/5892104">https://www.digikey.ca/en/products/detail/onsemi/S310FA/5892104</a>
F1	Fuse	1	\$1.20	\$1.20	<a href="https://www.digikey.ca/en/products/detail/littelfuse-inc/0997020-WXN/701061">https://www.digikey.ca/en/products/detail/littelfuse-inc/0997020-WXN/701061</a>
F1	Fuse holder	1	\$1.18	\$1.18	<a href="https://www.digikey.ca/en/products/detail/littelfuse-inc/01000063Z/14641003">https://www.digikey.ca/en/products/detail/littelfuse-inc/01000063Z/14641003</a>
J1, J7	Connector 1776508	2	\$2.01	\$4.02	<a href="https://www.digikey.ca/en/products/detail/phoenix-contact/1776508/349000">https://www.digikey.ca/en/products/detail/phoenix-contact/1776508/349000</a>
J3, J6	Screw Terminal	2	\$1.07	\$2.14	<a href="https://www.digikey.ca/en/products/detail/keystone-electronics/8197-2/2746666">https://www.digikey.ca/en/products/detail/keystone-electronics/8197-2/2746666</a>
J4	JST 4POS2.54MM	1	\$0.23	\$0.23	<a href="https://www.digikey.ca/en/products/detail/jst-sales-america-inc./B4B-XH-A/1651047?">https://www.digikey.ca/en/products/detail/jst-sales-america-inc./B4B-XH-A/1651047?</a>
J5	Conn_01x08_Socket	1	\$0.29	\$0.29	<a href="https://www.digikey.ca/en/products/detail/adam-tech/PH1RB-08-UA/9831008?">https://www.digikey.ca/en/products/detail/adam-tech/PH1RB-08-UA/9831008?</a>
L1	Inductor Toroidal 0077443A7	1	\$7.38	\$7.38	<a href="https://www.digikey.ca/en/products/detail/magnetics-a-division-of-spang-co/0077443A7/18626894?">https://www.digikey.ca/en/products/detail/magnetics-a-division-of-spang-co/0077443A7/18626894?</a>
Q1, Q2	MOSFET CSD19533KCS	2	\$1.71	\$3.42	<a href="https://www.digikey.ca/en/products/detail/texas-instruments/CSD19533KCS/4806074">https://www.digikey.ca/en/products/detail/texas-instruments/CSD19533KCS/4806074</a>
R1, R2	47 Ohm 0805	2	\$0.02	\$0.04	<a href="https://www.digikey.ca/en/products/detail/stackpole-electronics-inc/RMCF0805FT47R0/1713163">https://www.digikey.ca/en/products/detail/stackpole-electronics-inc/RMCF0805FT47R0/1713163</a>

R3, R4	220 Ohm 0805	2	\$0.02	\$0.04	<a href="https://www.digikey.ca/en/products/detail/stackpole-electronics-inc/RMCF0805FT220R/1760238">https://www.digikey.ca/en/products/detail/stackpole-electronics-inc/RMCF0805FT220R/1760238</a>
R5, R7, R9, R10	100k Ohm 0805	4	\$0.02	\$0.08	<a href="https://www.digikey.ca/en/products/detail/stackpole-electronics-inc/RMCF0805FT100K/1760712">https://www.digikey.ca/en/products/detail/stackpole-electronics-inc/RMCF0805FT100K/1760712</a>
R6, R8	10k Ohm 0805	2	\$0.02	\$0.04	<a href="https://www.digikey.ca/en/products/detail/stackpole-electronics-inc/RMCF0805FT10K0/1760676">https://www.digikey.ca/en/products/detail/stackpole-electronics-inc/RMCF0805FT10K0/1760676</a>
U1	MOSFET driver IR2104	1	\$5.36	\$5.36	<a href="https://www.digikey.ca/en/products/detail/infineon-technologies/IR2104PBF/812198">https://www.digikey.ca/en/products/detail/infineon-technologies/IR2104PBF/812198</a>
U2	LM7805_TO 220	1	\$0.79	\$0.79	<a href="https://www.digikey.ca/en/products/detail/stmicroelectronics/L7805CV/585964">https://www.digikey.ca/en/products/detail/stmicroelectronics/L7805CV/585964</a>
U3	LM7812_TO 220	1	\$0.98	\$0.98	<a href="https://www.digikey.ca/en/products/detail/stmicroelectronics/L7812CV/585973">https://www.digikey.ca/en/products/detail/stmicroelectronics/L7812CV/585973</a>
U4	ACS712. 20A	1	\$4.29	\$4.29	<a href="https://www.digikey.ca/en/products/detail/allegro-microsystems/ACS712ELCTR-20A-T/1284607">https://www.digikey.ca/en/products/detail/allegro-microsystems/ACS712ELCTR-20A-T/1284607</a>
-	Heat sink	3	\$1.17	\$3.50	<a href="https://www.amazon.ca/Easycargo-Heatsink-Insulator-Regulator-Transistor/dp/B08MW1YNJM/ref=asc_df_B08MW1YNJM/?th=1">https://www.amazon.ca/Easycargo-Heatsink-Insulator-Regulator-Transistor/dp/B08MW1YNJM/ref=asc_df_B08MW1YNJM/?th=1</a>
-	PCB	1	\$2.33	\$2.33	<a href="https://jlepcb.com/">https://jlepcb.com/</a>
			Total	\$55.8 1	

Bill of material of boost converter

Desig nator	Value	Qty	Cost per unit	Total cost	Source of materials
A4	Arduino_Na no_v3.x	1	\$10.66	\$10.6 6	<a href="https://www.amazon.ca/ELEGOO-Arduino-ATmega328P-Without-Compatible/dp/B0713XK923/?th=1">https://www.amazon.ca/ELEGOO-Arduino-ATmega328P-Without-Compatible/dp/B0713XK923/?th=1</a>
C1, C18	Cap 470uF, 100V	2	\$1.57	\$3.15	<a href="https://www.digikey.ca/en/products/detail/rubycon/100ZLH470MEFC16X31-5/3564548">https://www.digikey.ca/en/products/detail/rubycon/100ZLH470MEFC16X31-5/3564548</a>
C2, C11	Cap 470uF, 50V	2	\$0.98	\$1.95	<a href="https://www.digikey.ca/en/products/detail/nichicon/UPW1H471MHD/589652">https://www.digikey.ca/en/products/detail/nichicon/UPW1H471MHD/589652</a>
C3, C4, C5	Cap .22uF, 50V	3	\$0.26	\$0.77	<a href="https://www.digikey.ca/en/products/detail/nichicon/VR1HR22MDD/588837">https://www.digikey.ca/en/products/detail/nichicon/VR1HR22MDD/588837</a>
C9, C10	10nF,0805 SMD	2	\$0.10	\$0.21	<a href="https://www.digikey.ca/en/products/detail/kemet/C0805X103K1RAC3316/10315780">https://www.digikey.ca/en/products/detail/kemet/C0805X103K1RAC3316/10315780</a>
C12, C15	4.7u,0805 SMD	2	\$0.06	\$0.12	<a href="https://www.digikey.ca/en/products/detail/samsung-electro-mechanics/CL21A475KAQNNNE/3886902">https://www.digikey.ca/en/products/detail/samsung-electro-mechanics/CL21A475KAQNNNE/3886902</a>
C13, C17, C14, C16	2.2u 0805 SMD	4	\$0.19	\$0.77	<a href="https://www.digikey.ca/en/products/detail/samsung-electro-mechanics/CL21B225KAFNFNE/3888611">https://www.digikey.ca/en/products/detail/samsung-electro-mechanics/CL21B225KAFNFNE/3888611</a>
C19	10uF,0805 SMD	1	\$0.06	\$0.06	<a href="https://www.digikey.ca/en/products/detail/samsung-electro-mechanics/CL21A106KOQNNNE/3886754">https://www.digikey.ca/en/products/detail/samsung-electro-mechanics/CL21A106KOQNNNE/3886754</a>
D2, D3	SS310 0805 SMD	2	\$0.74	\$1.47	<a href="https://www.digikey.ca/en/products/detail/onsemi/S310FA/5892104">https://www.digikey.ca/en/products/detail/onsemi/S310FA/5892104</a>
D4	APT60S20B G 75A	1	\$5.60	\$5.60	<a href="https://www.digikey.ca/en/products/detail/microchip-technology/APT60S20BG/1494822?">https://www.digikey.ca/en/products/detail/microchip-technology/APT60S20BG/1494822?</a>

F0	Fuse	1	\$1.20	\$1.20	<a href="https://www.digikey.ca/en/products/detail/littelfuse-inc/0997020-WXN/701061">https://www.digikey.ca/en/products/detail/littelfuse-inc/0997020-WXN/701061</a>
F1	Fuse holder	1	\$1.18	\$1.18	<a href="https://www.digikey.ca/en/products/detail/littelfuse-inc/01000063Z/14641003">https://www.digikey.ca/en/products/detail/littelfuse-inc/01000063Z/14641003</a>
J2, J3, J6, J7	Screw Terminal 8197 2	4	\$1.07	\$4.28	<a href="https://www.digikey.ca/en/products/detail/keystone-electronics/8197-2/2746666">https://www.digikey.ca/en/products/detail/keystone-electronics/8197-2/2746666</a>
J4	JST 4POS2.54M M	1	\$0.23	\$0.23	<a href="https://www.digikey.ca/en/products/detail/jst-sales-america-inc./B4B-XH-A/1651047?">https://www.digikey.ca/en/products/detail/jst-sales-america-inc./B4B-XH-A/1651047?</a>
J5	Conn_01x08 _header	1	\$0.29	\$0.29	<a href="https://www.digikey.ca/en/products/detail/adam-tech/PH1RB-08-UA/9831008?">https://www.digikey.ca/en/products/detail/adam-tech/PH1RB-08-UA/9831008?</a>
L1	Inductor toroidal 0077443A7	1	\$7.38	\$7.38	<a href="https://www.digikey.ca/en/products/detail/magnetics-a-division-of-spang-co/0077443A7/18626894?">https://www.digikey.ca/en/products/detail/magnetics-a-division-of-spang-co/0077443A7/18626894?</a>
Q2	MOSFET CSD19533K CS	1	\$1.71	\$1.71	<a href="https://www.digikey.ca/en/products/detail/texas-instruments/CSD19533KCS/4806074">https://www.digikey.ca/en/products/detail/texas-instruments/CSD19533KCS/4806074</a>
R1, R3, R12, R13, R14, R15	0-ohm, Jumper, 0805	6	\$0.01	\$0.09	<a href="https://www.digikey.ca/en/products/detail/stackpole-electronics-inc/RMCF0805ZT0R00/1756901">https://www.digikey.ca/en/products/detail/stackpole-electronics-inc/RMCF0805ZT0R00/1756901</a>
R2	47 Ohm 0805 SMD	1	\$0.02	\$0.02	<a href="https://www.digikey.ca/en/products/detail/stackpole-electronics-inc/RMCF0805FT47R0/1713163">https://www.digikey.ca/en/products/detail/stackpole-electronics-inc/RMCF0805FT47R0/1713163</a>
R5, R7, R9	100k Ohm 0805 SMD	3	\$0.02	\$0.06	<a href="https://www.digikey.ca/en/products/detail/stackpole-electronics-inc/RMCF0805FT100K/1760712">https://www.digikey.ca/en/products/detail/stackpole-electronics-inc/RMCF0805FT100K/1760712</a>
R6, R8, R11, R16, R17	10k Ohm 0805 SMD	5	\$0.02	\$0.10	<a href="https://www.digikey.ca/en/products/detail/stackpole-electronics-inc/RMCF0805FT10K0/1760676">https://www.digikey.ca/en/products/detail/stackpole-electronics-inc/RMCF0805FT10K0/1760676</a>
U2	LM7805CV TO220	1	\$0.79	\$0.79	<a href="https://www.digikey.ca/en/products/detail/stmicroelectronics/L7805CV/585964">https://www.digikey.ca/en/products/detail/stmicroelectronics/L7805CV/585964</a>
U3	LM7812CV TO220	1	\$0.98	\$0.98	<a href="https://www.digikey.ca/en/products/detail/stmicroelectronics/L7812CV/585973">https://www.digikey.ca/en/products/detail/stmicroelectronics/L7812CV/585973</a>
U4, U5	ACS712 20A	2	\$4.29	\$8.58	<a href="https://www.digikey.ca/en/products/detail/allegro-microsystems/ACS712ELCTR-20A-T/1284607">https://www.digikey.ca/en/products/detail/allegro-microsystems/ACS712ELCTR-20A-T/1284607</a>
U6	ADS1115ID GSR 16Bit	1	\$8.59	\$8.59	<a href="https://www.digikey.ca/en/products/detail/texas-instruments/ADS1115IDGSR/2231567">https://www.digikey.ca/en/products/detail/texas-instruments/ADS1115IDGSR/2231567</a>
-	Heat sink	3	1.17	\$3.50	<a href="https://www.amazon.ca/Easycargo-Heatsink-Insulator-Regulator-Transistor/dp/B08MW1YNJM/ref=asc_df_B08MW1YNJM/?th=1">https://www.amazon.ca/Easycargo-Heatsink-Insulator-Regulator-Transistor/dp/B08MW1YNJM/ref=asc_df_B08MW1YNJM/?th=1</a>
-	PCB	1	2.33	2.33	<a href="https://jlcpcb.com/">https://jlcpcb.com/</a>
			Total	\$66.07	

Bill of material of Bidirectional converter

Designator	Value	Qty	Cost per unit	Total cost	Source of materials
A4	Arduino_Nano_v3.x	1	\$10.66	\$10.66	<a href="https://www.amazon.ca/ELEGOO-Arduino-ATmega328P-Without-Compatible/dp/B0713XK923/?th=1">https://www.amazon.ca/ELEGOO-Arduino-ATmega328P-Without-Compatible/dp/B0713XK923/?th=1</a>
C1, C18	Cap 470uF, 100V	2	\$1.57	\$3.15	<a href="https://www.digikey.ca/en/products/detail/rubycon/100ZLH470MEFC16X31-5/3564548">https://www.digikey.ca/en/products/detail/rubycon/100ZLH470MEFC16X31-5/3564548</a>
C2, C11	Cap 470uF, 50V	2	\$0.98	\$1.95	<a href="https://www.digikey.ca/en/products/detail/nichicon/UPW1H471MHD/589652">https://www.digikey.ca/en/products/detail/nichicon/UPW1H471MHD/589652</a>
C3, C4	Cap.33uF, 50V	2	\$0.26	\$0.51	<a href="https://www.digikey.ca/en/products/detail/nichicon/VR2AR33MDD/588879">https://www.digikey.ca/en/products/detail/nichicon/VR2AR33MDD/588879</a>
C5	Cap .22uF, 50V	1	\$0.26	\$0.26	<a href="https://www.digikey.ca/en/products/detail/nichicon/VR1HR22MDD/588837">https://www.digikey.ca/en/products/detail/nichicon/VR1HR22MDD/588837</a>
C6, C7	0.1uF, 0805 SMD	2	\$0.04	\$0.08	<a href="https://www.digikey.ca/en/products/detail/samsung-electro-mechanics/CL21B104KCFNNE/5961324?">https://www.digikey.ca/en/products/detail/samsung-electro-mechanics/CL21B104KCFNNE/5961324?</a>
C8, C19	10uF,0805 SMD	2	\$0.06	\$0.12	<a href="https://www.digikey.ca/en/products/detail/samsung-electro-mechanics/CL21A106KQNNNE/3886754">https://www.digikey.ca/en/products/detail/samsung-electro-mechanics/CL21A106KQNNNE/3886754</a>
C9, C10	10nF,0805 SMD	2	\$0.10	\$0.21	<a href="https://www.digikey.ca/en/products/detail/kemet/C0805X103K1RAC3316/10315780">https://www.digikey.ca/en/products/detail/kemet/C0805X103K1RAC3316/10315780</a>
C12, C15	4.7uF,0805 SMD	2	\$0.06	\$0.12	<a href="https://www.digikey.ca/en/products/detail/samsung-electro-mechanics/CL21A475KAQNNNE/3886902">https://www.digikey.ca/en/products/detail/samsung-electro-mechanics/CL21A475KAQNNNE/3886902</a>
C13, C17, C14, C16	2.2uF 0805 SMD	4	\$0.19	\$0.77	<a href="https://www.digikey.ca/en/products/detail/samsung-electro-mechanics/CL21B225KAFNFNE/3888611">https://www.digikey.ca/en/products/detail/samsung-electro-mechanics/CL21B225KAFNFNE/3888611</a>
D1, D3, D4, D6	SS310 0805 SMD	4	\$0.74	\$2.94	<a href="https://www.digikey.ca/en/products/detail/onsemi/S310FA/5892104">https://www.digikey.ca/en/products/detail/onsemi/S310FA/5892104</a>
D5	APT60S20BG 75A	1	\$5.60	\$5.60	<a href="https://www.digikey.ca/en/products/detail/microchip-technology/APT60S20BG/1494822?">https://www.digikey.ca/en/products/detail/microchip-technology/APT60S20BG/1494822?</a>
F1, F2	Fuse	2	\$1.20	\$2.40	<a href="https://www.digikey.ca/en/products/detail/littelfuse-inc/0997020-WXN/701061">https://www.digikey.ca/en/products/detail/littelfuse-inc/0997020-WXN/701061</a>
J1	Fuse holder	1	\$1.18	\$1.18	<a href="https://www.digikey.ca/en/products/detail/littelfuse-inc/01000063Z/14641003">https://www.digikey.ca/en/products/detail/littelfuse-inc/01000063Z/14641003</a>
J2, J3, J6, J7	Screw Terminal 8197 2	4	\$1.07	\$4.28	<a href="https://www.digikey.ca/en/products/detail/keystone-electronics/8197-2/2746666">https://www.digikey.ca/en/products/detail/keystone-electronics/8197-2/2746666</a>
J4	Screw_Terminal_01x02	1	\$0.52	\$0.52	<a href="https://www.digikey.ca/en/products/detail/cui-devices/TB002-500-02BE/10064069">https://www.digikey.ca/en/products/detail/cui-devices/TB002-500-02BE/10064069</a>
J5	Conn_01x08_header	1	\$0.29	\$0.29	<a href="https://www.digikey.ca/en/products/detail/adam-tech/PH1RB-08-UA/9831008?">https://www.digikey.ca/en/products/detail/adam-tech/PH1RB-08-UA/9831008?</a>
L1	Inductor toroidal 0077443A7	1	\$7.38	\$7.38	<a href="https://www.digikey.ca/en/products/detail/magnetics-a-division-of-spang-co/0077443A7/18626894?">https://www.digikey.ca/en/products/detail/magnetics-a-division-of-spang-co/0077443A7/18626894?</a>
Q1, Q2	MOSFET CSD19533KCS	2	\$1.71	\$3.42	<a href="https://www.digikey.ca/en/products/detail/texas-instruments/CSD19533KCS/4806074">https://www.digikey.ca/en/products/detail/texas-instruments/CSD19533KCS/4806074</a>
R1, R2	47 Ohm 0805 SMD	2	\$0.02	\$0.04	<a href="https://www.digikey.ca/en/products/detail/stackpole-electronics-inc/RMCF0805FT47R0/1713163">https://www.digikey.ca/en/products/detail/stackpole-electronics-inc/RMCF0805FT47R0/1713163</a>
R3, R4, R18	220 Ohm 0805 SMD	2	\$0.02	\$0.04	<a href="https://www.digikey.ca/en/products/detail/stackpole-electronics-inc/RMCF0805FT220R/1760238">https://www.digikey.ca/en/products/detail/stackpole-electronics-inc/RMCF0805FT220R/1760238</a>

R5, R7, R9, R10	100k Ohm 0805 SMD	4	\$0.02	\$0.08	<a href="https://www.digikey.ca/en/products/detail/stackpole-electronics-inc/RMCF0805FT100K/1760712">https://www.digikey.ca/en/products/detail/stackpole-electronics-inc/RMCF0805FT100K/1760712</a>
R6, R8, R11, R16, R17	10k Ohm 0805 SMD	5	\$0.02	\$0.10	<a href="https://www.digikey.ca/en/products/detail/stackpole-electronics-inc/RMCF0805FT10K0/1760676">https://www.digikey.ca/en/products/detail/stackpole-electronics-inc/RMCF0805FT10K0/1760676</a>
R12, R13, R14, R15	0-ohm, Jumper, 0805	4	\$0.01	\$0.06	<a href="https://www.digikey.ca/en/products/detail/stackpole-electronics-inc/RMCF0805ZT0R00/1756901">https://www.digikey.ca/en/products/detail/stackpole-electronics-inc/RMCF0805ZT0R00/1756901</a>
U1	MOSFET driver IR2104	1	\$5.36	\$5.36	<a href="https://www.digikey.ca/en/products/detail/infineon-technologies/IR2104PBF/812198">https://www.digikey.ca/en/products/detail/infineon-technologies/IR2104PBF/812198</a>
U2	LM7805CV TO220	1	\$0.79	\$0.79	<a href="https://www.digikey.ca/en/products/detail/stmicroelectronics/L7805CV/585964">https://www.digikey.ca/en/products/detail/stmicroelectronics/L7805CV/585964</a>
U3	LM7812CV TO220	1	\$0.98	\$0.98	<a href="https://www.digikey.ca/en/products/detail/stmicroelectronics/L7812CV/585973">https://www.digikey.ca/en/products/detail/stmicroelectronics/L7812CV/585973</a>
U4, U5	ACS712 20A	2	\$4.29	\$8.58	<a href="https://www.digikey.ca/en/products/detail/allegro-microsystems/ACS712ELCTR-20A-T/1284607">https://www.digikey.ca/en/products/detail/allegro-microsystems/ACS712ELCTR-20A-T/1284607</a>
U6	ADS1115ID GSR 16Bit	1	\$8.59	\$8.59	<a href="https://www.digikey.ca/en/products/detail/texas-instruments/ADS1115IDGSR/2231567">https://www.digikey.ca/en/products/detail/texas-instruments/ADS1115IDGSR/2231567</a>
-	Heat sink	3	\$1.17	\$3.50	<a href="https://www.amazon.ca/Easycargo-Heatsink-Insulator-Regulator-Transistor/dp/B08MW1YNJM/ref=asc_df_B08MW1YNJM/?th=1">https://www.amazon.ca/Easycargo-Heatsink-Insulator-Regulator-Transistor/dp/B08MW1YNJM/ref=asc_df_B08MW1YNJM/?th=1</a>
-	PCB	1	\$2.33	\$2.33	<a href="https://jlcpcb.com/">https://jlcpcb.com/</a>
			Total	\$76.28	-

#### Bill of material of Master Controller

Designator	Value	Qty	Cost per unit	Total cost	Source of materials
A4	Arduino_Nano_v3.x	1	\$10.66	\$10.66	<a href="https://www.amazon.ca/ELEGOO-Arduino-ATmega328P-Without-Compatible/dp/B0713XK923/?th=1">https://www.amazon.ca/ELEGOO-Arduino-ATmega328P-Without-Compatible/dp/B0713XK923/?th=1</a>
C4, C5	.22uF	2	\$0.26	\$0.51	<a href="https://www.digikey.ca/en/products/detail/nichicon/UV1HR22MDD/588837">https://www.digikey.ca/en/products/detail/nichicon/UV1HR22MDD/588837</a>
D2	SS310 0805 SMD	1	\$0.74	\$0.74	<a href="https://www.digikey.ca/en/products/detail/onsemi/S310FA/5892104">https://www.digikey.ca/en/products/detail/onsemi/S310FA/5892104</a>
J1, J3	JST 4POS2.54MM	2	\$0.23	\$0.46	<a href="https://www.digikey.ca/en/products/detail/jst-sales-america-inc./B4B-XH-A/1651047?">https://www.digikey.ca/en/products/detail/jst-sales-america-inc./B4B-XH-A/1651047?</a>
J2, J4	Screw_Terminal_01x02	1	\$0.52	\$0.52	<a href="https://www.digikey.ca/en/products/detail/cui-devices/TB002-500-02BE/10064069">https://www.digikey.ca/en/products/detail/cui-devices/TB002-500-02BE/10064069</a>
J5	Conn_01x08 Pin header	1	\$0.29	\$0.29	<a href="https://www.digikey.ca/en/products/detail/adam-tech/PH1RB-08-UA/9831008?">https://www.digikey.ca/en/products/detail/adam-tech/PH1RB-08-UA/9831008?</a>
J6, J7	Conn_01x06_Socket	2			

R3, R4	10k Ohm 0805 SMD	2	\$0.02	\$0.04	<a href="https://www.digikey.ca/en/products/detail/stackpole-electronics-inc/RMCF0805FT10K0/1760676">https://www.digikey.ca/en/products/detail/stackpole-electronics-inc/RMCF0805FT10K0/1760676</a>
R1, R2	220 Ohm 0805 SMD	2	\$0.02	\$0.04	<a href="https://www.digikey.ca/en/products/detail/stackpole-electronics-inc/RMCF0805FT220R/1760238">https://www.digikey.ca/en/products/detail/stackpole-electronics-inc/RMCF0805FT220R/1760238</a>
U2	LM7805CV TO220	1	\$0.79	\$0.79	<a href="https://www.digikey.ca/en/products/detail/stmicroelectronics/L7805CV/585964">https://www.digikey.ca/en/products/detail/stmicroelectronics/L7805CV/585964</a>
-	Heat sink	3	\$1.17	\$3.50	<a href="https://www.amazon.ca/Easycargo-Heatsink-Insulator-Regulator-Transistor/dp/B08MW1YNJM/ref=asc_df_B08MW1YNJM/?th=1">https://www.amazon.ca/Easycargo-Heatsink-Insulator-Regulator-Transistor/dp/B08MW1YNJM/ref=asc_df_B08MW1YNJM/?th=1</a>
-	15W Converter for pi	1	\$8.90	\$8.90	<a href="https://www.amazon.ca/DKARDU-Converter-Voltage-Regulator-Charger/dp/B0B2RF1L92/">https://www.amazon.ca/DKARDU-Converter-Voltage-Regulator-Charger/dp/B0B2RF1L92/</a>
-	PCB	1	\$2.33	\$2.33	<a href="https://jlcpcb.com/">https://jlcpcb.com/</a>
			Total	\$28.78	

#### Bill of material of communication bus

Designator	Value	Qty	Cost per unit	Total cost	Source of materials
J2, J3, J4, J6	Conn_01x08 _Socket	4	\$0.41	\$1.64	<a href="https://www.digikey.ca/en/products/detail/w%C3%BCrth-elektronik/61300811821/17737805?">https://www.digikey.ca/en/products/detail/w%C3%BCrth-elektronik/61300811821/17737805?</a>
J1,	Conn_01x08 _Socket vertical	1	\$0.77	\$0.77	<a href="https://www.digikey.ca/en/products/detail/sullins-connector-solutions/PPPC081LGBN-RC/775941?">https://www.digikey.ca/en/products/detail/sullins-connector-solutions/PPPC081LGBN-RC/775941?</a>
J7	Conn_01x08 Pin Right angle	1	\$0.29	\$0.29	<a href="https://www.digikey.ca/en/products/detail/adam-tech/PH1RB-08-UA/9831008?">https://www.digikey.ca/en/products/detail/adam-tech/PH1RB-08-UA/9831008?</a>
-	PCB	1	\$2.33	\$2.33	<a href="https://jlcpcb.com/">https://jlcpcb.com/</a>
			Total	\$5.03	

#### Bill of material of monitoring system

Component	Qty	Cost per unit	Total cost	Source of materials
Raspberry Pi	1	\$45.00	\$45.00	<a href="https://www.digikey.ca/en/products/detail/raspberry-pi/SC0193(9)/10258782?">https://www.digikey.ca/en/products/detail/raspberry-pi/SC0193(9)/10258782?</a>
7 Inch Touchscreen	1	\$0.77	\$0.77	<a href="https://www.digikey.ca/en/products/detail/sullins-connector-solutions/PPPC081LGBN-RC/775941?">https://www.digikey.ca/en/products/detail/sullins-connector-solutions/PPPC081LGBN-RC/775941?</a>
Conn_01x08 Pin Right angle	1	\$63.95	\$63.95	<a href="https://www.amazon.ca/dp/B0B44VZTRG/">https://www.amazon.ca/dp/B0B44VZTRG/</a>
DIN rail	1	\$7.26	\$7.26	<a href="https://www.digikey.ca/en/products/detail/altech-corporation/2511120%2F1M/8546913?">https://www.digikey.ca/en/products/detail/altech-corporation/2511120%2F1M/8546913?</a>
Bus bar	1	\$31.31	\$31.31	<a href="https://www.digikey.ca/en/products/detail/weidm%C3%BCler/0280300000/491744?">https://www.digikey.ca/en/products/detail/weidm%C3%BCler/0280300000/491744?</a>
		Total	\$147.52	

# Curriculum Vitae

**Name:** Md Motakabbir Rahman  
**Post-secondary Education and Degrees:** The University of Western Ontario  
London, Ontario, Canada  
2022-2024 MEdSc.

Rajshahi University of Engineering and Technology  
Rajshahi, Bangladesh  
2015-2019 BSc.

**Honors and Awards:** Hydro One Graduate Scholarships  
2024

**Related Work Experience:** Graduate Research Assistant  
The University of Western Ontario  
2022-2024

## Publications:

M. M. Rahman and J. Pearce, "Modular Open Source Solar Photovoltaic-Powered DC Nanogrids with Efficient Energy Management System," *Solar Energy and Sustainable Development Journal*, vol. 13, no. 1, Art. no. 1, Feb. 2024, doi: 10.51646/jsesd.v13i1.169.

M. Mottaghi, M. Rahman, A. Kulkarni, and J. M. Pearce, "AC/off-grid photovoltaic powered open-source ball mill," *HardwareX*, vol. 14, p. e00423, Jun. 2023, doi: 10.1016/j.ohx.2023.e00423.

S. Khan and M. M. Rahman, "Design and Simulation of Solar DC Nanogrid System from Bangladesh Perspective," *2021 International Conference on Automation, Control and Mechatronics for Industry 4.0 (ACMI), 2021*, pp. 1-6, <https://doi.org/10.1109/ACMI53878.2021.9528159>

Rahman, M. M., & Islam, M. S. (2020). PSO and ANN Based Hybrid MPPT Algorithm for Photovoltaic Array under Partial Shading Condition. *Engineering International*, 8(1), 9-24. <https://doi.org/10.18034/ei.v8i1.481>

Islam, M. S., Sultana, S., & Rahman, M. M. (2019). Protection of Power System during Cyber-Attack using Artificial Neural Network. *Engineering International*, 7(2), 73-84. <https://doi.org/10.18034/ei.v7i2.478>

M. M. Rahman and M. S. Islam, "Artificial Neural Network Based Maximum Power Point Tracking of a Photovoltaic System," *2019 3rd International Conference on Electrical, Computer & Telecommunication Engineering (ICECTE)*, Rajshahi, Bangladesh, 2019, pp. 117-120, <https://doi.org/10.1109/ICECTE48615.2019.9303531>